REPORT DOCUMENTATION PAGE

2

Form Approved OMB NO. 0704-0188

1. REPORT DATE (DD-MM-YYYY)	2. REPORT TYPE	3. DATES COVERED (From - To)
24-08-2014	MS Thesis	-

4. TITLE AND SUBTITLE
Peroxiredoxins: A Model for a Self-Assembling Nanoscale System

5a. CONTRACT NUMBER
W911NF-12-1-0554

5b. GRANT NUMBER

5c. PROGRAM ELEMENT NUMBER
611102

6. AUTHORS
Jacob LIttlejohn

5d. PROJECT NUMBER

5e. TASK NUMBER

5f. WORK UNIT NUMBER

7. PERFORMING ORGANIZATION NAMES AND ADDRESSES
University of Canterbury
20 Kirkwood Ave
Ilam
-

8. PERFORMING ORGANIZATION REPORT NUMBER

9. SPONSORING/MONITORING AGENCY NAME(S) AND ADDRESS (ES)
U.S. Army Research Office
P.O. Box 12211
Research Triangle Park, NC 27709-2211

10. SPONSOR/MONITOR'S ACRONYM(S)
ARO

11. SPONSOR/MONITOR'S REPORT NUMBER(S)
61663-CH.3

12. DISTRIBUTION AVAILIBILITY STATEMENT
Approved for public release; distribution is unlimited.

13. SUPPLEMENTARY NOTES
The views, opinions and/or findings contained in this report are those of the author(s) and should not contrued as an official Department of the Army position, policy or decision, unless so designated by other documentation.

14. ABSTRACT
The formation of large, complex structures from small building blocks through self-assembly is widely seen in proteins and provides a tool for the creation of functional nanoscale devices. However, the factors controlling protein self-assembly are complex and often poorly understood. Peroxiredoxins are a large family of proteins, many of which are able to form a variety of large structures from a small, basic unit. This assembly has been shown to be strongly influenced by the redox state of the enzyme, which functions as a switch, controlling

15. SUBJECT TERMS
peroxiredoxin, tecton, supramolecular assembly

16. SECURITY CLASSIFICATION OF:			17. LIMITATION OF ABSTRACT	15. NUMBER OF PAGES	19a. NAME OF RESPONSIBLE PERSON
a. REPORT	b. ABSTRACT	c. THIS PAGE			Juliet Gerrard
UU	UU	UU	UU		19b. TELEPHONE NUMBER +64-364-2987

Report Title

Peroxiredoxins: A Model for a Self-Assembling Nanoscale System

ABSTRACT

The formation of large, complex structures from small building blocks through self-assembly is widely seen in proteins and provides a tool for the creation of functional nanoscale devices. However, the factors controlling protein self-assembly are complex and often poorly understood. Peroxiredoxins are a large family of proteins, many of which are able to form a variety of large structures from a small, basic unit. This assembly has been shown to be strongly influenced by the redox state of the enzyme, which functions as a switch, controlling self-assembly. This thesis uses a protein from this family, human peroxiredoxin 3 (hPrx3) as a model system to investigate whether the self-assembly properties of hPrx3 can be influenced by rational protein engineering.

Three forms of hPrx3 were purified and examined. These were the wild type and two variants: a mutant (S78A) and a His-tagged form. Size exclusion chromatography showed that each form showed a different ratio of dimers and larger species. Both variants showed preference for larger species, especially in the His-tagged form. This was shown to be partially dependent on metal binding in the His-tagged form. Larger species formed from multiple rings were also identified. SAXS measurement indicated that in the wild type enzyme, higher order species were dodecameric rings. For the His-tagged variant, SAXS measurement showed that the species observed had a different structure than that of the wild type. Electron microscopy showed that higher order structures seen in both wild type hPrx3 and His-tagged hPrx3 were ring shaped, with dimensions consistent with dodecamers. A competitive assay showed that the wild type, with kcat/km values near 2 × 107, consistent with published results. Both variant forms showed evidence of slightly higher activity than the wild type, indicating a link between activity and assembly.

A peroxiredoxin from the thermophilic bacteria Thermus aquaticus, TaqPrx was also examined, in an attempt to investigate a peroxiredoxin capable of self-assembly at high temperatures, which would be very useful for a nanoscale device. TaqPrx was cloned, purified and examined, however, no evidence of self-assembly was observed. Protein modelling and dynamic light scattering measurement indicated that the protein purified was monomeric and had a structure. Sparse matrix crystal screening identified conditions that allowed crystal formation, although strongly diffracting crystals were not produced. A novel assay for peroxiredoxin activity was developed, and suggested that TaqPrx shows peroxiredoxin activity. This thesis shows that peroxiredoxins are a useful model system for the investigation of how protein self-assembly is controlled, and how it can be influenced by protein engineering.

Peroxiredoxins: A Model for a Self-Assembling Nanoscale System

A thesis submitted in partial fulfilment

of the requirements for the degree of

Master of Science

at the

University of Canterbury

by

Jacob Littlejohn

Table of Contents

Table of contents……*i*

Abstract……..……..*vii*

Abbreviations……...*viii*

Acknowledgements……..*xii*

Chapter One

Introduction

1.1 Protein quaternary structure and self-assembly 1

1.1.1 Quaternary structure 1

1.1.2 Quaternary structure formation through self-assembly 1

1.1.3 Quaternary structure and protein function 3

1.2 Nanobiotechnology and protein self-assembly 3

1.3 Overview of peroxiredoxins 4

1.4 The biological role of peroxiredoxins 6

1.4.1 Overview 6

1.4.2 Peroxiredoxins as cellular antioxidants 6

1.4.3 Peroxiredoxins as chaperones 6

1.4.4 Overoxidation and the floodgate model 7

1.5 The peroxiredoxin mechanism and active site 8

1.5.1 Peroxiredoxin substrate preference 8

1.5.2 Peroxiredoxin active site 9

1.5.3 Peroxiredoxin catalytic cycle 10

1.5.4 Rate of reaction 12

1.6 Peroxiredoxin classes 12

1.6.1 Sequence based divisions 12

1.7 Peroxiredoxin structure and assembly 13

1.7.1 Peroxiredoxin fold 13

1.7.2 Dimer formation 14

1.7.3 Assembly of larger species 17

1.8 Control of AhpC-Prx1 self-assembly and protein dynamics 18

1.8.1 The redox switch 19

1.8.2 Protein dynamics in the catalytic cycle of peroxiredoxins 21

1.8.3 The link between activity and oligomerisation 21

1.8.4 Overoxidation 22

1.9 Human Peroxiredoxin 3 22

1.10 Summary and project overview 23

Chapter Two

Results and Discussion (hPrx3)

2.1 Purification 25

2.1.1 Purification of wild type hPrx3 and S78A 26

2.1.2 Purification of His-tagged hPrx3 27

2.1.3 Purification of His-tagged hPrx3 S78A 28

2.2 Analysis of the quaternary structure of hPrx3 28

2.2.1 SEC analysis of hPrx3 30

2.2.2 SAXS analysis of wild type hPrx3 34

2.2.3 TEM of wild type hPrx3 40

2.3 Analysis of the quaternary structure of hPrx3 S78A 42

2.3.1 SEC Analysis of S78A mutant hPrx3 42

2.4 Analysis of the quaternary structure of His-tagged hPrx3 44

2.4.1 SEC Analysis of His-tagged hPrx3 44

2.4.2 SAXS analysis of His-tagged hPrx3 47

2.4.3 TEM of His-tagged Prx3 50

2.4.4 Effects of EDTA on His-tagged hPrx3 52

2.5 His-tagged hPrx3 S78A 55

2.6 Preliminary comparison of activity of hPrx3 variants 56

2.5.1 Activity assay for wild type hPrx3 56

2.5.2 Activity assay for hPrx3 S78A 58

2.5.3 Activity assay for His-tagged hPrx3 59

2.6 Summary of Results 60

Chapter Three

Results and Discussion (TaqPrx)

3.1 Sequence comparisons of hPrx3 and thermophilic peroxiredoxins 61

3.1.1 Clustal Omega alignment of peroxiredoxins 61

3.1.2 BLAST comparisons of reported peroxiredoxins in *T.aquaticus* 63

3.2 PCR and transformation 64

3.3 Overexpression and purification of TaqPrx 66

3.4 Melting temperature analysis or TaqPrx..... 67

3.5 Quaternary structure of TaqPrx by DLS 69

3.6 Structural homology modelling..... 70

3.6.1 Homology model of TaqPrx 70

3.6.2 Evaluation of homology model accuracy 71

3.7 Sparse matrix crystal screening 73

3.7.1 Initial screening 73

3.7.2 JCSG+ and PACT screens..... 74

3.8 Activity assay of TaqPrx 75

3.9 Summary of results..... 80

Chapter Four

Conclusion and Summary

Chapter Five

General Methods

5.1 Chemicals, buffers and equipment 86

5.2 Bacterial cultures..... 87

5.3 Plasmid extraction..... 87

5.4 DNA gel electrophoresis..... 87

5.5 Production of chemically competent cells 88

5.6 Heat shock transformation..... 88

5.7 Preparation of freezer stocks..... 88

5.8 Protein SDS-PAGE 88

5.9 Expression and purification of Tobacco etch virus protease 89

Chapter Six

Experimental Method (hPrx3)

6.1 pEt 151 plasmids 90

6.2 Overexpression and purification 90

6.3 Transition electron microscopy 91

6.4 Analytical size exclusion chromatography 92

6.4.1 Concentration, pH and buffer variations 92

6.4.2 EDTA and His-tagged hPrx3 92

6.5 SAXS 93

6.6 Competitive activity assay 93

Chapter Seven

Experimental Method (TaqPrx)

7.1.1 Comparisons of thermophilic peroxiredoxin genes to hPrx3 95

7.1.2 The *TaqPRDX1* gene 95

7.2 Gateway cloning of *TaqPRDX1* 95

7.2.1 PCR 95

7.2.2 Cloning of *TaqPRDX1* into pDONR221 donor plasmid 97

7.2.3 Transformation of pDONR221 plasmid into *E.coli* DH5α 98

7.2.4 BsrG1 digest of pDONR221 plasmid 98

7.2.5 Cloning of *TaqPRDX1* into pDEST 17 expression plasmid 98

7.2.6 Transformation of pDEST17 into *E.coli* Rosetta 98

7.3 Overexpression and purification of TaqPrx 99

7.4 Protein melting temperature analysis 100

7.5 Dynamic light scattering measurement of TaqPrx 100

7.6 Structural homology modelling 100

7.7 Sparse matrix crystal screening 100

7.7.1 Initial screening 100

7.7.2 JCSG+ and PACT screening 102

7.8 Activity assay 103

References 104

Abstract

The formation of large, complex structures from small building blocks through self-assembly is widely seen in proteins and provides a tool for the creation of functional nanoscale devices. However, the factors controlling protein self-assembly are complex and often poorly understood. Peroxiredoxins are a large family of proteins, many of which are able to form a variety of large structures from a small, basic unit. This assembly has been shown to be strongly influenced by the redox state of the enzyme, which functions as a switch, controlling self-assembly. This thesis uses a protein from this family, human peroxiredoxin 3 (hPrx3) as a model system to investigate whether the self-assembly properties of hPrx3 can be influenced by rational protein engineering.

Three forms of hPrx3 were purified and examined. These were the wild type and two variants: a mutant (S78A) and a His-tagged form. Size exclusion chromatography showed that each form showed a different ratio of dimers and larger species. Both variants showed preference for larger species, especially in the His-tagged form. This was shown to be partially dependent on metal binding in the His-tagged form. Larger species formed from multiple rings were also identified. SAXS measurement indicated that in the wild type enzyme, higher order species were dodecameric rings. For the His-tagged variant, SAXS measurement showed that the species observed had a different structure than that of the wild type. Electron microscopy showed that higher order structures seen in both wild type hPrx3 and His-tagged hPrx3 were ring shaped, with dimensions consistent with dodecamers. A competitive assay showed that the wild type, with k_{cat}/km values near 2×10^7, consistent with published results. Both variant forms showed evidence of slightly higher activity than the wild type, indicating a link between activity and assembly.

A peroxiredoxin from the thermophilic bacteria *Thermus aquaticus*, TaqPrx was also examined, in an attempt to investigate a peroxiredoxin capable of self-assembly at high temperatures, which would be very useful for a nanoscale device. TaqPrx was cloned, purified and examined, however, no evidence of self-assembly was observed. Protein modelling and dynamic light scattering measurement indicated that the protein purified was monomeric and had a structure. Sparse matrix crystal screening identified conditions that allowed crystal formation, although strongly diffracting crystals were not produced. A novel assay for peroxiredoxin activity was developed, and suggested that TaqPrx shows

peroxiredoxin activity. This thesis shows that peroxiredoxins are a useful model system for the investigation of how protein self-assembly is controlled, and how it can be influenced by protein engineering.

Abbreviations

A, Ala	alanine
A_{600}	absorbance at 600 nm
AhpC	alkyl hydroperoxidase C
AhpE	alky hydroperoxidase E
AhpF	alkyl hydroperoxidase F
Amp	ampicillin
ATP	adenosine triphosphate
BCP	bacterioferritin comigratory protein
BLAST	basic local alignment sequence tool
C, Cys	cysteine
Chl	chloramphenicol
C_P	peroxidatic cysteine
C_R	resolving cysteine
D_{MAX}	maximum distance
DNA	deoxyribonucleic acid
DTPA	diethylene triamine pentaacetic acid
DTT	dithiothreitol
E. coli	*Echerischia coli*
EDTA	ethylenediaminetetraacetic acid
EMBL	european microbiology lab
F, Phe	phenylalanine
FPLC	fast protein liquid chromatography

Abbreviations x

G,Gly	glycine
G.stearothermophilus	*Geobacillus stearothermophilus*
H, His	histidine
H. sapiens	*Homo sapiens*
HMW	high molecular weight
HRP	horseradish peroxidase
I. aggregans	*Ignispaera aggregans*
IPTG isopropyl β-D-1	thiogalactopyranoside
Kan	kanamycin
L, Leu	leucine
LB	lysogeny broth
M. tuberculosis	*Mycobacterium tuberculosis*
MBP	maltose binding protein
mPEG	poly (ethylene glycol) methyl ester
MW	molecular mass
MX1	macromolecular crystallography
NADH	reduced nicotinamide adenosine dinucleotide
NADPH	reduced nictotinamide adenosine dinucleotide phosphate
NEM	*N*-ethyl maleimide
OD_{600}	optical density at 600 nm
P. aerophilum	*Pyrobaculum aerophilum*
P. furiosus	*Pyrococcus furiosus*
PAGE	polyacrylamide gel electrophoresis

PCR	polymerase chain reaction
PDB	protein databank
PEG	poly(ethylene glycol)
Prx	peroxiredoxin
Q, Gln	glutamine
R, Arg	arginine
RFU	relative fluorescence units
R_g	radius of gyration
RI	refractive index
RNA	ribonucleic acid
ROS	reactive oxygen species
rpm	revolutions per minute
S, Ser	serine
S. acidocaldarius	*Sulfolobus acidocaldarius*
S. sulfataricus	*Sulfolobus sulfataricus*
SAXS	small angle x-ray scattering
SDS	sodium dodecyl sulfate
SEC	size exclusion chromatography
T, Thr	threonine
T. aquaticus	*Thermus aquaticus*
T. maritima	*Thermotoga maritima*
TAE	tris acetate EDTA
TaqPRDX1	*Thermus aquaticus* peroxiredoxin gene 1

TaqPrx	*Thermus aquaticus* peroxiredoxin
TCEP	tris(2-carboxyethyl)phosphine
TEM	transition electron microscopy
TEM	transmission electron microscopy
Tet	tetracyclin
TEV	tobacco etch virus
Tpx	thiol peroxidise
UV	ultraviolet
w/v	weight/volume
Y, Tyr	tyrosine
β-ME	β-mercaptoethanol

Acknowlegments

Firstly, a big thanks to Juliet Gerrard, my supervisor for this project, for fantastic supervision, inspiration and support through researching and writing this thesis. Thanks for keeping me positive and always having ideas for moving forwards in my research, and for giving me the opportunity to learn so much.

To my co-supervisors, Celine, Ren and Shaun, thanks for the support and advice you gave me over course of my study. Thanks especially to Shaun for taking me in as a lab refugee, and to everyone in the AgResearch lab at the University of Auckland for their help and support in my time there.

A huge thank-you to Celine and Amy, thanks so much for all your help with peroxiredoxin work, for your help and advice and ideas for new experiments, I really couldn't have done it without you.

Thanks to Mark, Christine and everyone else in the peroxiredoxin team from the Otago medical school for providing the hPrx3 gene, and immense expertise on the protein. Thanks especially to Alexander Peskin for teaching me how to run and interpret the activity assays.

To everyone in the BIC lab, thanks for your help in the lab, advice on methods, proof reading this thesis and general support, especially in the lead up to handing this thesis in, and for making research such an enjoyable experience.

Thank you to everyone who provided and helped me with the various techniques I used in this project: Grant and Jeremy for help with SAXS data collection and analysis, Jackie for TEM images and for being a fantastic lab manager, Marie Squire for mass spec, Hugh Morgan for providing the *Thermus aquaticus* genomic DNA and, of course, to Pam for getting me started on peroxiredoxin and showing me the ropes in the lab.

Finally, to my friends and family and especially Kathleen, for all your encouragement and support through my studies, I couldn't have done this without you.

CHAPTER ONE

Introduction

Human peroxiredoxin 3 (hPrx3) is a protein that is able to form large, highly ordered structures from a small, dimeric building block through self-assembly. This thesis investigates what conditions affect self-assembly in hPrx3 and whether mutations can be used to alter the equilibrium, between oligomeric forms.

1.1 Protein quaternary structure and self-assembly

1.1.1 Quaternary structure

Protein structure can be examined on several levels of increasing complexity. The sequence of amino acids in the polypeptide chain is the primary sequence. Amino acids interact to form secondary structural elements such as α-helices and β-sheets, which themselves assemble to form the three dimensional shape of a protein, its tertiary structure. Many proteins show a higher level of organisation, termed quaternary structure (Klotz, Langebman, and Dahnall 1970; Matthews and Sunde 2012). This is achieved by multiple polypeptide chains interacting permanently or transiently with each other to form larger structures (Ali and Imperiali 2005). The subunits in a protein complex may be identical, or a complex may be made up of multiple different types of subunit. Quaternary structures in proteins show a wide array of possible forms, from dimers made of two identical subunits (Marianayagam, Sunde, and Matthews 2004) to large, complex structures made of many different types of subunit, for example the F_1F_0 ATPases (Nakamoto, Baylis Scanlon, and Al-Shawi 2008).

1.1.2 Quaternary structure formation through self-assembly

Quaternary structure in proteins is generally achieved by self-assembly (Figure 1.1) This is the ability of small units to assemble into a larger, ordered structure defined only by the structure of the subunits themselves (Whitesides and Boncheva 2002; Whitesides and Grzybowski 2002). In order to do this, proteins use interface regions to specifically and

stably interact with their binding partner. Interfaces between proteins vary widely in terms of area, residues and forces involved (Jones 2012). In general, interfaces with larger surface areas show stronger interactions (Horton and Lewis 1992), however, research has shown that different parts of an interface can contribute much more to its stability than others (Bogan and Thorn 1998).

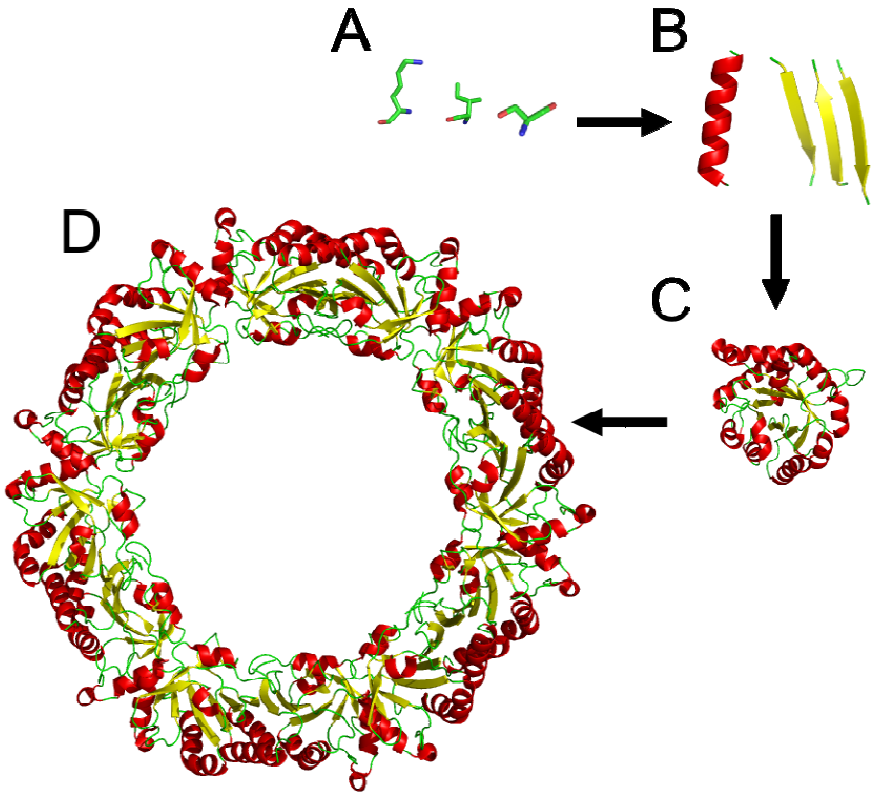

Figure 1.1: Schematic representation of self-assembly using proteins. **(A)** Amino acids assemble into **(B)** Secondary structural elements, which form **(C)** protein subunits, which themselves assemble to **(D)** oligomers. The image was created using PDB structures 1ZYE (Cao et al. 2005).

The interfaces of many oligomers show a large number of polar residues able to form hydrogen bonds or ionic interactions across the interface (Sheinerman, Norel, and Honig 2000). These may be direct, or mediated by water molecules trapped in cavities in the interface (Sonavane and Chakrabarti 2008). While these interactions are quite strong, residues must lose favourable interactions with the solvent, lessening their stabilising effect (Hendsch and Tidor 1994). Hydrophobic interactions, which increase stability by burying hydrophobic residues away from solution, are very important in the folding of a protein to its native form (Dill 1990). However, analysis of the role of hydrophobic interactions in assembly showed that its role is likely to be less important than that of hydrogen bonds and ionic interactions (Tsai et al. 1997).

Another important consideration is the three dimensional structure of the interface. In general, it has been seen that loop regions are more common in protein-protein interfaces than β-strands or α-helices (Ansari and Helms 2005). This may be due to the higher level of flexibility in these regions, allowing tighter, more stable interfaces to form (Jones 2012).

1.1.3 Quaternary structure and protein function

While it is known that many proteins form quaternary structures, the reasons for this are less well undersood (Griffin and Gerrard 2012). A variety of reasons have been proposed as to why oligomerisation is so widely observed.

Some proteins show obvious functional benefits to assembly, such as having active sites located in interfaces between subunits (Marianayagam, Sunde, and Matthews 2004). This would allow for regulation of activity, as disrupting the interface would prevent enzyme activity. For structural proteins such as tubulin, formation from oligomers enhances a cell's efficiency, as structures of varying lengths can be created by adding or removing subunits (Job, Valiron, and Oakley 2003). Another advantage for oligomerisation is increasing metabolic efficiency by substrate channelling. Several complexes made up of multiple different enzymes from the same metabolic pathway have been identified (Ovádi 1991). This allows substrates to pass from one active site to another without the risk of loss to competing reactions (Miles, Rhee, and Davies 1999). For many other proteins, no such obvious advantages to oligomerisation are known. It has been proposed that oligomerisation can influence protein dynamics in the active site (Griffin et al. 2008).

1.2 Nanobiotechnology and protein self-assembly

Nanobiotechnology is an emerging field of research aiming to utilise biological systems in the creation of devices at the nanometre scale that can carry out useful tasks (Whitesides 2003; Lowe 2000). Biological systems contain extremely complex nanoscale systems. Examples are the F_1F_0 ATPase, a rotary molecular motor powered by an ion gradient (Nakamoto, Baylis Scanlon, and Al-Shawi 2008) and viral capsids, cage-like structures that encase the viral genome (Angelescu and Linse 2008). These structures are built from smaller subunits by self-assembly. By understanding the molecular basis of the assembly of these species, and how this assembly is controlled, biologically based nanodevices can be designed (Zhang 2003).

Extensive work has been carried out in the use of DNA for this role: DNA can be folded into a wide range of two and three dimensional shapes using its ability to specifically bind to

complementary sequences (Rothemund 2006). Functional DNA based nanomachines have been demonstrated, such as walkers capable of moving along a track (Bath and Turberfield 2007).

Proteins have also drawn attention as building blocks for nanoscales structures (Bromley et al. 2008; Papapostolou and Howorka 2009). Proteins have a unique set of properties that make them attractive as self-assembling building blocks. They possess diverse chemical functionality, and display a wide variety of three dimensional structures that could be used as the basis for nanoscale devices (Astier, Bayley, and Howorka 2005).

As described in 1.1.2, the control of protein self-assembly is quite poorly understood, since many competing forces are involved. Thus, more extensive research is necessary to gain a better understanding of how protein self-assembly allows large structures to be built from smaller subunits. Peroxiredoxins are a family of proteins with members that show well defined self-assembly, as well as strong control of assembly based on their redox state. They can therefore be used as a model system by making changes to the protein and analysing how self-assembly is influenced.

1.3 Overview of peroxiredoxins

Peroxiredoxins (Prx) are a group of antioxidant enzymes found in all domains of life (Chae et al. 1994). First discovered in yeast (Kim et al. 1988), they have been shown to be present in almost every organism examined (Hofmann, Hecht, and Flohé 2005), with many producing multiple forms. Peroxiredoxins have been identified in the cytosol, membranes and inside organelles (Bernier-Villamor et al. 2004; Cao, Lindsay, and Isaacs 2007; Tavender, Sheppard, and Bulleid 2008), and are often among the most abundant proteins produced by both eukaryotic and bacterial cells (Rhee, Chae, and Kim 2005; Wood et al. 2003; Link, Robison, and Church 1997). The primary function of peroxiredoxin enzymes is to reduce peroxides, which are potentially damaging reactive oxygen species (ROS), formed as side reactions from the mitochondrial electron transport chain (Boveris and Chance 1973). However, peroxiredoxins have been implicated in numerous other roles, including cellular signalling (Wood, Poole, and Karplus 2003) and chaperone activity (Jang et al. 2004). Recent research has even shown evidence for a role of peroxiredoxin in the regulation of circadian rhythms (Edgar et al. 2012). The biological role of peroxiredoxins is discussed further in section 1.4.

Peroxiredoxins are unique among the several peroxide reducing enzymes in that they use no cofactors, relying instead on a conserved cysteine residue termed the peroxidatic cysteine, or C_P. This reacts directly with peroxides to form an oxidised cysteine intermediate. The active enzyme is regenerated *via* a disulfide (Wood et al. 2003) using other enzymes in the cell as the reductant (Figure 1.2).

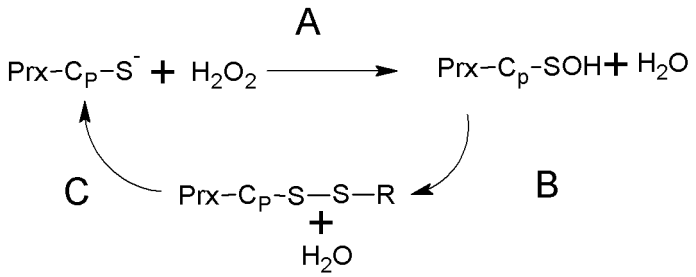

Figure 1.2: Basic reaction mechanism of peroxiredoxins. **(A)** The active cysteine reacts with hydrogen peroxide, forming the intermediate. **(B)** A disulfide is formed between the active cysteine and a second thiol group. **(C)** The active form is regenerated by reduction of the disulfide bond. CP is the active cysteine, Prx is the peroxiredoxin enzyme, R is a thiol containing species.

Peroxiredoxins show variation in the details of this mechanism. The identity of the thiol containing group used to generate the disulfide form varies widely, as does the reductant used to regenerate the active enzyme. Section 1.5 further discusses the mechanism of peroxiredoxins, while section 1.6 contains details on the differences between groups of enzymes within the peroxiredoxin family.

Certain peroxiredoxin enzymes have been shown to form a wide range of complex oligomeric structures. These are built using self-assembly from small, basic subunits. The most commonly seen structure is a ring formed by multiple dimers, often a decamer. The assembly of these has been shown to be strongly linked to the redox state of the active cysteine residue (Alphey et al. 2000; Barranco-Medina, Lázaro, and Dietz 2009). This acts as part of a switch to change proteins between a state favouring the dimer and a state favouring the decamer (Wood et al. 2002). Peroxiredoxin rings have themselves been shown to self-assemble into even larger structures, including stacks and tubes, catenanes and cage-like structures. The details of this self-assembly process from small subunits to large and complex species, and how it is linked to the mechanism of peroxiredoxin activity is discussed further in section 1.7.

Peroxiredoxins have the ability to form complex and well ordered structures through self-assembly, and show well understood redox based control over this process. This makes

them a useful model system to investigate how protein self-assembly can be controlled through rational design of mutations to the protein sequence. How this thesis will achieve this goal is described further in section 1.8.

1.4 The biological role of peroxiredoxins

1.4.1 Overview

A large amount of research into the biological role of peroxiredoxins has been carried out, primarily in mammalian systems. Much of this research is beyond the scope of this review, so instead a brief overview will be given, with a focus on the biological role of structural changes in peroxiredoxin.

Peroxiredoxins are just one of several enzyme families that react with peroxides. Others are the catalases, glutathione peroxidases and thioredoxins. This indicates the importance of ROS removal in biology. Of these, peroxiredoxins are often the most abundant, and many organisms express multiple different peroxiredoxin enzymes. Some organisms that have been modified not to express peroxiredoxins show severe symptoms (Lee et al. 2007), while others demonstrate no visible detrimental effects (Li et al. 2007). Upregulation of peroxiredoxins has been associated with drug resistance in the pathogenic bacterium *Mycobacterium tuberculosis (M. tuberculosis)* (Guimarães et al. 2005) and certain cancers (Park et al. 2000).

1.4.2 Peroxiredoxins as cellular antioxidants

Peroxiredoxins were first identified by their ability to protect proteins from oxidative damage, indicating a role as antioxidants (Kim et al. 1988). Others peroxide reducing enzymes include the catalases and the glutathione peroxidases, which are both known to have very high reaction rates (Salvi et al. 2007; Ursini, Maiorino, and Gregolin 1985). Activity assays have shown that peroxiredoxin enzymes have similar levels of activity, with k_{cat}/k_m on the order of 1×10^7 $M^{-1}s^{-1}$ (Ogusucu et al. 2007; Nelson et al. 2008). Due to their high abundance, it has been calculated that they react with almost all peroxide present in the cytosol of eukaryotes, (Winterbourn 2008) and around 90% of peroxide in the mitochondria (Cox, Winterbourn, and Hampton 2010).

1.4.3 Peroxiredoxins as chaperones

Certain peroxiredoxins have been investigated as chaperone proteins (Jang et al. 2004). Other small proteins with chaperone activity have been shown to have assembly properties

(Benesch et al. 2008), and peroxiredoxins have been hypothesised to be involved in the evolution of the chaperonin class of chaperones (Dekker, Willison, and Taylor 2011). An investigation into two very similar peroxiredoxins from yeast, cytosolic Prx 1 and Prx 2, found that oxidative stress and heat shock triggered both assembly into higher molecular weight structures (HMW) and an increase in chaperone activity, with a decrease in peroxide reducing ability (Yang et al. 2002). A crystal structure of a peroxiredoxin in its HMW form has been published, and is formed by two stacked decameric rings (Saccoccia et al. 2012).

A study of mammalian Prx1 and Prx2 showed that the Prx1 had higher chaperone activity, while Prx2 had higher antioxidant activity, even though the enzymes are 91% homologous (Lee et al. 2007). They also showed differences in oligomeric state, with Prx1 favouring larger assemblies. This was found to be caused by a cysteine residue unrelated to the active site that could form disulfide bonds between proteins. Mutation of this residue reduced the chaperone activity of Prx1 as well as its preference for the formation of larger species.

1.4.4 Overoxidation and the floodgate model

Several eukaryotic peroxiredoxins show susceptibility to overoxidation peroxide (Figure 1.3) (Yang et al. 2002). Unusually, this appears to be a derived trait – only a few prokaryotic peroxiredoxins are susceptible (Pascual et al. 2010), although extremely high concentrations of peroxide can cause overoxidation in any peroxiredoxin (Parsonage et al. 2005). Moreover, overoxidation susceptibility is strongly conserved across eukaryotic species. This has led to a hypothesis that overoxidation has a functional explanation in hydrogen peroxide signalling (Wood, Poole, and Karplus 2003). It is known that hydrogen peroxide is used in eukaryotic cells as a signalling molecule, with diverse biological roles (Veal, Day, and Morgan 2007). These include the regulation of the mitogen activated protein kinase and nuclear factor κB, which are involved in apoptosis (Allen and Tresini 2000).

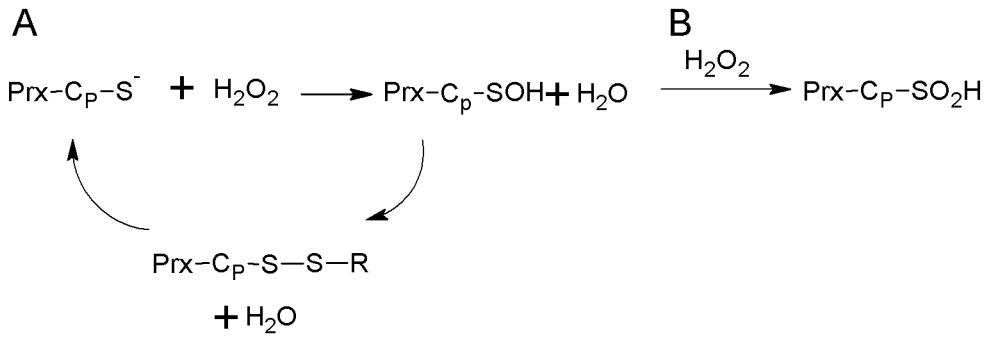

Figure 1.3 Overoxidation of peroxiredoxin. **(A)** The standard peroxiredoxin cycle. CP is the peroxidatic cysteine, Prx is peroxiredoxin, R is a thiol containing species. **(B)** Reaction of the cysteine sulfenic acid intermediate with hydrogen peroxide forms a cysteine sulfinic acid.

The floodgate model is a hypothesis that attempts to explain this (Wood, Poole, and Karplus 2003). In the model peroxide levels are kept low by the actions of peroxiredoxins, as well as the other antioxidant enzymes under normal conditions. However when hydrogen peroxide levels are increased in a signalling event, peroxiredoxins are quickly overoxidised and inactivated. The normal, low flux of hydrogen peroxide produced by cell metabolism is prevented from activating hydrogen peroxide regulated pathways. This may explain the upregulation of peroxiredoxins in certain cancers – an increase in hydrogen peroxide would not overoxidise enough peroxiredoxins to activate the pro-apoptotic signal (Wood, Poole, and Karplus 2003; Cao, Bhella, and Lindsay 2007).

The floodgate model was strengthened by the discovery that overoxidised peroxiredoxin was rapidly reactiviated in the cytosol (Woo et al. 2003). This was found to be due to a protein called sulfiredoxin (Biteau, Labarre, and Toledano 2003), which reduces cysteine sulfinic acids at the cost of ATP.

There has been criticism of the floodgate model, however, as no evidence of overoxidised peroxiredoxin has been identified during peroxide mediated cell signalling (Cox, Winterbourn, and Hampton 2010).

1.5 The peroxiredoxin mechanism and active site

1.5.1 Peroxiredoxin substrate preference

Peroxiredoxins react primarily with hydrogen peroxide, which is mainly produced by side reactions of oxygen in the mitochondria (Boveris and Chance 1973). However, activity with

other peroxide species has been identified. Organic peroxides (ROOH) such as tBuOOH have been shown to react with certain peroxiredoxins (Cao, Bhella, and Lindsay 2007; Trujillo, Clippe, et al. 2007). Similar molecules are produced in organisms by the reaction of hydrogen peroxide with metabolites such as lipids and peptides. There is some evidence for peroxiredoxins reacting with these molecules *in vivo* (Cox, Winterbourn, and Hampton 2010). Another species that peroxiredoxins have shown reactivity towards is peroxynitrite ($ONOO^-$) (Manta et al. 2009; Bryk, Griffin, and Nathan 2000; Trujillo, Ferrer-Sueta, et al. 2007). Peroxinitrite is formed by the reaction of the signalling molecule nitrous oxide (NO) with either the superoxide radical anion (O_2^-) or hydrogen peroxide. It is highly reactive and capable of nitrating various organic molecules (Pacher, Beckman, and Liaudet 2007; Ferrer-Sueta and Radi 2009).

There appears to be variation between peroxiredoxins in substrate reactivity, with some being shown to prefer H_2O_2, while others react with peroxynitrite or organic peroxides (Bryk, Griffin, and Nathan 2000).

1.5.2 Peroxiredoxin active site

All peroxiredoxins have an active site architecture using four conserved amino acid residues (Figure 1.4A). These are the peroxidatic cysteine residue, also called C_P, a proline residue, a threonine residue (in some cases a serine) and an arginine residue (Chae et al. 1994). These are very strongly spatially conserved in an active site pocket, with all but the arginine located in a conserved motif: PXXXT(/S)XXC. The arginine residue is located in a distant part of the protein sequence (Hall et al. 2010).

The thiol group of the cysteine residue is thought to be deprotonated, in the thiolate form, which better allows a nucleophilic attack on peroxides (Alphey et al. 2000). While a standard cysteine thiol group has a pK_a near 8, the active cysteine in peroxiredoxins has been shown to a significantly lower pK_a, leading to a calculated 90% of C_P thiol deprotonated (Nelson et al. 2008; Hugo et al. 2009).

The thiolate form is stabilised primarily by the positively charged conserved arginine residue (Figure 1.4B), which is locked into orientation by nearby residues, usually a histidine or a glutamine residue (Hall et al. 2010; Karplus and Hall 2007). Furthermore, C_P is located near the N-terminus of an alpha helix, which has an overall dipole moment due to the alignment of hydrogen bonds within the helix (Hol, Duijnen, and Berendsen 1978). The N-terminus has a positive dipole, helping to stabilise the negatively charged thiolate. Structural alignment of numerous peroxiredoxin crystal structures including molecules bound in the active site

shows that the conserved threonine (or serine) accepts a hydrogen bond from the peroxide substrate. This draws electron density away from the peroxide oxygen, activating it for nucleophilic attack by C_P. The role of the conserved proline appears to be to block C_P from the surrounding solvent (Hall et al. 2010; Nelson et al. 2011).

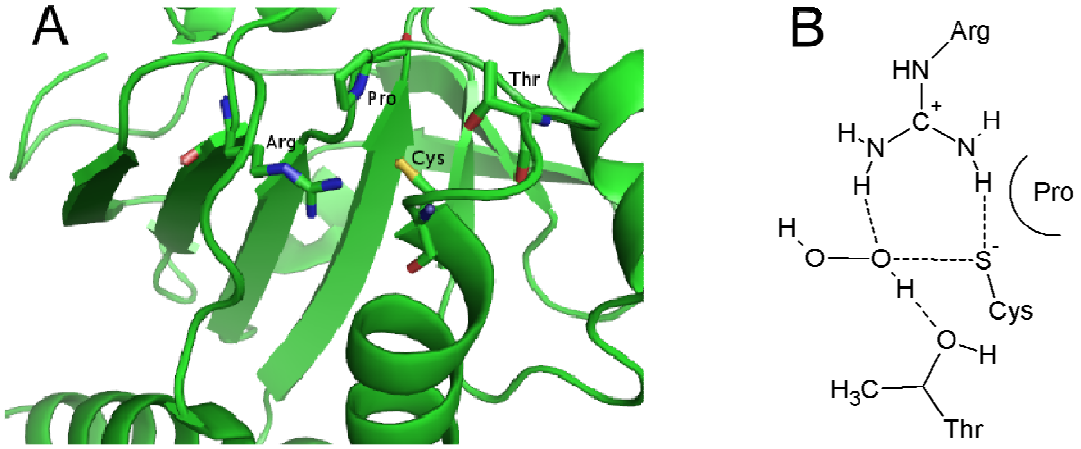

Figure 1.4: (A) The peroxiredoxin active site, the conserved Cys, Thr, Arg and Pro residues are labelled (from PDB file 1ZYE (Cao et al. 2005)). **(B)** Schematic representation of the active site with hydrogen peroxide bound. Hydrogen bonds are represented as dashed bonds.

1.5.3 Peroxiredoxin catalytic cycle

The peroxiredoxin catalytic cycle can be divided into three steps (Figure 1.2). These are: peroxidation – the reaction of C_P with peroxide to form an oxidised cysteine derivative called a cysteine sulfenic acid; resolution – the reaction of the cysteine sulfenic acid with another thiol to form a disulfide bond; and reduction – the regeneration of the initial thiolate form of C_P (Wood et al. 2002). The first step is identical in all peroxiredoxins, but the next two can be accomplished in a variety of ways, depending on the enzyme.

There are two ways in which the resolution step can occur. Most peroxiredoxins use a second cysteine residue located elsewhere in the amino acid sequence. These peroxiredoxins are termed 2-Cys Prx (Poole 2007). Many of these enzymes are dimers, and use a cysteine residue from the other subunit for resolution. The location of this residue in the protein sequence is generally conserved, and enzymes using this method of resolution are termed typical 2-Cys Prx. Other enzymes use a cysteine residue in the same peptide chain as the peroxidatic cysteine for resolution, and are termed atypical 2-Cys. The location of the resolving cysteine is not conserved across this group. The second way in which resolution can occur is through a mixed disulfide bond between the peroxidatic cysteine and another species, such as the thiol containing protein glutaredoxin (Pedrajas et al. 2010).

Peroxiredoxins that use this method of resolution are termed 1-Cys Prx. These differences are summarised in Figure 1.5.

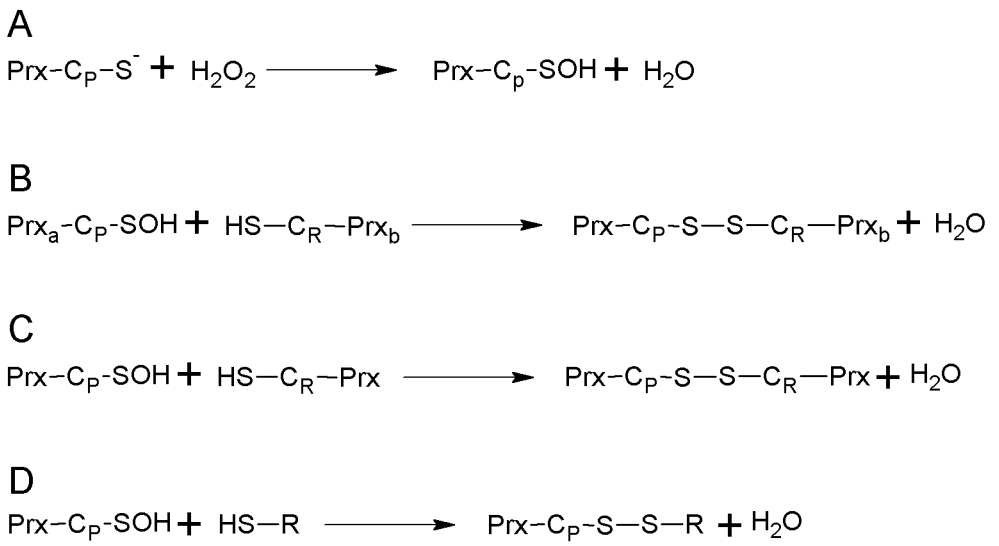

Figure 1.5: Differences in the resolution step between peroxiredoxins. **(A)** The peroxidation step shared by all peroxiredoxins. The peroxidatic cysteine reacts with hydrogen peroxide to form a cysteine sulfenic acid. C_P is the peroxidatic cysteine, Prx is the peroxidatic cysteine. **(B)** The resolution step in typical 2-Cys Prx. The cysteine sulfenic acid from one subunit reacts with the resolving cysteine from another subunit to form an intermolecular disulfide bond. Prx_a and Prx_b are two separate chains in a dimeric peroxiredoxin, C_R is the resolving cysteine. **(C)** The resolution step in atypical 2-Cys Prx. The cysteine sulfenic acid reacts with a resolving cysteine on the same chain to form a intramolecular disulfide bond. **(D)** The resolution step in 1-Cys Prx. The cysteine sulfenic acid reacts with a thiol containing species to form a mixed disulfide bond.

Reduction is accomplished by a variety of different enzymes, but reducing power is ultimately derived from NADPH or NADH (Poole 2005). This is achieved by forming an intermolecular disulfide with the oxidised peroxiredoxin, which is then reduced by the flavomolecule (Hofmann, Hecht, and Flohé 2005). In mammals, thioredoxin is used to reduce the peroxiredoxin. This effectively passes the oxidation onto thioredoxin, which is itself reduced by thioredoxin reductase (Cao, Bhella, and Lindsay 2007). AhpC proteins, which are a group of peroxiredoxins found in bacteria, use an enzyme called AhpF to reduce them, which combines the activities of thioredoxin and thioredoxin reductase (Poole et al. 2000). Some organisms use different systems – parasitic trypanosomatids use a unique peptide called trypanothione and an enzyme called tryparedoxin, which has some similarities to thioredoxin (Nogoceke et al. 1997).

1.5.4 Rate of reaction

Peroxiredoxins have generally be shown to have high rates of reaction similar magnitude to other peroxide reducing enzymes such as catalase (Schonbaum and Chance 1976). This is accomplished by the stabilisation of the transition state of the peroxidation step (1.5.3). Neither the starting materials (the cysteine thiolate and peroxide) or the products (the cysteine sulfenic acid and a hydroxyl anion) can form optimal hydrogen bonds in the active site (Hall et al. 2010).

1.6 Peroxiredoxin classes

The peroxiredoxin family of enzymes is large, and can be divided up into several groups. Peroxiredoxin naming is not consistent through the literature, especially in earlier research, when fewer examples were well studied. The first way that peroxiredoxins were categorised was by their mechanism of H_2O_2 reduction, specifically how they accomplish resolution of the cysteine sulfenic acid form. As described in 1.5.3, this gives three groups: typical 2-Cys, atypical 2-Cys and 1-Cys peroxiredoxins (Barranco-Medina, Lázaro, and Dietz 2009).

1.6.1 Sequence based divisions

Examination of sequences and crystal structures showed that the mechanism based divisions of peroxiredoxins do not accurately represent the evolutionary relationships within the family. Using sequence alignments, peroxiredoxins were divided into 6 groups (Karplus and Hall 2007; Hall et al. 2011). These do not preserve the previous 1-Cys/2-Cys, typical/atypical divisions – many groups contain examples of multiple types, indicating that certain features have arisen multiple times in the course of the evolutionary history of these proteins.

AhpC-Prx1 is the best studied group and is named for two of the first peroxiredoxins investigated; the bacterial AhpC and the mammalian Prx1. This group is widely distributed, being found in archaea, bacteria and in every order of eukaryotes (Nelson et al. 2011). All AhpC-Prx1 peroxiredoxins are dimeric in their most basic form and use the typical 2-Cys mechanism (1.5.3) with the resolving cysteine located in a C-terminal extension. Some mammalian enzymes in this class show susceptibility to overoxidation in high concentrations of peroxide, which may be linked to cellular signalling (1.4.4). Many proteins in this group demonstrate intriguing self-assembly properties which are regulated by the redox state of the peroxidatic cysteine.

The **BCP-PrxQ** is a group found mainly in bacteria, though examples exist in plants and yeast. The name comes from bacterioferritin comigratory protein, a former name for peroxireodoxins, and the plant PrxQ. Many of these proteins are monomeric, though some dimeric forms have been identified (Nelson et al. 2011). This group contains proteins using both the atypical 2-Cys mechanism (D'Ambrosio et al. 2009) and the 1-Cys mechanism (Wakita et al. 2007).

Prx6 is a group that is closely related to the AhpC-Prx1 group and is named after human peroxiredoxin 6. They are found in bacteria and eukaryotes. Prx6 peroxiredoxins are dimeric, but mainly use the 1-Cys Prx mechanism, although some use the typical 2-Cys mechanism (Deponte and Becker 2005). Another dimeric group is the **Prx5** group, named after human Prx5. Found in bacteria and eukaryotes; the group mainly includes members that use the 1-Cys Prx mechanism, though others use the atypical 2-Cy Prx mechanism.

Two other groups exist; both contain very few known enzymes. The **Tpx** are named for thiol peroxidase, another former name for peroxiredoxins, and are found only in bacteria. They are dimeric and use the atypical 2-Cys Prx mechanism (Hall, Karplus, and Poole 2009). The **AhpE** peroxiredoxins are also dimeric, but use the 1-Cys Prx mechanism (Hugo et al. 2009). They are named for the first example of the group, which was discovered in *M. tuberculosis* (Li et al. 2005) and are found only in closely related bacteria.

1.7 Peroxiredoxin structure and assembly

1.7.1 Peroxiredoxin fold

All peroxiredoxins share a similar structure called the thioredoxin fold, an α/β fold which is also seen in several other proteins that catalyse disulfide related reactions, including thioredoxin and glutathione peroxidase (Schröder and Ponting 1998). The core of this fold consists of 7 β-strands, forming a 5 stranded β-sheet (β3 to β7) and a β-hairpin (β1 and β2). As there is some interaction between the sheet and the hairpin, it is sometimes referred to as a 7 stranded β-sheet. The sheet is antiparallel, and is surrounded by 5 α-helices (Figure 1.6A). The key reactive cysteine is located in the first turn of α2 (Figure 1.6B) (Choi et al. 1998). Peroxiredoxins have been characterised in which the basic fold with differing loop lengths, and extensions at both the N- and C-termini (Schröder and Ponting 1998).

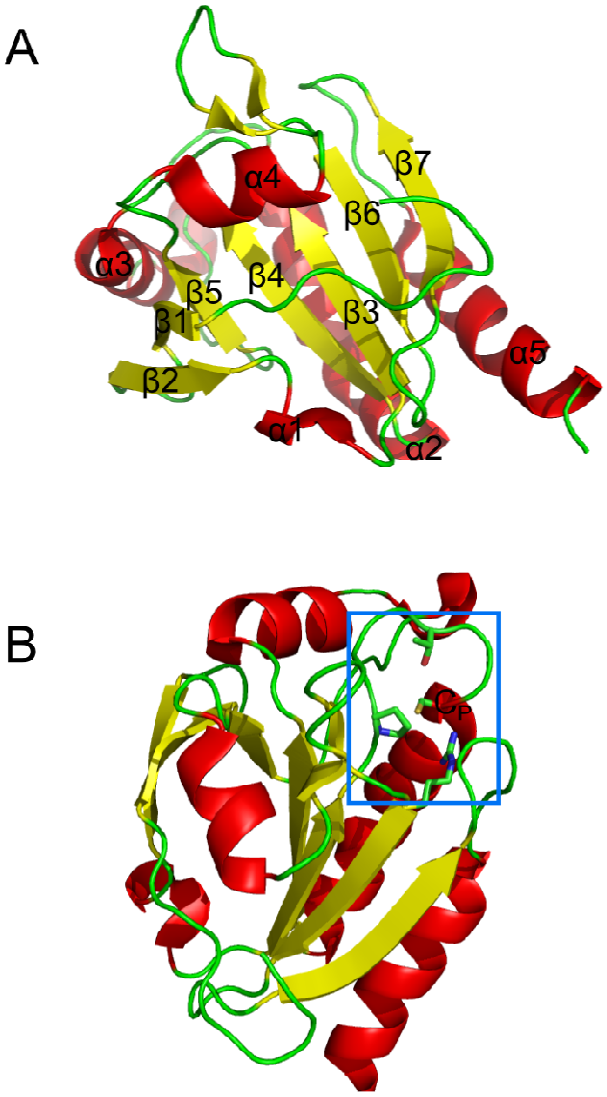

Figure 1.6: (A) The core structure of the peroxiredoxins, with secondary structural elements labelled. **(B)** Rotated image showing the location of the active site. The active site is highlighted in blue. The conserved active site residues are shown, and the peroxidatic cysteine is marked as C_P. β-strands are shown in yellow, α-helices are shown in red. Images were created from PDB file 1ZYE (Cao et al. 2005).

1.7.2 Dimer formation

Peroxiredoxins can form oligomers through two main interfaces. These are termed the A-type and B-type interfaces. The A-type interface (Figure 1.7A) involves four regions of contact between four regions of the protein, which have been termed regions I to IV (Figure 1.7B) (Wood et al. 2002). The main contributions to this interface are from the interaction between region I, which is the loop between β3 and α2, region II, which is α3. Region I borders on the active site of the enzyme, and is very important in the redox switching

behaviour seen in some peroxiredoxins (1.7.3). The A-type interface is more common across the peroxiredoxin family than the B-type interface, and shows considerable variation in the angle of the two groups (Sarma et al. 2005).

The B-type interface is formed through β7 in an antiparallel arrangement, creating an extended β-sheet across the subunits of the dimer (Figure 1.7C). Enzymes using this interface have a C-terminal extension that helps provide stability to the dimer (Karplus and Hall 2007). This interface is seen only in the AhpC-Prx1 and Prx6 groups, where it forms the basic unit of the protein in these families (1.6.1).

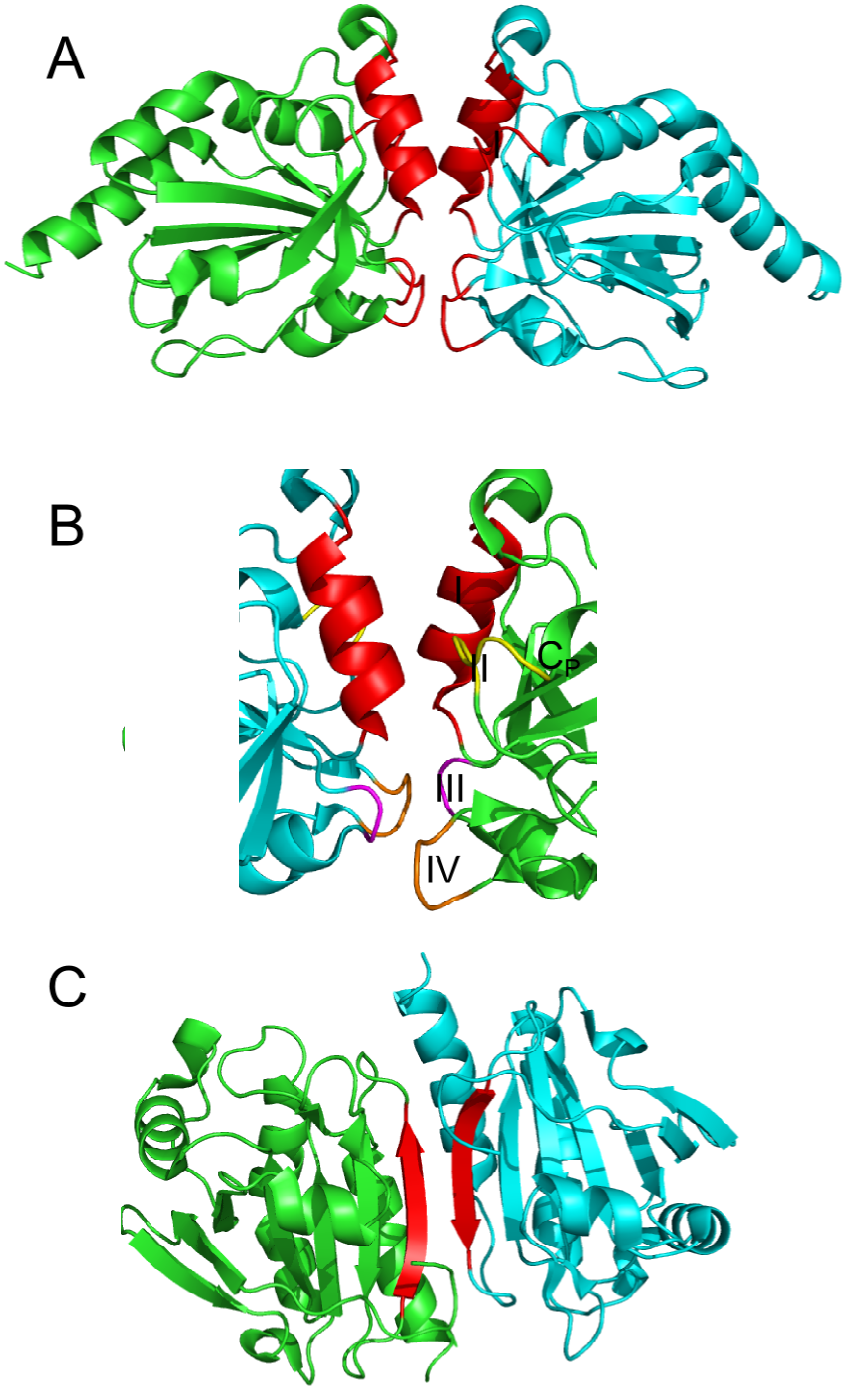

Figure 1.7: (A) The A-type interface. Interacting regions are shown in red. **(B)** The B-type interface. Interacting regions are shown in red. **(C)** The A-type interface. Region I is shown in red, region II is shown in yellow, region III is shown in magenta and region IV is shown in orange. Images were created from PDB file 1ZYE (Cao et al. 2005).

1.7.3 Assembly of larger species

Peroxiredoxins of the AhpC-Prx1 group have been shown to be able to form higher order species from dimers. Best known is the decameric form (Schröder et al. 2000), though octameric and dodecameric forms have also been identified (Figure 1.8A-C) (Li et al. 2005; Cao et al. 2005). These peroxiredoxins are B-type dimers, but use the A-type interface to assemble into ring shaped species that have been observed both by electron microscopy and X-ray crystallography.

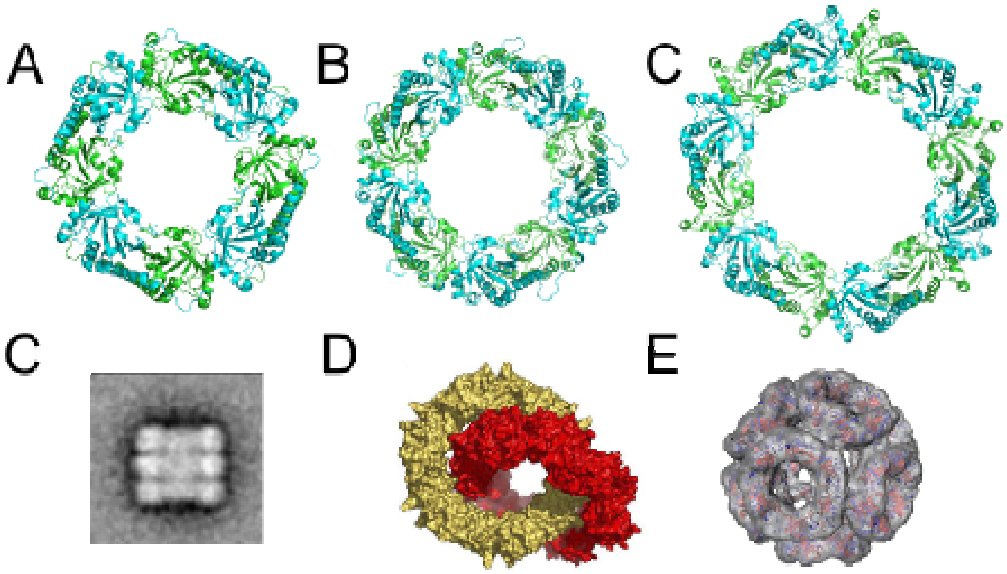

Figure 1.8: Oligomeric assemblies in peroxiredoxins. **(A)** An octomeric peroxiredoxin ring (PDB code 2H01, unpublished). **(B)** Decameric peroxiredoxin ring (PDB code 1N8J, (Wood, Poole, and Karplus 2003)). **(C)** Dodecameric peroxiredoxin ring (PDB code 1ZYE, (Cao et al. 2005)). **(D)** Stack of three dodecameric rings. Image from (Gourlay et al. 2003). **(D)** Catenane of dodecamers. Image was taken from (Cao et al. 2005). **(E)** Dodecahedron formed from decamers. Image from (Meissner et al. 2007).

In several studies, a wide range of even larger structures have been identified that are assembled from ring shaped species (Figure 1.8C-E). The most common form seen is a stack of rings. These have been identified by transition electron microscopy (TEM), and may be anything from a pair of rings (Saccoccia et al. 2012), to a long tube built from as many as 60 rings stacked on top of each other (Gourlay et al. 2003). Other structures include a catenane formed of two interlocking dodecamers that was identified by X-ray crystallography (Cao et al. 2005), and a cage shape dodecahedral structure made of 12 decamers, identified by TEM (Meissner et al. 2007). Finally, regular but less well defined structures termed ‘high

molecular weight complexes (HMW)' have been identified in certain peroxiredoxins in response to increased oxidative stress (Jang et al. 2004).

A recent X-ray structure has identified the interface giving rise to stacked species, which was termed the R-interface (Saccoccia et al. 2012). This main interactions involved are thought to be electrostatic (Figure 1.9).

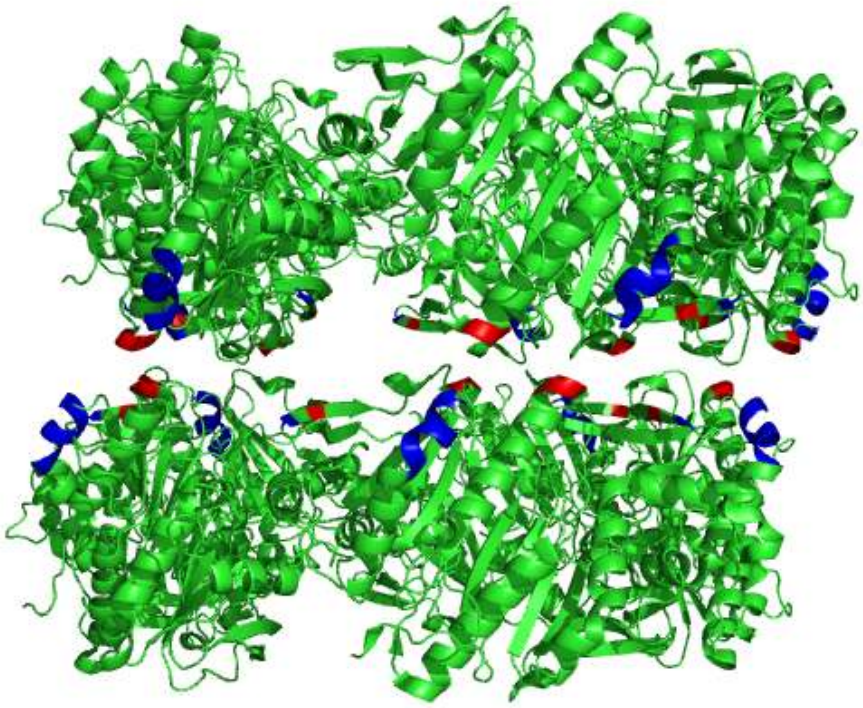

Figure 1.9: The proposed R- interface between decameric peroxiredoxin. Negatively charged regions are shown in blue, positively charged regions are shown in red. Image was created from PDB file 3ZTL (Saccoccia et al. 2012).

1.8 Control of AhpC-Prx1 self-assembly and protein dynamics

1.8.1 The redox switch

Several studies have investigated the conditions that favour self-assembly in peroxiredoxins that form higher order structures. A wide variety of factors have been implicated, including low pH, high or low ionic strength and increased protein concentration (Matsumura et al. 2008; Bernier-Villamor et al. 2004; Kitano et al. 1999). The most important factor, however, is the redox state of the peroxidatic cysteine, with the reduced, dithiol form favouring higher order species, and the oxidised, disulfide form favouring the dimer (Wood et al. 2002; Barranco-Medina et al. 2008).This was found to be caused by movements in the region of the protein containing the active site, a region termed the C_P loop.

In the reduced form, this forms the first turn of the helix α2 and is directly adjacent to region I of the A-type interface (Figure 1.10A). When the enzyme is oxidised to the cysteine sulfenic acid intermediate form, the C_P loop unfolds, allowing the resolving cysteine access to peroxidatic cysteine and the formation of the disulfide bond between them (Figure 1.10B) (Wood et al. 2002). However, this unfolding causes region I to shift, which destabilises the A-type interface and disrupts the formation of larger, ring shaped species (Poole 2007).

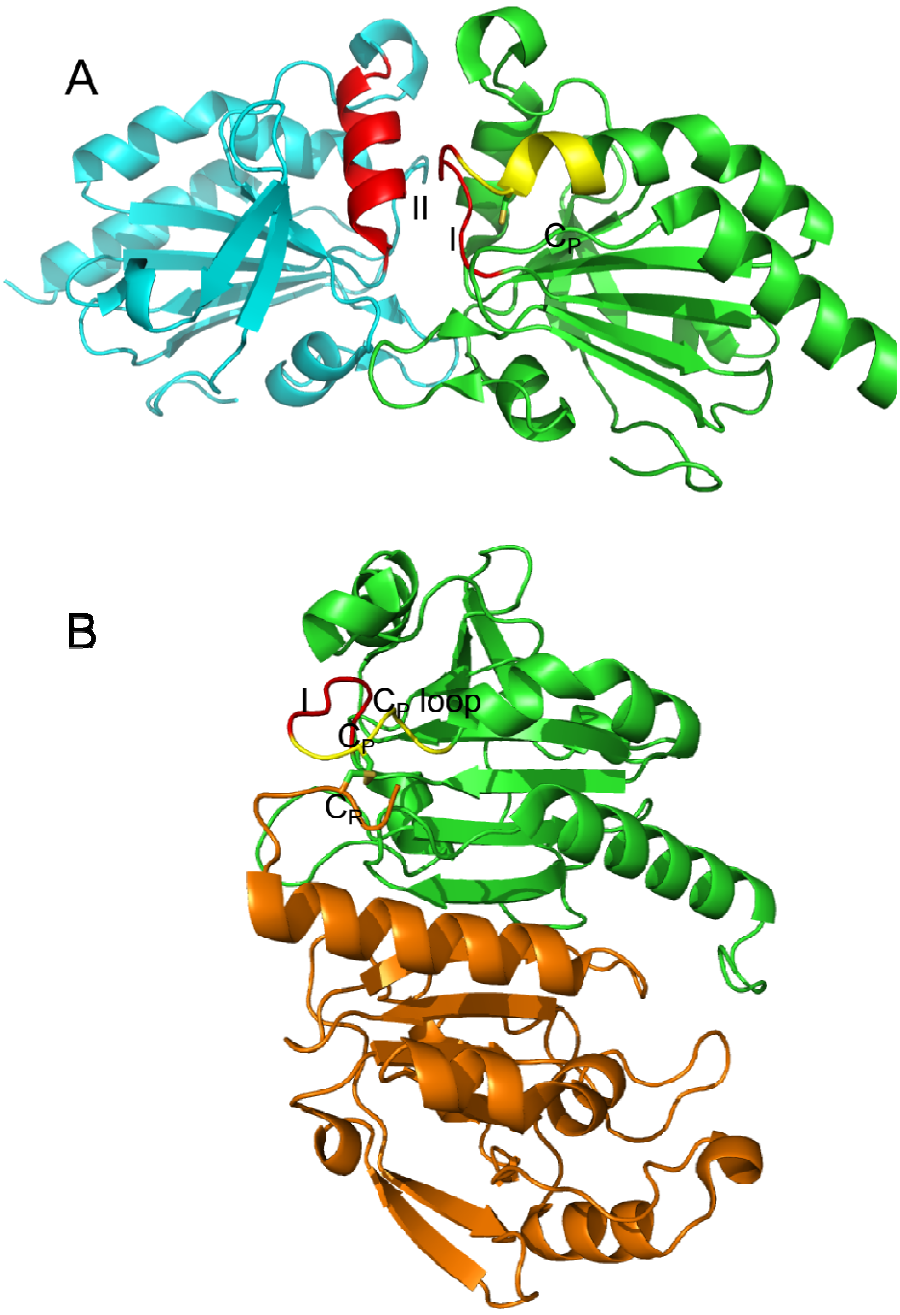

Figure 1.10: (A) The A-type interface and the C_P loop in the reduced form. The C_P loop is shown in yellow, region I and II interfaces are shown in red, the subunit across the A-type interface is shown in cyan. The peroxidatic cysteine is labelled C_P. (PDB code 1ZYE (Cao et al. 2005)). **(B)** The oxidised form. The C_P loop is shown in yellow, region I is shown in red, the subunit across the B-type interface that contributes C_R is shown in orange. The peroxidatic cysteine is labelled C_P, the resolving cysteine is labelled C_R. (PDB code 1QQ2 (Hirotsu et al. 1999))

1.8.2 Protein dynamics in the catalytic cycle of peroxiredoxins

When the peroxidatic cysteine reacts with its peroxide substrate, a local unfolding event occurs. This causes the C_P loop on helix α2 to unfold, exposing the cysteine sulfenic acid to the solution. This can be seen in all crystal structures of oxidised peroxiredoxins, and allows the resolving cysteine residue to approach the normally buried C_P (Karplus and Hall 2007).

In the typical 2-Cys mechanism, the two cysteine residues involved in the reaction mechanism are very distant from each other – as much as 14 Å. Moreover, the resolving cysteine (C_R) is buried within a subdomain formed by the C-terminal extension which these peroxiredoxins contain. In order to form the disulfide bond, further unfolding of the protein is necessary. After the formation of the cysteine sulfenic acid and the local unfolding that exposes it, the region containing C_R also unfolds, allowing it to reach across the dimer interface and react to form the disulfide form (Figure 1.10B) (Wood et al. 2002).

Local unfolding also plays a role in peroxiredoxins using the atypical 2-Cys Prx mechanism, though this has been investigated to a much lesser extent than those that use the typical 2-Cys mechanism. There is great variation in resolving cysteine location in proteins that use this mechanism, ranging from a few amino acids away from the peroxidatic cysteine (Liao et al. 2009) to distances close to those seen in peroxiredoxins using the 2-Cys Prx (Hall, Karplus, and Poole 2009). However, the oligomerisation of peroxiredoxins using the atypical 2-Cys mechanism is not affected by their redox conditions (Sarma et al. 2005; Hall, Karplus, and Poole 2009).

1.8.3 The link between activity and oligomerisation

The oligomeric state of AhpC-Prx1 family peroxiredoxins is strongly influenced by the redox state of the peroxidatic cysteine residue. As this residue changes its oxidation state as part of its catalytic cycle (Figure 1.2), it has been hypothesised that self-assembly of these are linked, and that the assembly of higher order species enhances the catalytic activity of peroxiredoxins (Barranco-Medina, Lázaro, and Dietz 2009). Mutations to residues in the A-type interface have been shown to influence activity in AhpC, with mutants where the decameric form was less favoured showing lower activity than the wild-type, and a mutant where the decamer form was favoured showed higher activity (Parsonage et al. 2005).

1.8.4 Overoxidation

Several mammalian peroxiredoxins show a susceptibility to inactivation by excess hydrogen peroxide (1.4.4). This is caused by the cysteine sulfenic acid intermediate form reacting with hydrogen peroxide and forming a cysteine sulfinic acid (Figure 1.3)

The basis for this is two conserved motifs that all overoxidation sensitive peroxiredoxins contain: Gly-Gly-Leu-Gly (GGLG) and Tyr-Phe (YF). GGLG is found between α3 and β5, and the YF motif is found in the C-terminal extension found in typical 2-Cys peroxiredoxins (Wood, Poole, and Karplus 2003). These are thought to make the local unfolding of the C_P loop less favourable, allowing for the cysteine sulfenic acid to persist long enough to react with a further molecule of peroxide (Sayed and Williams 2004). Truncation of the C-terminal extension has been shown to prevent overoxidation (Koo et al. 2002) and it has been hypothesised that lower mobility in the C-terminal tail also contributes to overoxidation, by slowing down the reaction of C_R with the cysteine sulfenic acid (Wood et al. 2002). As the C_R cannot react with the sulfinic acid to form, overoxidised peroxiredoxins favour a decameric form (Schröder et al. 2000).

1.9 Human Peroxiredoxin 3

Human peroxiredoxin 3 (hPrx3) is found in the mitochondria, where it is responsible for the reduction for the majority of hydrogen peroxide generated there (Cox, Winterbourn, and Hampton 2010). The other peroxiredoxin in the mitochondria is peroxiredoxin 5, which is a member of the Prx5 group (1.5.1) and uses the atypical 2-Cys Prx mechanism (Cao, Lindsay, and Isaacs 2007).

Peroxiredoxin 3 belongs to the AhpC-Prx1 group, and uses the typical 2-Cys Prx mechanism, as do all members of this group (Cao, Lindsay, and Isaacs 2007). It was first identified as MER 5 (Tohru et al. 1989) and was later termed SP-22 (Watabe et al. 1994) before being renamed hPrx3. It shows a similar level of activity to other peroxiredoxins, though tuned for the different pH conditions of the mitochondria (Cox et al. 2009). Like other mammalian AhpC-Prx1 peroxiredoxins, it contains the overoxidation motifs (1.8.4) and is susceptible to overoxidation, though to a slightly lesser extent than its closest relatives, human peroxiredoxins 1 and 2 (Cox, Winterbourn, and Hampton 2010). It also contains the residues proposed to allow the formation of stacked ring structures (Saccoccia et al. 2012).

While little research has been carried out on the structure of human peroxiredoxin 3, the very similar bovine homolog has been examined by electron microscopy and X-ray

crystallography (Gourlay et al. 2003; Cao et al. 2005). These studies revealed that the protein formed ring shaped species, as well as stacks of two or three rings. Moreover, in a mutant replacing the active cysteine with a serine, long tubes of up to 60 rings were observed (Gourlay et al. 2003). A crystal structure of the bovine homolog has been published (Cao et al. 2005). This shows the protein forms a dodecameric ring (it was previously thought to be decameric), and also reveals a unique catenane arrangement, where two dodecameric rings interlock.

1.10 Summary and project overview

Peroxiredoxins are an enzyme family that use a conserved cysteine residue to reduce peroxides. Many display self-assembly that is strongly influenced by the redox state of the active site cysteine. This regulated self-assembly property makes it attractive as a model system to investigate how engineering of the protein can be used to influence self-assembly.

Human peroxiredoxin 3 was selected for study as it demonstrates a wide variety of the unique oligomeric properties of peroxiredoxins. As an AhpC-Prx1 group peroxiredoxin, it shows self-assembly linked to the redox state of the enzyme active site. The closely related bovine Prx3 has been shown to form a wide range of higher order structures, including stacks, catenanes and tubes.

This thesis aimed to investigate the self-assembly of hPrx3, and to examine whether modifications to the sequence of the protein could be used to alter these self-assembly properties. This could be through altering the proportions of dimers and ring shaped species observed; or by altering the chemical and physical conditions where different forms were favoured.

There were also two secondary goals. First, to investigate whether any hPrx3 variants with altered self-assembly properties had altered enzymatic activity; and secondly, to investigate self-assembling thermophilic peroxiredoxins and identify any altered oligomeric properties they had compared to the wild type.

Chapter Two describes the overexpression and purification of 4 different forms of hPrx3. These are the wild type enzyme, the hPrx3 S78A mutant, His-tagged hPrx3 and His-tagged hPrx3 S78A. It then describes the methods used to determine the oligomeric size and shape of the species observed, as well as an assay to find the K_m/K_{cat} of each purified enzyme variant.

Chapter Three describes the identification of a potential peroxiredoxin enzyme in the genome of the thermophilic bacterium *Thermus aquaticus*, TaqPrx. The gene coding for it was cloned into a plasmid and the protein was overexpressed and purified. The size and oligomeric state of the protein was investigated. A novel assay was designed in order to identify any evidence for peroxide reducing activity in TaqPrx.

CHAPTER TWO

Results and Discussion (hPrx3)

Four forms of human peroxiredoxin 3 (hPrx3) were purified and analysed: wild type hPrx3; hPrx3 S78A, which contains a mutation in the A-type interface that forms ring shaped species such as decamers and dodecamers (1.7.3); His-tagged wild type; and His-tagged hPrx3 S78A. His-tagged hPrx3 S78A showed poor solubility, so limited work was carried out on this variant. These proteins were examined to determine their quaternary structure under various conditions and to investigate which higher order species the proteins could form. Protein activity was also examined to investigate whether differences in oligomeric state correlated with changes in the activity of the enzyme.

The presence of N-terminal His-tags has previously been implicated in promoting oligomerisation in peroxiredoxins (Cao, Bhella, and Lindsay 2007). It was examined in order to further investigate its effects of peroxiredoxin self-assembly, and to investigate the mechanism for any effects on self-assembly observed.

The mutant hPrx3 S78A contains a substitution in the A-type interface, which is used in the formation decamers and dodecamers (1.7.3). A mutation similar to this, T77V, was studied in a bacterial peroxiredoxin, where it was found to promote higher order structures (Parsonage et al. 2005). hPrx3 S78A was examined to investigate whether this property would also be observed. S78 is located in region II in the A-interface (1.7.2), and is thought to form water mediated hydrogen bonds across the interface.

2.1 Purification

Protein was purified following a protocol based of (Gourlay et al. 2003), as described in 6.2. This was modified by adding a His-tag cleavage step using tobacco etch virus (TEV) protease when purifying wild type hPrx3 and hPrx3 S78A. An anion exchange step was also added, as small amounts of contaminants were detected in early purifications.

After incubation overnight, *Escherichia coli* (*E. coli*) BL21 cells were harvested by centrifugation and resuspended in buffer. A cell press was used to disrupt cell walls and cell debris was removed by centrifugation. Nickel affinity chromatography was used to separate

protein from the lysate. Protein was then dialysed and cleaved using TEV protease overnight. Cleaved protein was separated from His-tags, uncleaved protein and TEV protease using a second nickel affinity chromatography step, collecting protein that did not interact with the column. Finally, samples were dialysed and purified further using anion exchange chromatography, then dialysed into storage buffer.

For His-tagged hPrx3 and His-tagged hPrx3 S78A, the TEV protease cleavage step was omitted. Samples separated from the bacterial lysate by nickel affinity chromatography were dialysed and purified by anion exchange chromatography, then dialysed into buffer.

Purification efficiency was analysed using SDS-PAGE as described in 4.8.

2.1.1 Purification of wild type hPrx3 and S78A

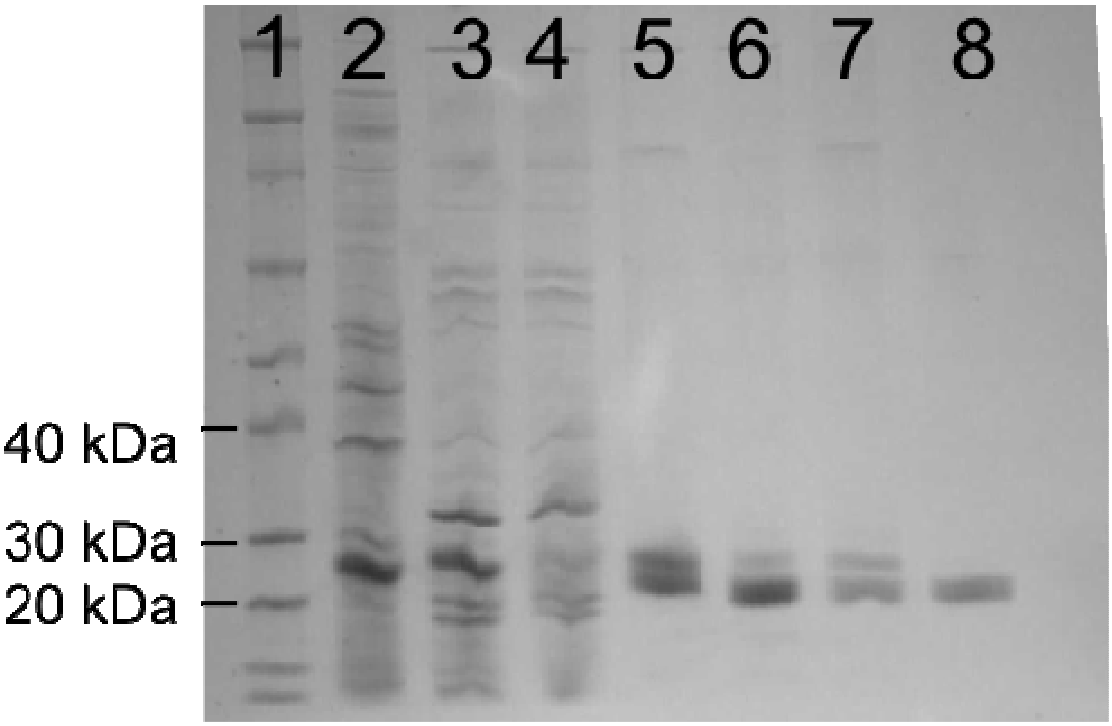

Figure 2.1: Purification of wild type hPrx3. **Lane 1:** Novex Sharp prestained protein standards. **Lane 2:** Bacterial lysate. **Lane 3:** Pellet from lysed bacteria. **Lane 4:** Nickel affinity column flowthrough. **Lane 5:**His-tagged hPrx3 after nickel affinity chromatography. **Lane 6:** His-tagged hPrx3 in TEV protease cleavage buffer. **Lane 7:** Uncleaved hPrx3, TEV protease and cleaved His-tags. **Lane 8:** hPrx3 after anion exchange chromatography.

The size of the band seen in Lane 8 is slightly larger than 20 kDa. This is consistent with the molecular mass of hPrx3, which is 22.0 kDa.

Both hPrx3 and hPrx3 S78A were purified using the same method. A representative SDS-PAGE gel is shown. For hPrx3, yields of up to 40 mg of protein per litre of culture were obtained. For hPrx3 S78A, yields of up to 25 mg of protein per litre of culture were obtained.

2.1.2 Purification of His-tagged hPrx3

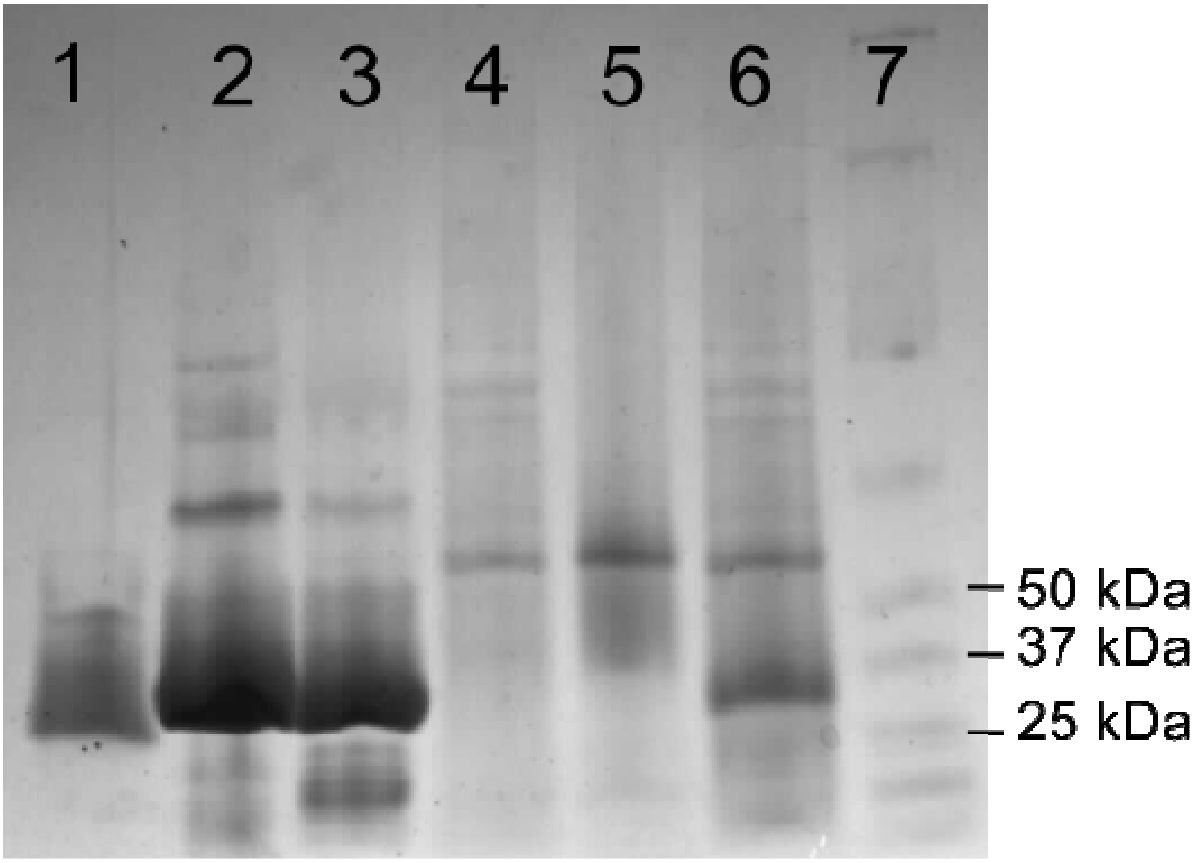

Figure 2.2: Purification of His-tagged hPrx3. **Lane1:** His-tagged hPrx3 after anion exchange chromatography. **Lane 2-3:** His-tagged hPrx3 after nickel affinity chromatography. **Lane 4:** Nickel affinity column flowthrough. **Lane 5:** Pellet from lysed bacteria. **Lane 6:** Bacterial lysate. **Lane 7:** Precision Plus Protein WesternC prestatined protein standards.

For His-tagged hPrx3, yields of up to 25 mg per litre of culture were obtained. In the final lane, a single band is present with a molecular mass of approximately 25 kDa, consistent with His-tagged hPrx3.

2.1.3 Purification of His-tagged hPrx3 S78A

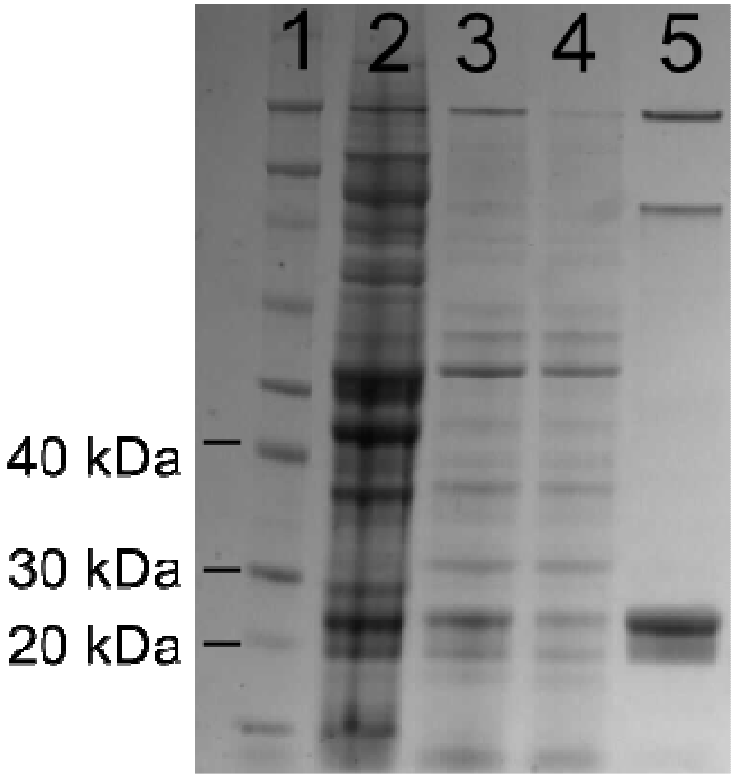

Figure 2.3: Purification of His-tagged hPrx3 S78A. **Lane 1:** Protein standards. **Lane 2:** Bacterial lysate. **Lane 3:** Pellet from lysed bacteria. **Lane 4:** Nickel affinity column flowthrough. **Lane 5:** Aggregated His-tagged hPrx3 S78A.

When His-tagged hPrx3 S78A was dialysed into low salt buffer in preparation of anion exchange chromatography, rapid aggregation was observed. The aggregated species has a mass of approximately 25 kDa, consistent with His-tagged hPrx3 S78A, which has a calculated molecular mass of 25.2 kDa.

2.2 Analysis of the quaternary structure of hPrx3

In order to examine the oligomeric state of hPrx3, methods to determine the molecular weight of species present under varying buffer conditions were necessary. Analytical size exclusion chromatography (SEC), which separates protein by their hydrodynamic radius using a column of gel beads, was employed to obtain an approximate molecular mass as described in 6.4.1. By comparing the volume of buffer required to elute the sample protein to a set of standards of known molecular mass, an estimate of the molecular weight of the species present can be obtained (Porath and Flodin 1959). However, SEC assumes that the protein of interest is of a similar shape to those used to make the calibration curve.

Moreover, larger species are more prone to error than smaller species, as the relationship between elution volume and hydrodynamic radius is logarithmic (Winzor 2003).

Despite these disadvantages, SEC offers the ability to screen a large range of different conditions, with few restrictions on buffer type. Additionally, the difference in mass between dimers and any higher order species present was expected to be large enough that meaningful results could be obtained despite the inherent limitation of the analytical method.

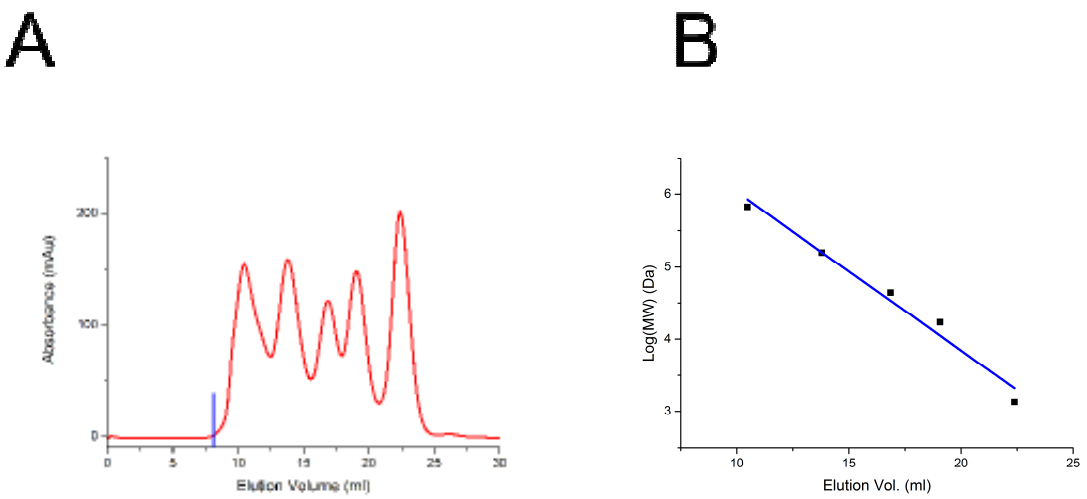

Figure 2.4: (A) Absorbance at 280 nm of Bio-Rad protein standards in 20 mM Tris, 150 mM NaCl, pH 7.5. Standards are, from left to right: Bovine thyroglobin (670 kDa); bovine γ-globulin (158 kDa); chicken ovalbumin (44 kDa); horse myoglobin (17 kDa); Vitamin B_{12} (1.35 kDa).The blue bar marks the void volume of the column, ~8 ml. **(B)** Calibration curve of protein standards.

Using the calibration curve, an equation to estimate the molecular mass of unknown samples can be derived.

$\log_{10}(MW) = -0.22(x) + 8.22$

Where *MW* is the molecular mass of the species in Daltons, and *x* is the elution volume in ml.

Several different SEC columns were used over the course of this thesis, each having slightly different volumes. When calculating masses, calibration curves appropriate to each column were used.

2.2.1 SEC analysis of hPrx3

Protein was examined in 20 mM Tris, 150 mM NaCl, pH 7.5 in both the presence and absence of DTT as a reductant. Tris was selected as it is capable of buffering between pH 7.5 and 9.0, so oligomeric state could be compared at both neutral and raised pH without altering buffer type. These peaks were then compared to the calibration curve in order to estimate their molecular mass. The calculated mass of the dimeric protein from the amino acid sequence is 44.1 kDa, while the decameric form is 220.5 kDa and the dodecameric form is 264.5 kDa.

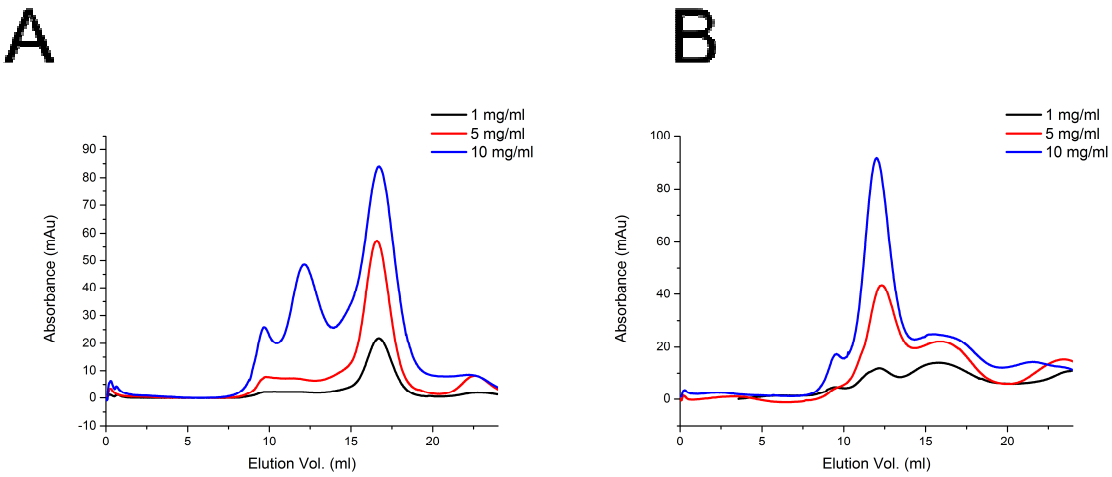

Figure 2.5: (A) Absorbance at 280 nm of hPrx3 in 20 mM Tris, 150 mM NaCl, pH 7.5. **(B)** Absorbance at 280 nm of hPrx3 in 20 mM Tris, 150 mM NaCl, 10 mM DTT, pH 7.5.

The trace for the protein in the presence of reductant shows an uneven baseline. This is due to the presence of DTT, which absorbs strongly at 280 nm.

For the protein in the absence of reductant, three peaks are present in the 10 mg/ml sample. The largest is close to, but not at the void volume. This corresponds to a species with a molecular mass of approximately 1 MDa. The second peak seen corresponds to a mass of approximately 390 kDa, while the third corresponds to a molecular mass of approximately 40 kDa. The 5 mg/ml and 1 mg/ml samples only show peaks corresponding to approximately 40 kDa.

For protein in the presence of reductant, two main peaks can also be seen, corresponding to species of similar size to those seen in the non-reduced sample. However, the peak corresponding to the larger species is significantly larger, and is present even at the lowest protein concentration measured.

The smaller of the two main peaks likely corresponds to the dimeric form of the protein, while the larger is probably a higher order structure such as a decamer or dodecamer. The increased levels of higher order species present in reduced conditions is consistent with previously reported results for peroxiredoxins, where reduction favoured higher order species (Wood et al. 2002). While the value calculated for the dimer is close to that seen in the size exclusion graph, the higher order species appears to be significantly larger. Although this may be due to the protein forming a species other than the ring shaped species reported in the literature, it is more likely to be due to the ring structure moving through the gel matrix at a different rate than would be predicted for more spherical protein.

Both conditions also showed a third, well defined peak at 10 mg/ml corresponding to an even larger species. While it is not possible to accurately determine the mass of such species using this technique, very large structures formed from peroxiredoxins have previously been reported (Jang et al. 2004).

Samples were also examined in 20 mM sodium phosphate (NaPi), 150 mM NaCl, pH 7.5 both in the presence and absence of reductant. NaPi is able to buffer at lower pH levels than Tris, and so was used to compare to samples examined in low pH conditions.

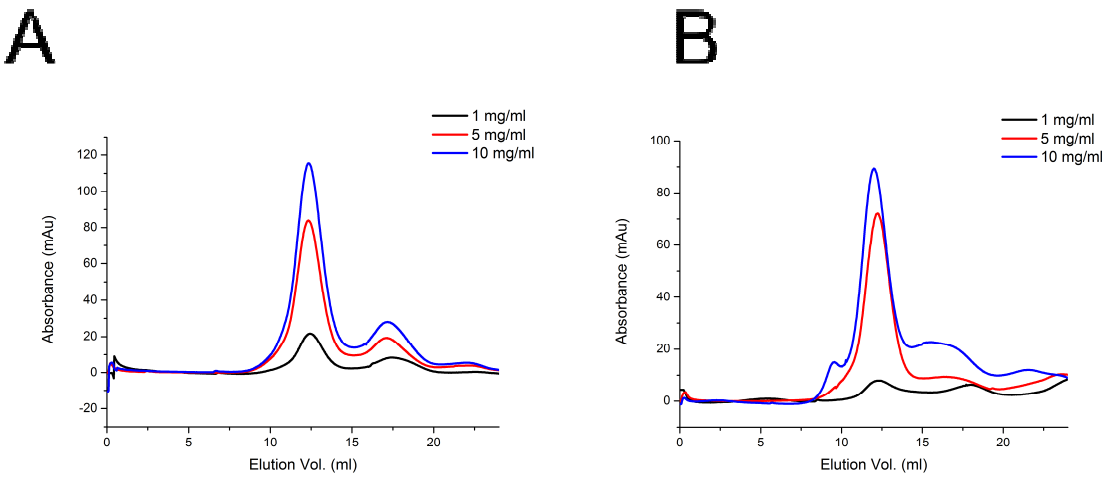

Figure 2.6: (A) Absorbance at 280 nm of hPrx3 in 20 mM NaPi, 150 mM NaCl, pH 7.5. **(B)** Absorbance at 280 nm of hPrx3 in 20 mM NaPi, 150 mM NaCl, 10 mM DTT, pH 7.5.

In the non-reduced conditions, two distinct peaks are present, at similar elution volumes to those seen for the protein in Tris at pH 7.5. These correspond to species with molecular masses of 390 kDa and 40 kDa. However, the ratio of species is different, with higher order species being favoured. This shows that buffer can have strong effects on the assembly of the protein into larger order structures.

In reduced conditions, two peaks are also present, with molecular weights of approximately 370 kDa and 40 kDa. These most likely correspond to dimeric and higher order forms of the protein. In the 10 mg/ml trace, evidence of an even larger species is present, similar to what was observed in Figure 2.5.

Samples were examined at increased pH levels, as the hPrx3 A-type interface (1.7.2) contains residues capable of forming hydrogen bonds, which could be strengthened or weakened by altering the pH.

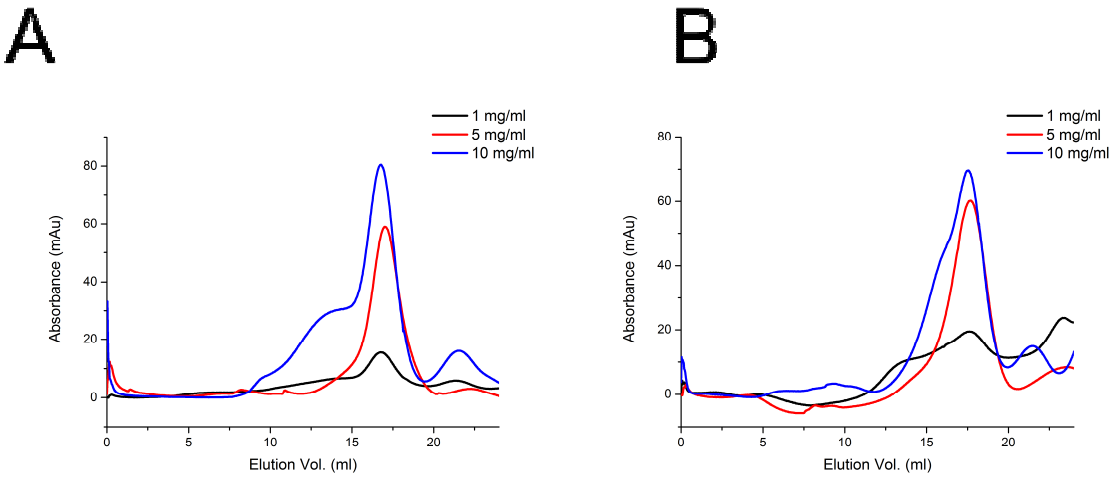

Figure 2.7: (A) Absorbance at 280 nm of hPrx3 in 20 mM Tris, 150 mM NaCl, pH 9.0. **(B)** Absorbance at 280 nm of hPrx3 in 20 mM Tris, 150 mM NaCl, 10 mM DTT, pH 9.0.

Under both conditions there is evidence of aggregation occurring in the 10 mg/ml samples, as peaks are not clearly defined and have broad shoulders. However, peaks were visible that corresponded to approximately 35 kDa, which would indicate that the dimeric form of the protein is favoured.

Higher pH favours the dimeric species, even in the presence of reductant. This may be due to the disruption of hydrogen bonds with in the A-type interface (1.7.2).

Samples were also examined at reduced pH, as the interface also contains His residues which, near pH 6.0, can become protonated and positively charged. The introduction of a charge in the interface could be disruptive to higher order species formation. At low pH, TCEP was used as the reductant instead of DTT as DTT is not able to act as a reductant below pH 7.

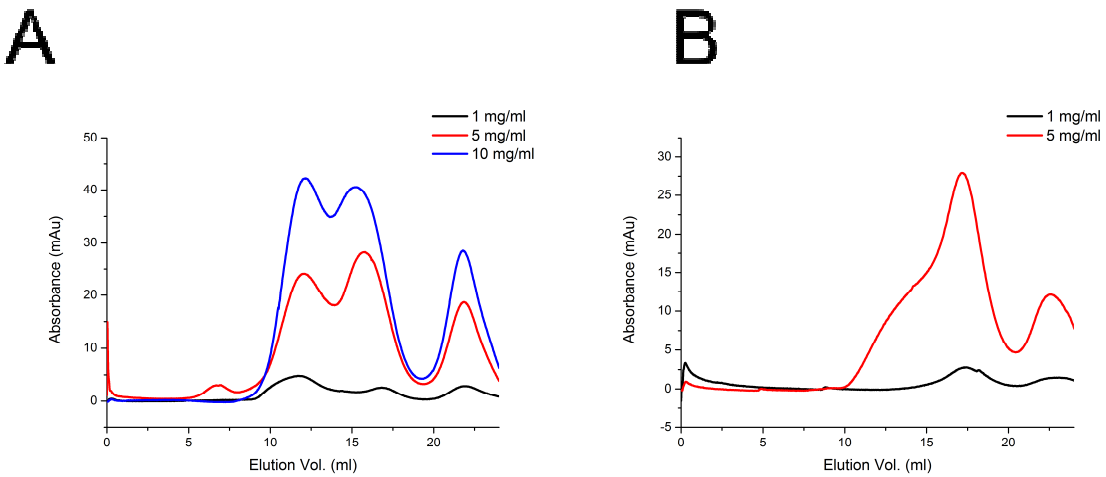

Figure 2.8: (A) Absorbance at 280 nm of hPrx3 in 20 mM NaPi, 150 mM NaCl, pH 6.0. **(B)** Absorbance at 280 nm of hPrx3 in 20 mM NaPi, 150 mM NaCl, 10 mM TCEP, pH 6.0.

In lowered pH, three peaks are visible. The first corresponds to a species with an approximate molecular mass of 390 kDa, while the second corresponds to a species with an approximate molecular mass of 50 kDa.

The third peak is near the column cutoff volume of 24 ml. The identity of this species is not clear, it is too small to be a protein, and is most likely a small molecule.

In the presence of reductant at pH 6.0, a high level of aggregation was apparent, with the protein visibly dropping out of solution at 10 mg/ml. For this reason, no data was collected for protein under these conditions. The peaks present correspond to species with molecular weights of approximately 40 kDa, indicating that the dimeric form may be favoured under these conditions.

Both pH 6.0 conditions show an increase in dimeric species compared to the protein in NaPi at pH 7.5 (Figure 2.6). This may be due to the protonation of a His residue present in the A-type interface, H76. Protonation of this residue would introduce a positive charge into the interface, which would destabilise assembly using this interface.

Across the samples examined, two main species are observed. The first is a high molecular mass species that is favoured by increased concentration, reductant and NaPi buffer. It is likely that this represents a ring shaped species, either a decamer or a dodecamer. It is not possible to accurately between these species using this technique, as their shapes means the elution volume observed will not correlate accurately with their molecular mass.

The second species observed has a low molecular mass, and is favoured in lower concentrations and at pH higher and lower than 7.5. This is likely the dimeric form of hPrx3. The more globular shape of the dimeric form of hPrx3 means that the values calculated for this species will be more accurate than for ring shaped species. The smaller species observed in wild type hPrx3 correspond to species with molecular masses of approximately 40 kDa, consistent with them being the dimer form of hPrx3.

2.2.2 SAXS analysis of wild type hPrx3

Small angle X-ray scattering (SAXS) is a powerful tool for investigating the three dimensional shape of proteins in solution. Samples are exposed to an X-ray beam, which is scattered by any particles present in the solution. The intensity of scattered X-rays and the angle at which they scatter yields information about the shape of the species that gave rise to them. As particles in solution have little long range order, accurate information can only be gained up to the nanometre range. Although SAXS cannot show the structure of a protein to atomic precision as X-ray crystallography can, it allows protein to be examined in solution and at relatively low concentrations, making it useful to compare to other experiments carried out in similar conditions (Mertens and Svergun 2010).

SAXS data can be analysed by various programs to derive the radius of gyration from the scattering data, and the molecular weight and dimensions of the species that produced the scattering pattern can be estimated (Konarev et al. 2006; Petoukhov et al. 2012).

As described in 6.5, SAXS data from hPrx3 was collected and analysed. SAXS measurement requires a homogenous sample to acquire useful data; as if multiple species are present, observed scattering will be derived from both species. Thus, samples were separated through a 3 ml gel filtration column before entering the X-ray beam. Scattering was collected from samples in 20 mM Tris, 150 mM NaCl at pH 7.5, as protein was known to be stable in these conditions, and contained a mixture of dimers and higher ordered species.

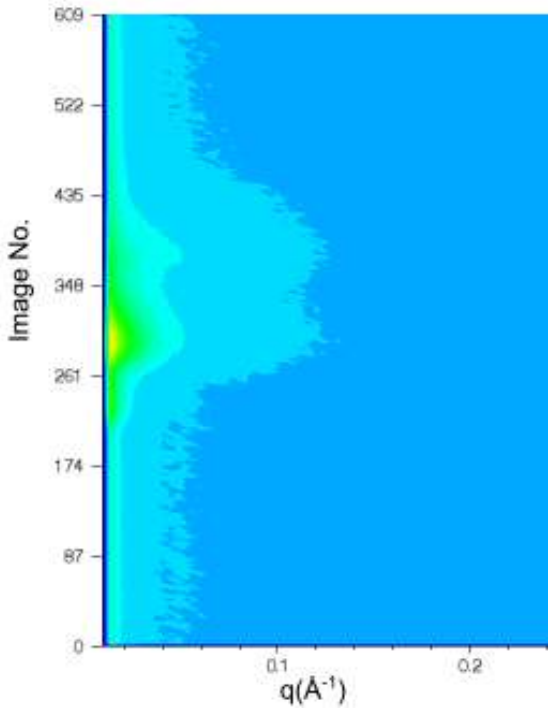

Figure 2.9: Contour graph showing the intensity of SAXS images of wild type hPrx3 collected after separation of species by gel filtration. Blue shows low intensity, while yellow shows high intensity. Image No. is the number of the scattering image used and is equivalent to the elution volume, while q is the scattering angle.

For the wild type enzyme, two species were detected. Images corresponding to each of these were averaged using the program Scatterbrain and used to calculate the properties of that species. For the first peak, frames 291-300 were used; for the second peak, frames 372-380 were used. Data collected were analysed using the program PRIMUS from the ATSAS package (Konarev et al. 2006).

Data corresponding to the two species observed were analysed in several ways. Guinier analysis was used to estimate the radius of gyration and evaluate the quality of the data by identifying if attractive interparticle effects were present (Mertens and Svergun 2010). The AutoPorod function of PRIMUS was used to calculate the Porod volume from the Guinier region of the data. This is used to estimate the maximum dimensions and molecular mass of the species present, as Porod volume is correlated to the molecular mass (Petoukhov et al. 2012).

GNOM analysis was used to calculate the distance distribution function, p(r). This gives an indication of the particle shape, as it shows the distribution of distances between points within the particle. It also gives a more accurate calculation of the radius of gyration than

Guinier analysis, as it uses all the scattering data rather than only the linear region (Mertens and Svergun 2010).

The program CRYSOL was used to compare the scattering observed to theoretical scattering calculated from the crystal structure of bovine Prx3 (PDB code 1 ZYE (Cao et al. 2005)). CRYSOL also calculated the theoretical radius of gyration of the crystal structure (Svergun, Barberato, and Koch 1995).

The results of these analyses are summarised in Table 1.

	Guinier		**GNOM**		**AutoPorod**	
	R_g	**Error**	**R_g**	**Error**	**D_{MAX}**	**MW**
Peak 1	60.5	±1.39	60.29	±0.98	188	293
Peak 2	42.7	±1.58	43.98	±0.33	78	53.3

Table 2.1: Analysis of SAXS data for wild type hPrx3. Data analysis was carried out using the programs Scatterbrain and PRIMUS. R_g is radius of gyration in Å, Error is the standard error in the radius of gyration in Å, D_{MAX} is the maximum dimensions of the species in Å and MW is the molecular weight in kDa. Peak 1 is made from images 291-300, Peak 2 is made from images 372-380.

For peak 1, analysis of the data shows the presence of a species with a radius of gyration of approximately 60 Å. AutoPorod indicates a species with a molecular weight of 293 kDa, which would correspond to a species made up of 13.3 monomers of 22 kDa, suggesting that the protein may be dodecameric in structure. The calculated molecular weight means that the Porod volume is approximately 451 nm^3, as molecular mass is approximately 0.65 times the Porod volume. The D_{MAX} value of 188 Å is close to the maximum dimension of the crystal structure of dodecameric bovine peroxiredoxin, which is 150 Å.

Examination of the p(r) plot (Figure 2.10A) for peak 1 is consistent with the protein being present as a ring shaped species. There are fewer medium distances within the particle than short or long distances, consistent with a space in the centre of the particle.

CRYSOL was used to align the observed data of peak 1 with the theoretical scattering of bovine Prx3 from the crystal structure (Figure 2.10B). This showed a strong alignment, with a Chi-squared value of 0.930. This is strong evidence for the species observed being dodecameric in structure. CRYSOL also produced calculated radius of gyration and volume calculations from the crystal structure. The calculated radius of gyration was 54.58 Å, while

the calculated volume was 441 nm^3. This is close to that seen in peak 1. The radius of gyration calculated is somewhat smaller than that of the observed species, this is likely due to the fact that the crystal structure 1ZYE (Cao et al. 2005) does not include the last 32 amino acid residues of the protein sequence.

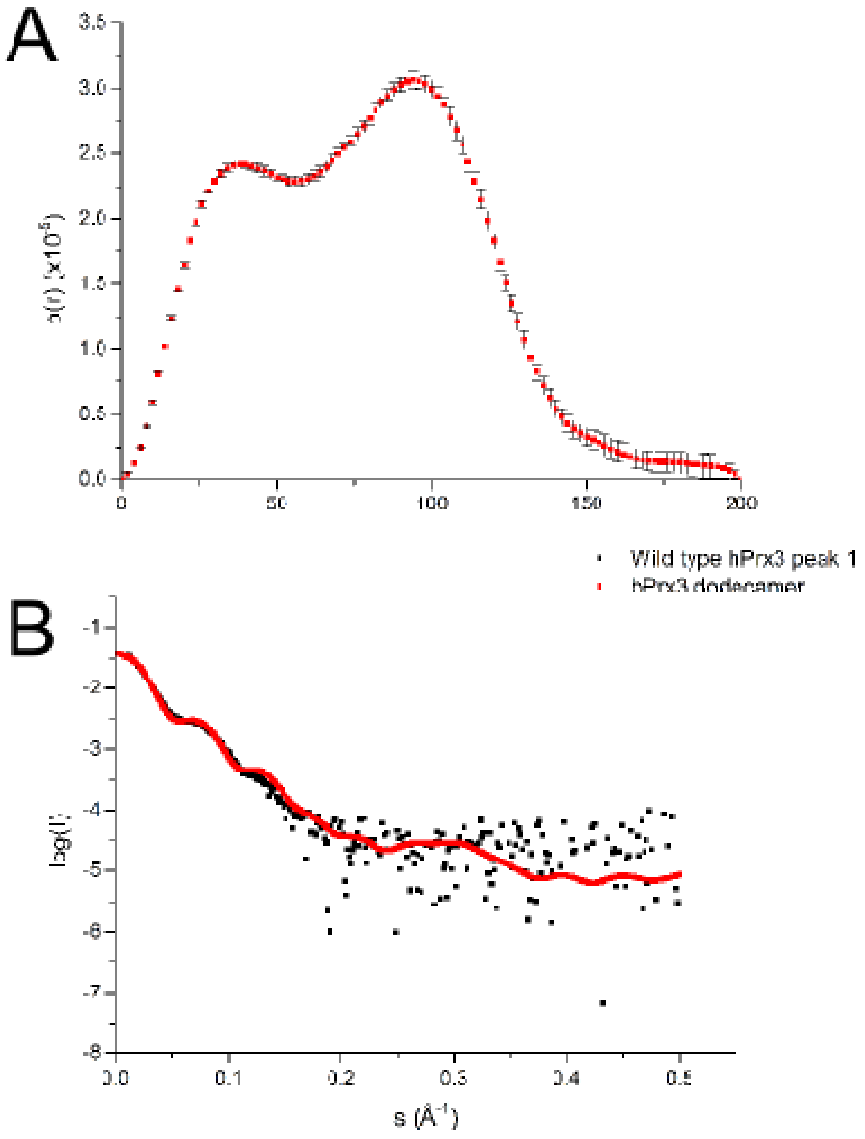

Figure 2.10: (A) p(r) plot of peak 1. Error bars are shown in black. **(B)** CRYSOL alignment of observed scattering of wild type hPrx3 peak 1 (black) and calculated scattering of dodecameric bovine Prx3. Chi-squared of the fit is 0.930. Log(I) is the log of the intensity of scattering observed, and s is the scattering angle in Å. Calculated scattering curves were generated from the PDB structure 1ZYE (Cao et al. 2005).

For peak 2, analysis of the data showed a species with a radius of gyration of approximately 43 Å. Guinier analysis showed evidence of self-association. Although this makes the data collected less reliable, it was expected as the dimer shows assembly to form the higher order species observed. AutoPorod indicates a species with a molecular weight of 53.3 kDa, which corresponds to 2.4 monomers of 22.0 kDa, suggesting that the species observed is dimeric. It also shows a Porod volume of approximately 120 nm^3. The D_{MAX} value of 78 Å is consistent with the species being a dimer, as the crystal structure of dimeric bovine peroxiredoxin shows a maximum dimension of approximately 67 Å.

Examination of the p(r) plot for peak 2 is consistent with the species being a dimeric peroxiredoxin (Figure 2.11A). Most distances are short, but a few longer, indicating an elongated structure.

The scattering observed in peak 2 aligned quite well with the calculated scattering of the dimeric form of bovine Prx3, with a Chi-squared value of 1.10 (Figure 2.11B). The observed data diverges at small angles, likely due to the self-association observed in the sample. The calculated radius of gyration of the dimer from the crystal structure is 20.3 Å, significantly smaller than what was observed for peak 2. The calculated volume was 50 nm^3, again much smaller than what was observed for peak 2. This may be due to the inaccuracies caused by the self-association of the species, or due to the species having a significantly different structure than seen in the crystal structure.

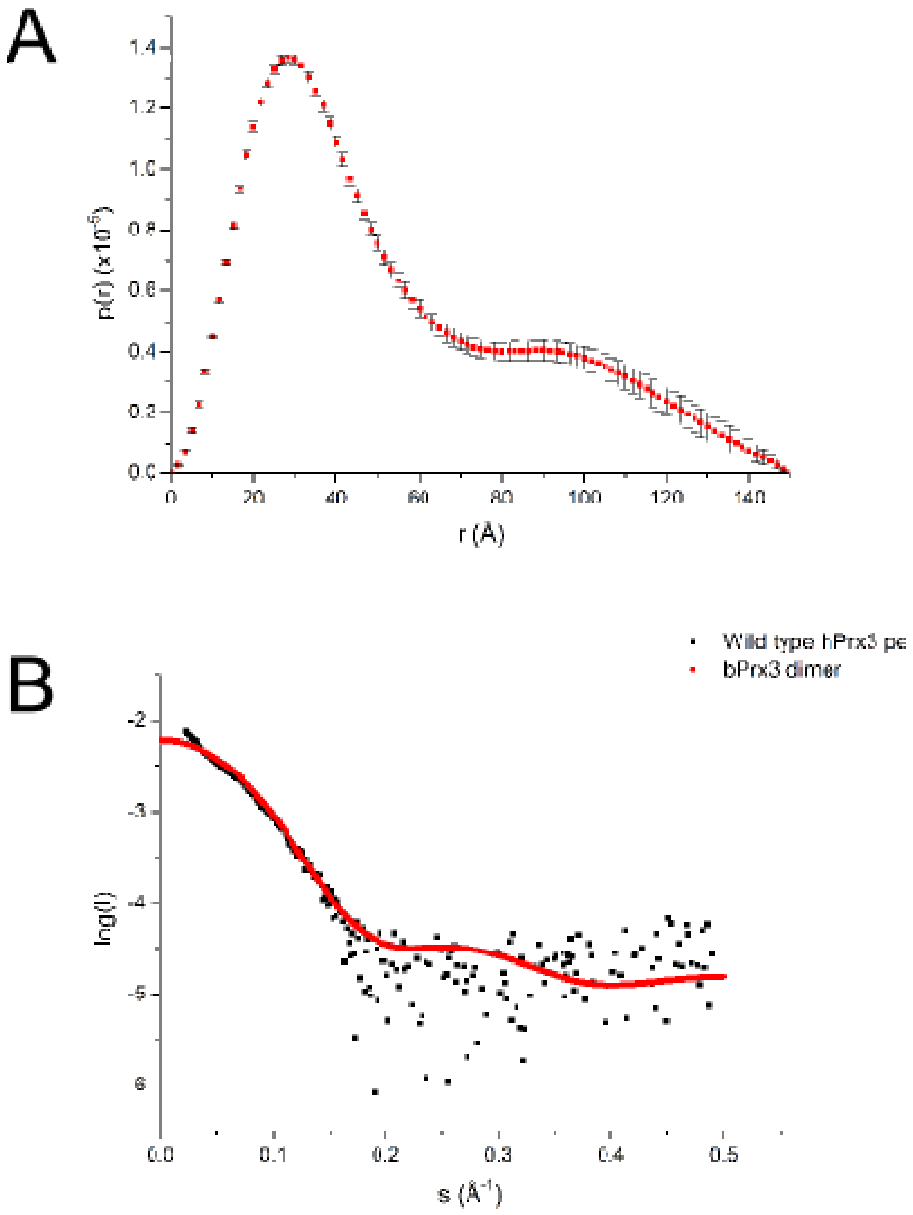

Figure 2.11: (A) p(r) plot of peak 2. Error bars are shown in black. **(B)** CRYSOL alignment of observed scattering of wild type hPrx3 peak 1 (black) and calculated scattering of dimeric bovine Prx3. Chi-squared of the fit is 1.10. Log(I) is the log of the intensity of scattering observed, and s is the scattering angle in Å. Calculated scattering curves were generated from the PDB structure 1ZYE (Cao et al. 2005).

2.2.3 TEM of wild type hPrx3

Electron microscopy provides the ability to directly observe the protein, allowing the accurate measurement of higher order structures, as well as the ability to observe species that may not be present in significant qualities to accurately characterise using other techniques.

As described in 6.3, samples of wild type hPrx3 were analysed by TEM after negative staining in order to directly image the species observed in SEC (2.2.1) and SAXS (2.2.2) and confirm that the higher order species were ring shaped dodecamers. Images were produced using a Morgagni 268D TEM, measuring at 100 kV by Dr Celine Valery. Images were captured images using a SIS/Olympus Megapixel III digital camera.

The TEM image clearly shows the presence of ring shaped structures in the sample. These structures have average external diameters of 140 Å and internal diameters of average 70 Å. This matches very closely to the size seen in the crystal structure of dodecameric bovine peroxiredoxin 3 (Cao et al. 2005), which shows a maximum external diameter of approximately 145 Å and an interior diameter of 70 Å.

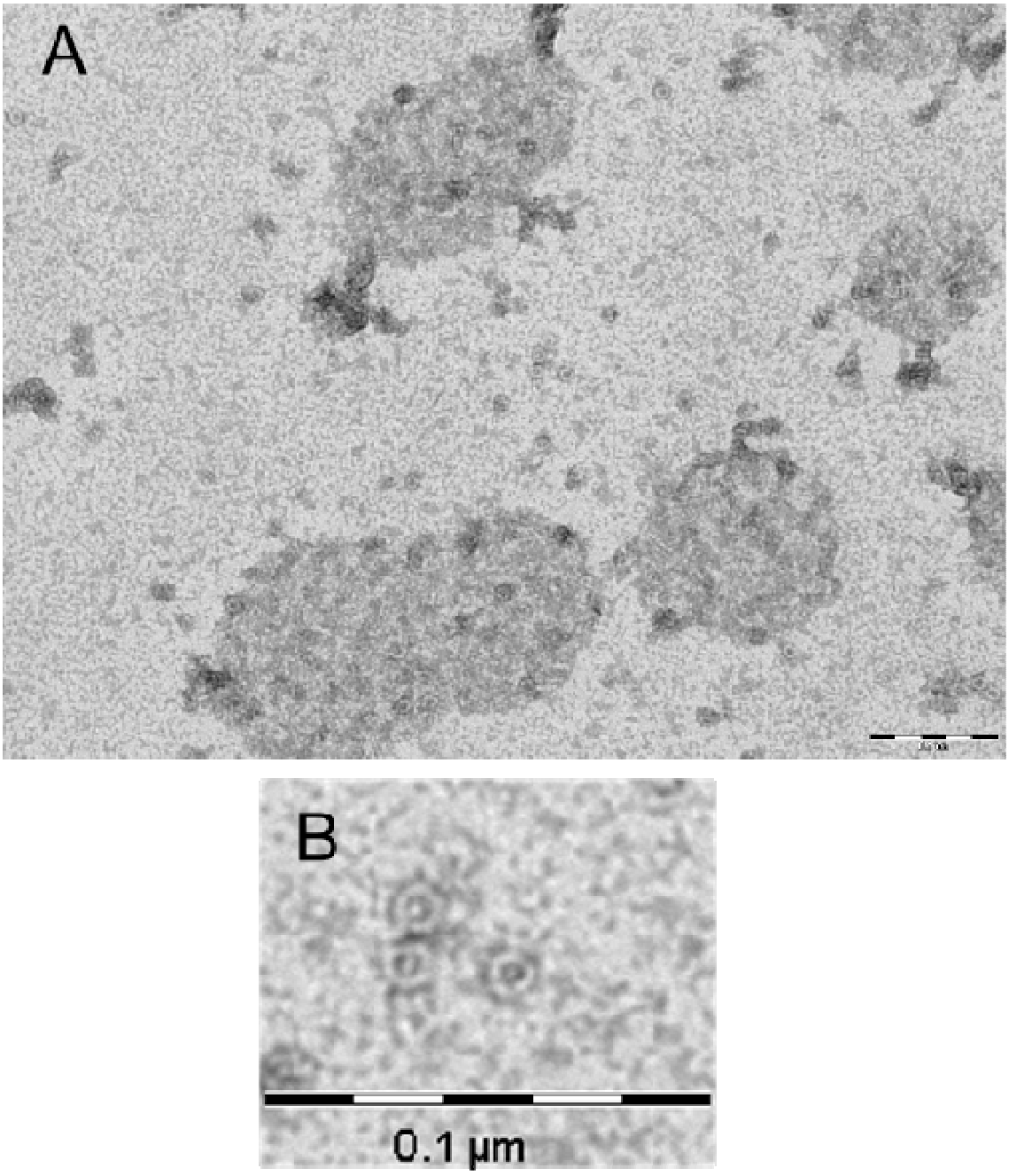

Figure 2.12: (A) Wild type hPrx3 at a concentration of 10 mg/ml in 20 mM Tris, 150 mM NaCl, 10 mM EDTA, pH 7.5. Samples are negatively stained using 1% Uranyl acetate. **(B)** Magnified view showing rings.

2.3 Analysis of the quaternary structure of hPrx3 S78A

An hPrx3 mutant was designed, hPrx3 S78A. This contains a residue substitution in the A-type interface, the interface used in building ring shaped structures. PISA analysis showed that S78 is likely to form a hydrogen bond across the interface, and previous research has indicated that a similar mutation in a bacterial peroxiredoxin favours assembly (Parsonage et al. 2005).

2.3.1 SEC Analysis of S78A mutant hPrx3

hPrx3 S78A was examined using SEC in the same conditions as the wild type enzyme (2.2.1). This protein has a calculated molecular mass of while the decameric form is 220.3 kDa and the dodecameric form is 264.3 kDa.

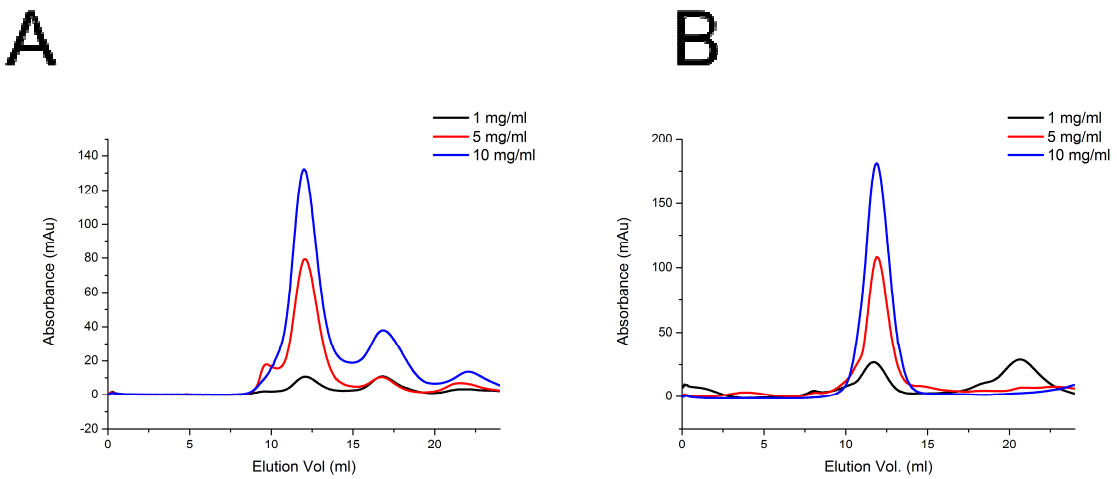

Figure 2.13: (A) Absorbance at 280 nm of S78A hPrx3 in 20 mM Tris, 150 mM NaCl, pH 7.5. **(B)** Absorbance at 280 nm of S78A hPrx3 in 20 mM Tris, 150 mM NaCl, 10 mM DTT, pH 7.5.

In the non-reduced sample, two main peaks can be seen. These correspond to species of approximately 390 kDa and 40 kDa. The proportions of species are different than that seen in the wild type enzyme, with more protein being seen in the higher order form, even at low concentrations.

In the reduced sample only one peak is visible, which corresponds to a species with an approximate molecular mass of 380 kDa.

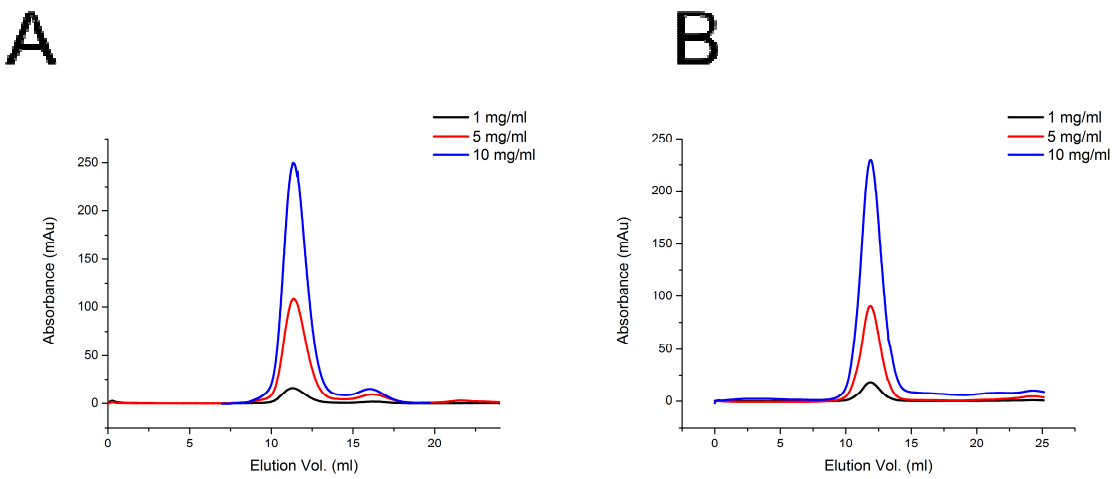

Figure 2.14: (A) Absorbance at 280 nm of S78A hPrx3 in 20 mM NaPi, 150 mM NaCl, pH 7.5. **(B)** Absorbance at 280 nm of S78A hPrx3 in 20 mM NaPi, 150 mM NaCl, 10 mM DTT, pH 7.5.

In the non-reduced sample, two peaks can be seen, a large peak corresponding to a higher order species of approximately 400 kDa, and a very small peak corresponding to approximately 50 kDa. Compared to the wild type in these conditions, hPrx3 S78A shows an increased proportion of the larger species, and a lower proportion of the smaller species.

In the reduced sample, only one peak can be seen, corresponding to the higher order species and having a molecular weight of approximately 380kDa. No evidence of any smaller species can be seen under these conditions, indicating that the higher order species, most likely a dodecamer, is very strongly favoured.

It was intended to analyse hPrx3 S78A at pH 9.0 in the presence and absence of reductant, however insufficient time was available to do so.

At pH 6.0, protein showed extensive aggregation, do no size exclusion analysis was carried out for protein under these conditions.

The species observed in hPrx3 S78A have similar masses to those seen in wild-type hPrx3 and are most likely the same forms of the protein, with the larger species being a ring shaped dodecamer, and the smaller being a dimer. This is as expected, as the mutant has a very similar molecular mass to the wild type. However, differences in proportions are apparent. hPrx3 S78A shows higher proportions of the larger species, consistent with the research carried out in the bacterial peroxiredoxin (Parsonage et al. 2005). The likely cause of this is that the serine residue formed a hydrogen bond to the solution in the wild type, and removing this removed an interaction favouring the dimeric form. As the mutation did not introduce any bulky or charged groups that could disrupt dodecamer formation, dodecamer

was favoured. There would also be a gain in stability for the dodecameric form due to the burial of the hydrophobic methyl group in the interface.

2.4 Analysis of the quaternary structure of His-tagged hPrx3

His-tagged hPrx3 was also purified and examined, to investigate whether the presence of N-terminal His-tags affected assembly, and whether this was linked to their metal ion binding abilities.

2.4.1 SEC Analysis of His-tagged hPrx3

His-tagged hPrx3 was examined using SEC in the same conditions as wild type hPrx3 (2.2.1). Calculation from the amino acid sequence gives a theoretical molecular mass of 50.4 kDa for the tagged dimer, 252.0 kDa for a decamer and 302.3 kDa for a dodecamer.

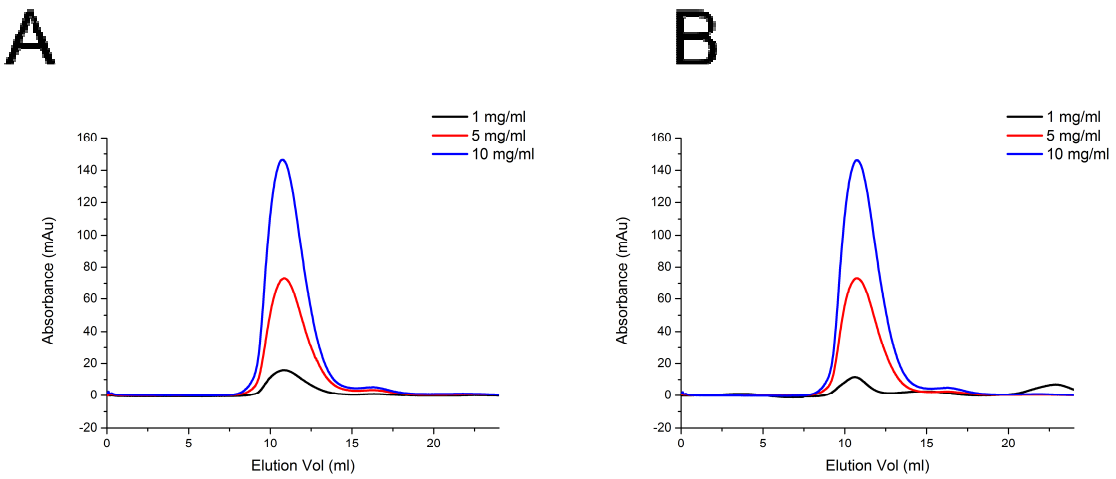

Figure 2.15: (A) Absorbance at 280 nm of His-tagged hPrx3 in 20 mM Tris, 150 mM NaCl, pH 7.5. **(B)** Absorbance at 280 nm of tagged hPrx3 in 20 mM Tris, 150 mM NaCl, 10 mM DTT, pH 7.5.

In non-reduced conditions, two peaks were observed. The first is very large and represents a species with an approximate molecular mass of 770 kDa, while the second peak shows a much smaller signal, and corresponds to a species with a molecular mass of 50 kDa. Compared to wild type hPrx3, a much higher proportion of the protein is present as large structures, indicating that the presence of His-tags strongly favour the formation of larger structures in these conditions. The size of the larger species is also much larger than what was seen in wild type hPrx. This may be due to the protein favouring a species even larger than a ring shaped dodecamer, such as a stack of multiple rings.

In reduced conditions, two peaks can be seen, with a higher proportion of the protein being present in the first peak. The peaks correspond to molecular mass of 650 kDa, while the smaller corresponded to 50 kDa.

Compared to the wild type enzyme, both conditions favour higher order species strongly, with almost no dimeric protein present.

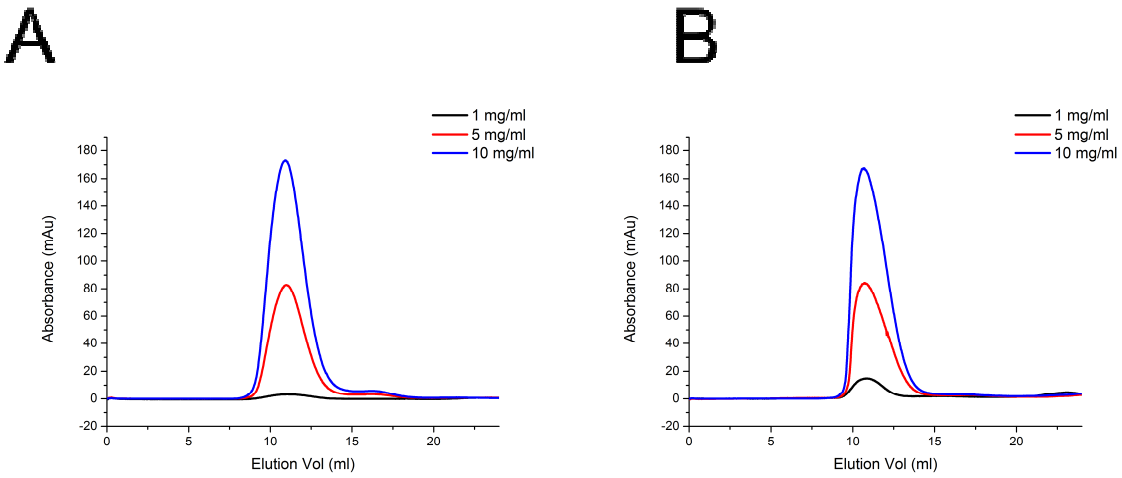

Figure 2.16: (A) Absorbance at 280 nm of tagged hPrx3 in 20 mM NaPi, 150 mM NaCl, pH 7.5. **(B)** Absorbance at 280 nm of tagged hPrx3 in 20 mM NaPi, 150 mM NaCl, 10 mM DTT, pH 7.5.

In the non-reduced sample, two peaks are again visible, with the majority of the protein being in higher order species with a molecular weight corresponding to approximately 670 kDa. The smaller peak corresponds to a molecular weight of approximately 50 kDa.

In the reduced sample, only one peak is present, with a molecular weight corresponding to approximately 750 kDa. Under these conditions, all protein is present in higher order species, even the lowest concentration measured.

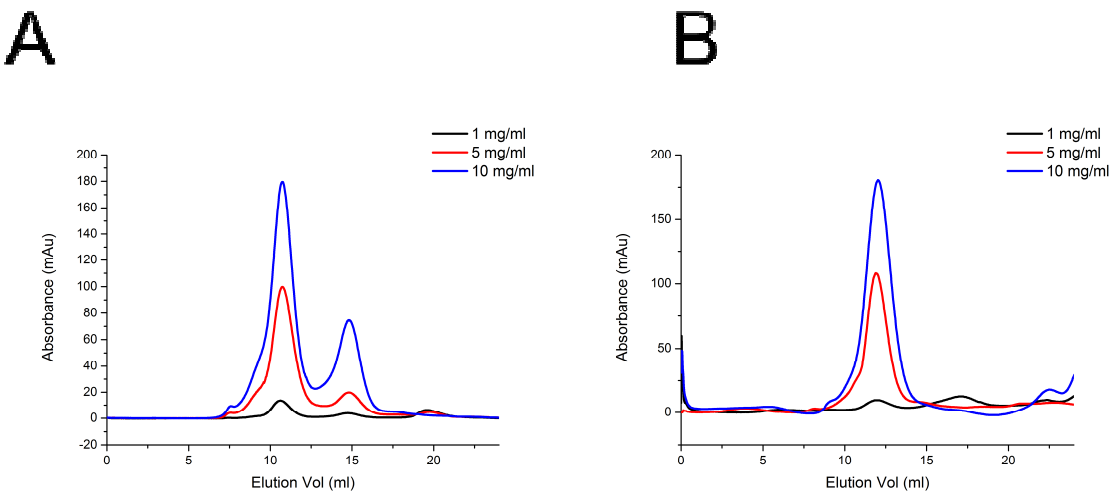

Figure 2.17: (A) Absorbance at 280 nm of tagged hPrx3 in 20 mM Tris, 150 mM NaCl, pH 9.0. **(B)** Absorbance at 280 nm of tagged hPrx3 in 20 mM Tris, 150 mM NaCl, 10 mM DTT, pH 9.0.

At elevated pH, two main peaks are visible, with the majority of protein in the higher order peak. These peaks correspond to species with approximate molecular weights of 780 kDa and 85 kDa. While the larger species has a similar estimated weight to the samples examined at pH 7.5, the smaller species seems too large for a dimeric protein. Its size makes a trimeric or tetrameric form seem more likely. A much higher proportion of the protein is present as the smaller species compared to His-tagged hPrx3 seen at neutral pH.

In reduced conditions, one main peak was visible. This corresponded to a molecular weight of approximately 395 kDa. In the 1 mg/ml trace, a second peak is also present, which corresponds to a molecular mass of approximately 40 kDa.

At pH 6.0, protein showed extensive aggregation, so no SEC analysis was carried out at this pH. The likely cause of this is that this is close to the isoelectric point of the protein, which was calculated to be pH 5.97 using the compute MW/pI tool from ExPASY (http://web.expasy.org/compute_pi/).

In the conditions examined, His-tagged hPrx3 showed two main species present. The larger species showed a wide variation in its mass, but tended to be larger than 650 kDa. The variation may be due to small errors in calibration, as in peaks close to the void volume such as these, small differences in elution volume can correspond to large changes in calculated mass. However, the data does indicate that very large species are present. It is not possible to accurately estimate whether they correspond to decamers, dodecamers or even larger higher order species. The smaller species seen, however, was generally calculated to have a mass near 50 kDa, consistent with it being the dimeric form of His-tagged hPrx3.

2.4.2 SAXS analysis of His-tagged hPrx3

SAXS data was collected from His-tagged hPrx3 to examine the size and shape of the species present.

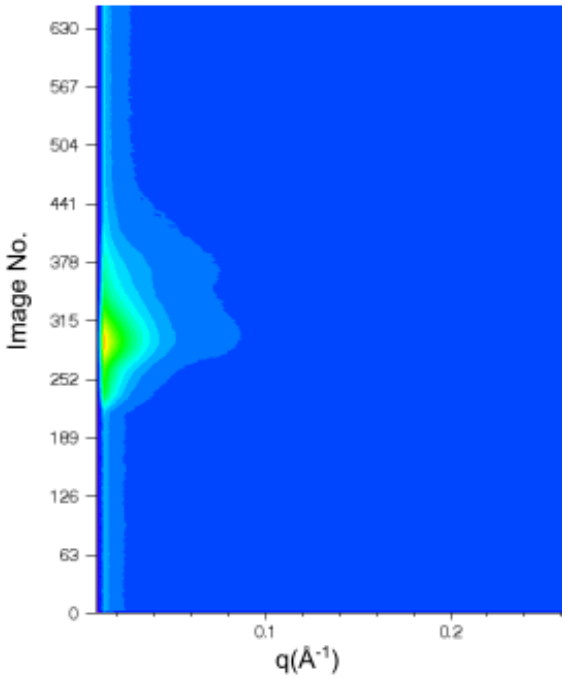

Figure 2.18: Contour graph intensity of SAXS images of His-tagged hPrx3 collected after separation of species by gel filtration. Blue shows low intensity, while yellow shows high intensity. Image No. is the number of the scattering image used and is equivalent to the elution volume, while q is the scattering angle.

Two peaks were observed for the His-tagged hPrx3 sample, however, the second did not provide enough useful data for analysis. The presence of two peaks, one corresponding to a much higher proportion of the protein in the sample, is consistent with the results of SEC (2.2.3). Images corresponding to the first peak (289-295) were averaged and used for analysis as in (2.3.1). The results are summarised in Table 2.

	Guinier		GNOM		AutoPorod	
	R_g	Error	R_g	Error	D_{MAX}	MW
Peak 1	60.8	±0.55	63.27	±0.78	212	424

Table 2: Analysis of SAXS data for His-tagged hPrx3. Peak 1 is made from frames 289-295. Data analysis was carried out using the programs Scatterbrain and PRIMUS. R_g is radius of gyration in Å, Error is the standard error in the radius of gyration in Å, D_{MAX} is the maximum dimensions of the species in Å and MW is the molecular weight in kDa.

Analysis of the data shows the presence of a species with a radius of gyration of approximately 62 Å. AutoPorod indicates a species with a molecular weight of 424 kDa, which would correspond to a species made up of 16.8 monomers of 25.2 kDa. The calculated molecular weight means the Porod volume is approximately 650 nm^3. The D_{MAX} value is 212 Å.

This data indicates that the overall size of the species observed is only slightly larger than the wild type hPrx3, however, the volume is significantly larger. This may indicate that the species observed is an assembly of multiple rings, such as a stack or a catenane.

Examination of the p(r) plot (Figure 2.19A) confirms that the structure is very different than that of wild type hPrx3. The distances seen are consistent with an ellipsoid or oblate structure (Mertens and Svergun 2010).

CRYSOL alignment of the observed data with theoretical scattering calculated from the bovine Prx3 also showed that the structure was very different from that of wild type hPrx3, as it did not closely match the calculated data, showing a Chi-squared value of 4.44 (Figure 2.19B). When compared to the catenane form, a slightly lower Chi-square value or 2.35 is seen (Figure 2.20). This may indicate that His-tagged hPrx3 is in a higher order form. It is not expected that the observed data match very closely with calculated data from the crystal structure, as His-tagged hPrx3 contains both the C-terminal region not present in the crystal structure and the additional His-tag, which increases the molecular mass per monomer by 8.5 kDa.

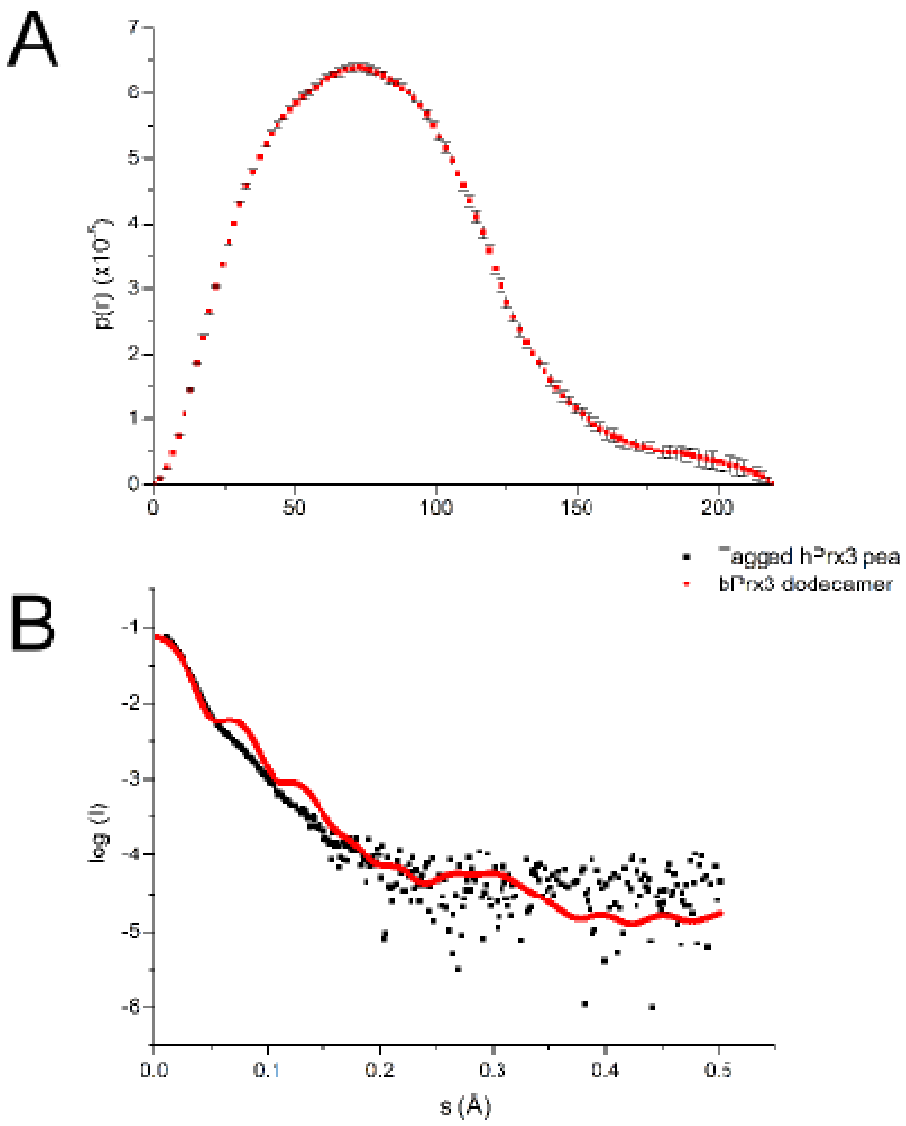

Figure 2.19: (A) p(r) plot of peak 1. Error bars are shown in black. **(B)** CRYSOL alignment of observed scattering of His-tagged hPrx3 peak 1 (black) and calculated scattering of dodecameric bovine Prx3. Chi-squared of the fit is 4.44. Log(I) is the log of the intensity of scattering observed, and s is the scattering angle in Å. Calculated scattering curves were generated from the PDB structure 1ZYE (Cao et al. 2005).

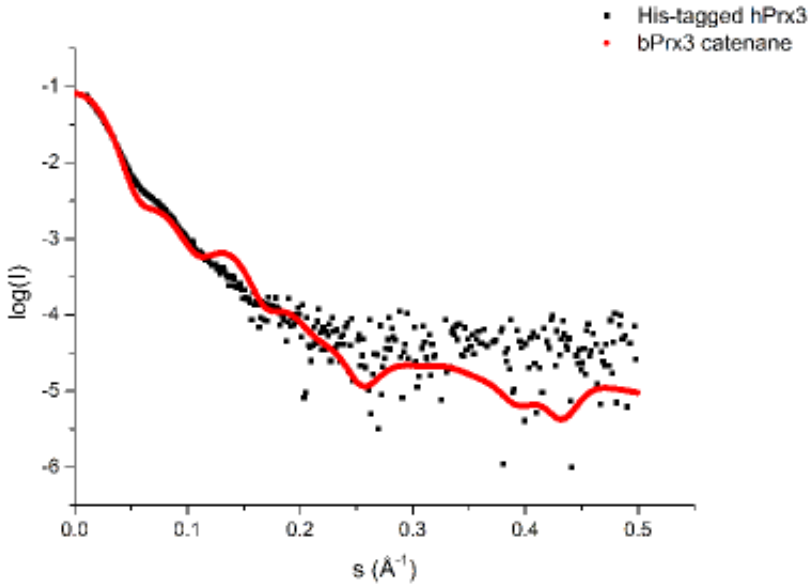

Figure 2.20: CRYSOL alignment of observed scattering of His-tagged hPrx3 peak 1 (black) and calculated scattering of bovine Prx3 catenane. Chi-squared of the fit is 2.35. Log(I) is the log of the intensity of scattering observed, and s is the scattering angle in Å. Calculated scattering curves were generated from the PDB structure 1ZYE (Cao et al. 2005).

2.4.3 TEM of His-tagged Prx3

As described in 6.3 TEM was used to investigate the structure of the higher order species observed by SEC (2.4.1), and to see if the shape of the species observed in SAXS (2.4.2) represented a higher order species. Images were produced Morgagni 268D TEM, measuring at 100 kV by Dr Celine Valery Images were captured using a SIS/Olympus Megapixel III digital camera.

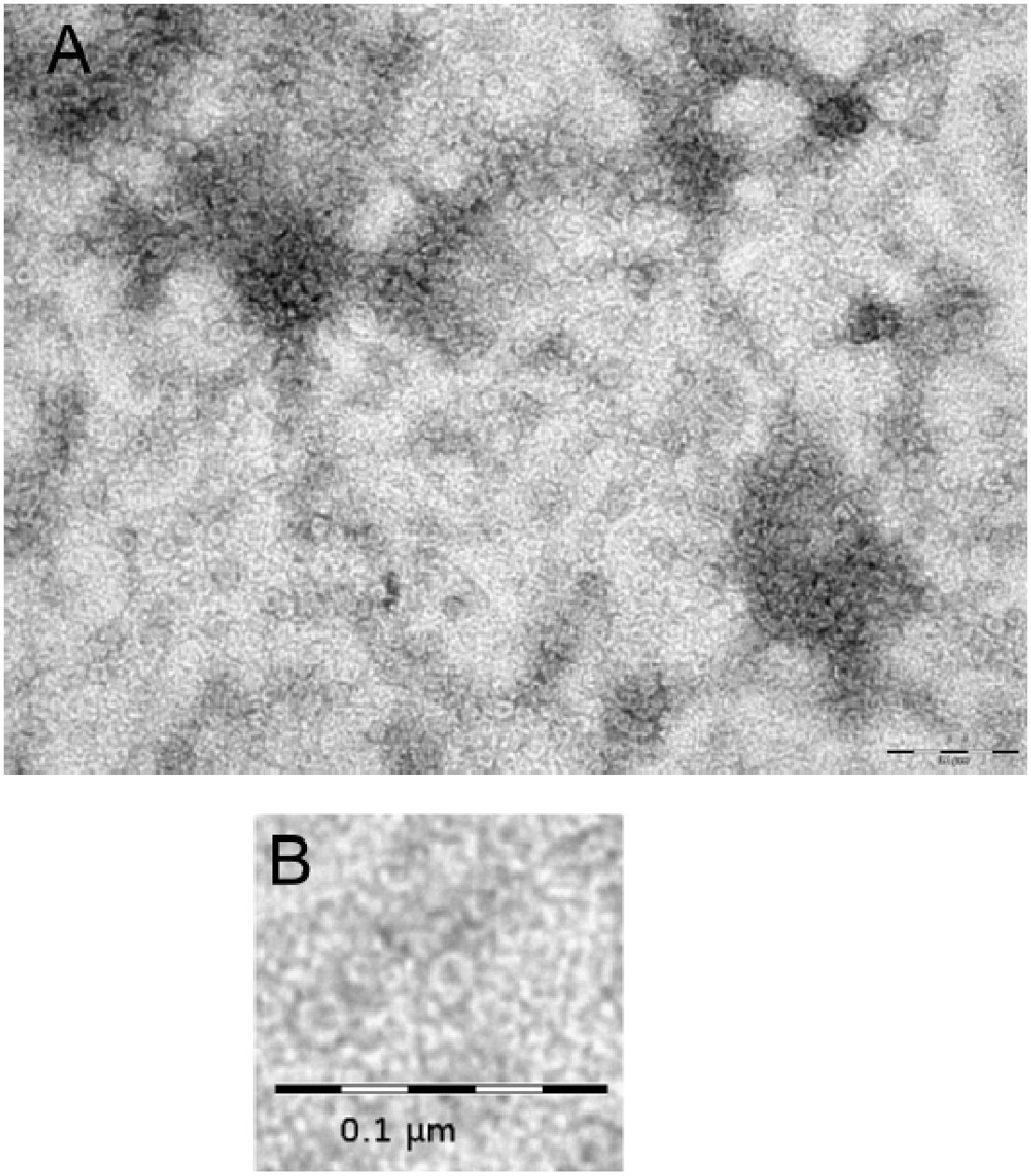

Figure 2.21: (A) His-tagged hPrx3 at a concentration of 10 mg/ml in 20 mM Tris, 150 mM NaCl, 10 mM EDTA, pH 7.5. Samples are negatively stained using 1% Uranyl acetate. **(B)** Magnified view showing rings.

The TEM image shows ring shaped species similar to those seen in wild type hPrx3 (2.2.3). These rings have an average external diameter of 140 Å, and an average internal diameter of 70 Å, the same as seen in the wild type enzyme. This indicates that the protein is most likely a dodecamer.

2.4.4 Effects of EDTA on His-tagged hPrx3

As the His-tag binds metal ions very tightly, the addition of metal ions was investigated to see whether this would alter the equilibrium between oligomeric states of the tagged protein. However, it was found that addition of nickel ions at concentrations as low as 1 mM caused rapid aggregation of protein. This aggregate was analysed by TEM (6.2), to observe any very high order species present. Images were produced Morgagni 268D TEM, measuring at 100 kV by Dr Celine Valery Images were captured using a SIS/Olympus Megapixel III digital camera.

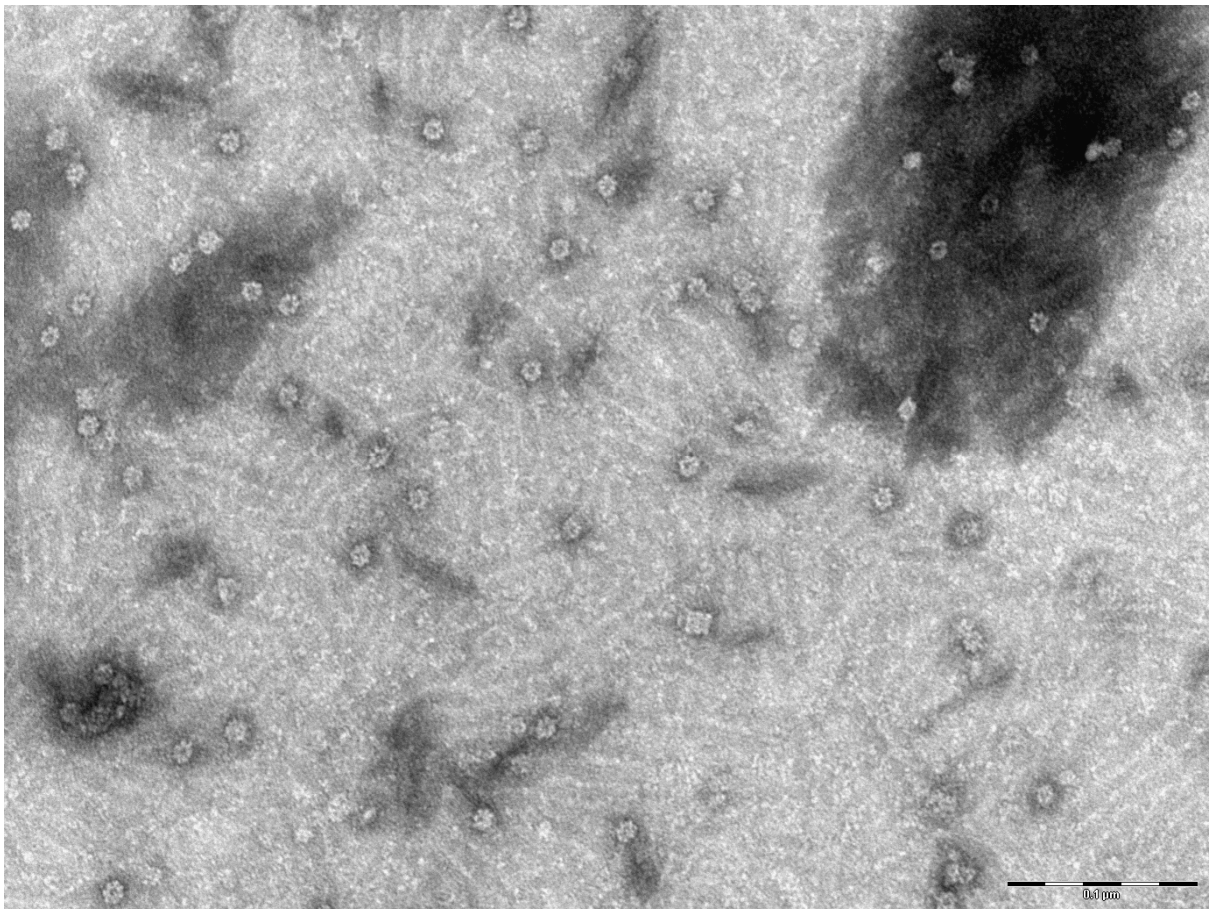

Figure 2.22: Tagged hPrx 3 at a concentration of 10 mg/ml in 20 mM Tris, 150 mM NaCl, 10 mM $NiCl_2$, pH 7.5.

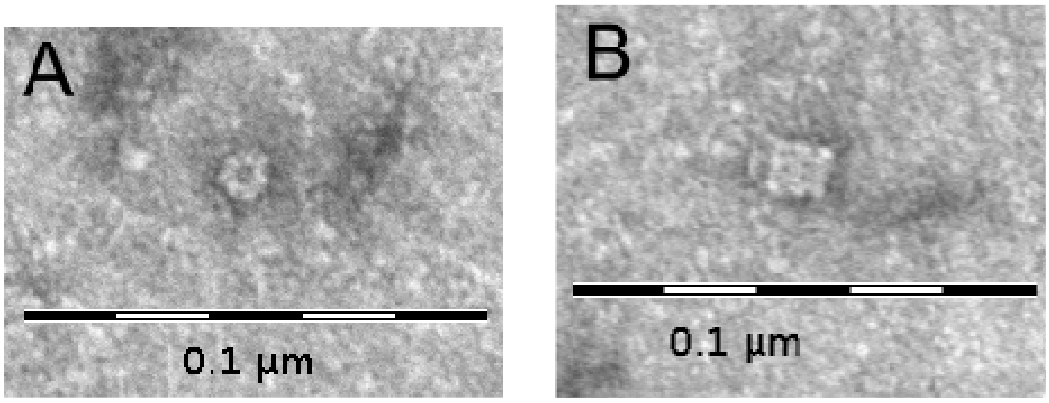

Figure 2.23 (B) Magnified view of the rings seen in Figure 2.22 showing rings. **(C)** Magnified view showing three stacked rings.

The TEM images revealed the presence of both ring and stack shaped formations. Rings had an average external diameter of approximately 140 Å, and an average interior diameter of approximately 46 Å, significantly less than that seen in the wild-type enzyme and the His-tagged wild type in the absence of nickel. A possible cause for this is that the N-terminus of the protein is on the inside face of the dodecamer, so His tags could project towards the centre of the ring. The presence of nickel could allow them to become ordered enough to be visible in the TEM image.

The stack of rings in Figure 2.22B is approximately 135 Å long, which corresponds to three rings stacked end to end, as each ring is approximately 45 Å tall in the crystal structure of bovine Prx3. The width of the stack is also consistent with the width of tagged hPrx3 rings. A structure such as this may be the identity of the species observed in the SAXS data (2.42).

Tagged protein was also analysed in the presence of the chelating agent EDTA to test whether metal ion binding played a role in the differences seen in the quaternary structure properties of His-tagged hPrx compared to wild type hPrx3.

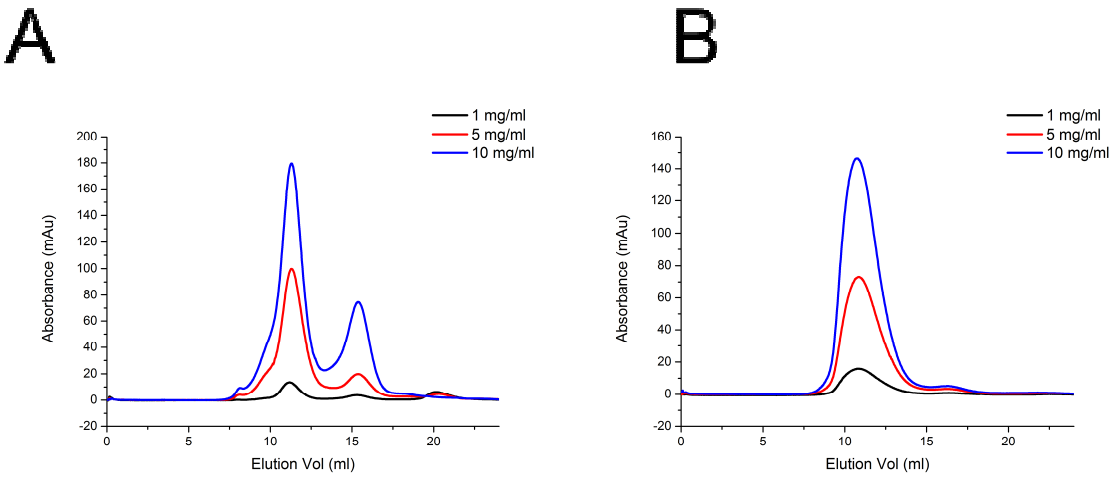

Figure 2.24: (A) Absorbance at 280 nm of His-tagged hPrx3 in 20 mM Tris, 150 mM NaCl, 10 mM EDTA, pH 7.5. **(B)** Absorbance at 280 nm of His-tagged hPrx3 in 20 mM Tris, 150 mM NaCl, pH 7.5.

With the addition of EDTA, two peaks are visible, corresponding to species with molecular weights of 720 kDa and 48 kDa. These are similar to the sizes seen for the protein in the absence of EDTA, shown in Figure 2.22 B. However, the proportions are different, with more protein being present in the dimeric form. This indicates that metal binding has an important role in the altered oligomeric properties of tagged hPrx3. The proportions do not match those seen for the wild type protein, which indicates that either metal binding does not account for all the differences between wild type and His-tagged hPrx3, or that EDTA is not able to completely remove all metal ions from the His-tagged protein. It also indicates that metal ions are present in His-tagged samples examined in (2.4.1) and (2.4.3). The origin of these ions may either be the metal affinity column used in purification of the enzyme, or the bacteria in which they were synthesised (6.2).

2.5 His-tagged hPrx3 S78A

As mentioned previously, His-tagged S78A showed poor solubility, and formed cloudy aggregates in solution. These aggregates were investigated using TEM to observe whether any higher order species were present.

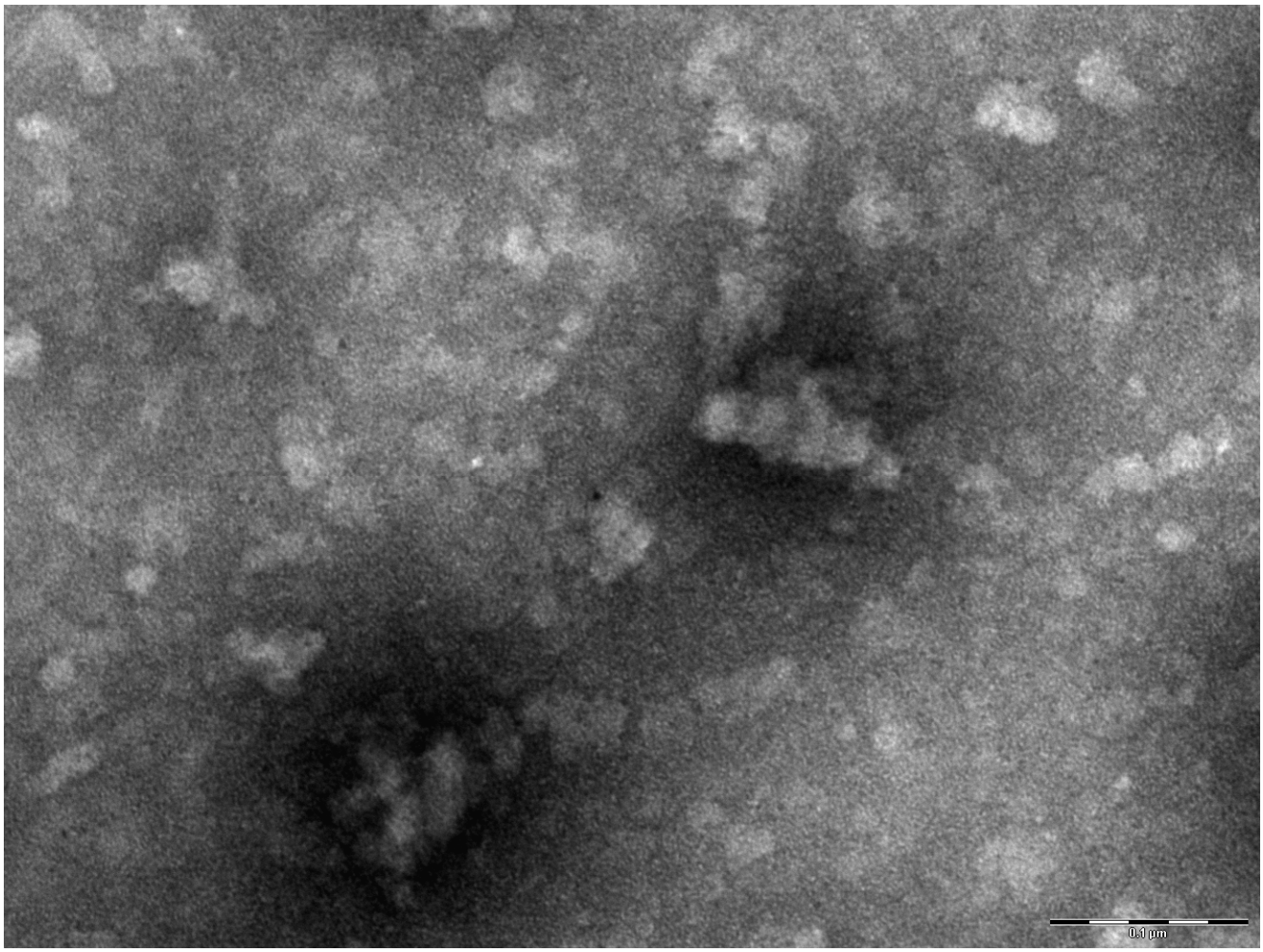

Figure 2.25: (A) His-tagged hPrx3 S78A at a concentration of 3 mg/ml in 20 mM Tris, 150 mM NaCl, 10 mM NiCl, pH 7.5.

TEM showed the presence of unordered aggregates and no evidence of ordered species. This indicates that aggregation was due to protein instability in these conditions, as opposed to the aggregation observed in His-tagged hPrx3 upon the addition of nickel ions (2.4.3).

2.6 Preliminary comparison of activity of hPrx3 variants

It has previously been reported that mutations affecting the quaternary structure of peroxiredoxins alter their activity (Parsonage et al. 2005). As the hPrx3 variants produced showed different oligomeric properties, their activity was measured to investigate whether their altered quaternary structure resulted in differing enzyme activity.

2.5.1 Activity assay for wild type hPrx3

An activity assay based on that described in (Ogusucu et al. 2007) was used to examine whether the different forms of hPrx3 had different levels of enzymatic activity. This assay was based on competition with horseradish peroxidase, an enzyme that degrades hydrogen peroxide with a known rate (Dolman et al. 1975). This enzyme contains a heme group with a distinctive absorbance. When reacting with hydrogen peroxide, this absorbance is lost. By comparing the change in absorbance of this enzyme in the presence of hydrogen peroxide and differing concentrations of peroxiredoxins to the absorbance of HRP in the absence of these reactants, the rate of reaction of the peroxiredoxin can be calculated (Nelson et al. 2008).

The k_{cat}/k_M of the enzyme can be calculated from the slope of a graph comparing the concentration of the peroxiredoxin enzyme used and the term $(F/F\text{-}1)k_{HRP}[HRP]$. In this term:

(F/1-F) is a ratio derived from the absorbance of the HRP heme with H_2O_2 present, its absorbance with H_2O_2 and hPrx3 present and its absorbance with neither reactant present

kHRP is the k_{cat}/k_M of HRP in $M^{-1}s^{-1}$

[HRP] is the concentration of HRP

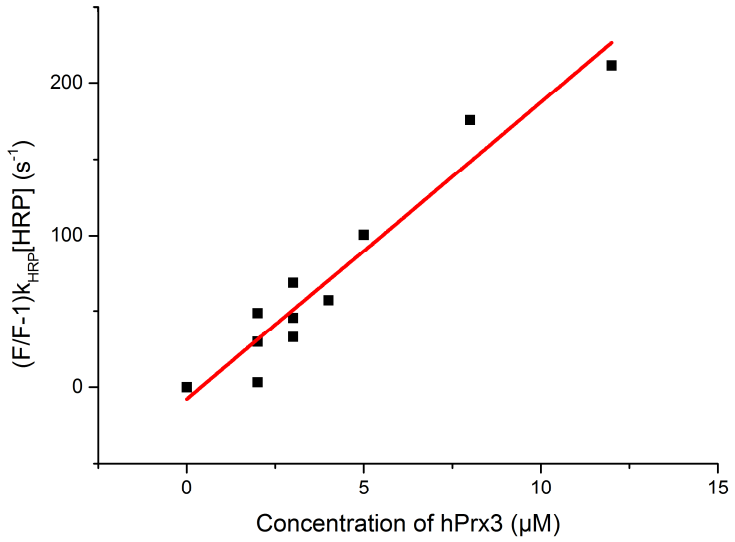

Figure 2.26: Results of the activity assay for wild type hPrx3. As preparation of samples produced a limited amount of protein to carry out assays, each point represents a single measurement.

The trend line of the graph for the activity assay of wild type hPrx3 gives a $k_{ca}t/k_M$ value of 2.0×10^7 $M^{-1}s^{-1}$. The trend line fits quite well to the data, with an R^2 value of 0.93. The calculated value of $k_{ca}t/k_M$ is close to the reported value for another peroxiredoxin enzyme, *Salmonella typhimurium* AhpC, which has a k_{cat}/k_M of 3.7×10^7 (Parsonage et al. 2005), as well as to the results reported in other uses of this assay (Ogusucu et al. 2007; Nelson et al. 2008).

2.5.2 Activity assay for hPrx3 S78A

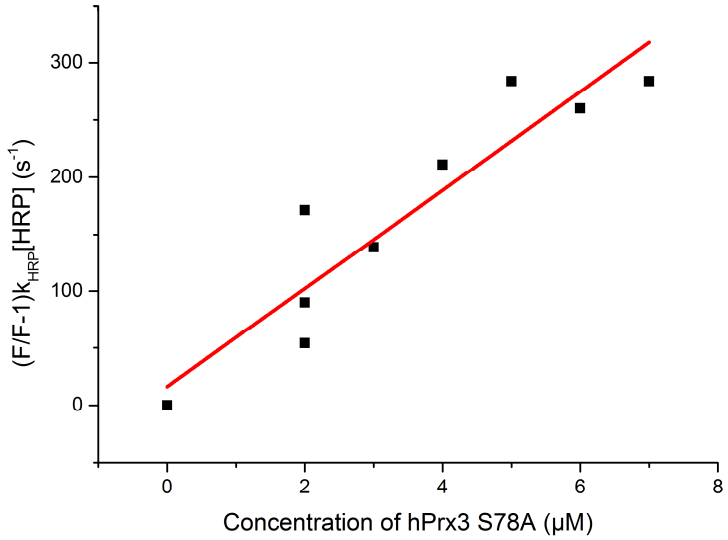

Figure 2.27: Results of the activity assay for S78A hPrx3.

The trend line of the graph for the activity assay of S78A hPrx3 gives a k_{cat}/k_M value of 4.3 $\times 10^7$ $M^{-1}s^{-1}$. Again, this is of the same order of magnitude as previously reported peroxiredoxin enzymes. The value is approximately twice that of the wild type enzyme, suggesting that this mutant reacts with H_2O_2 faster than the wild type enzyme. However, more replicates would be needed to confirm this, as the trend line does not fit as well to the data as that of the wild type enzyme, with an R^2 of 0.84.

2.5.3 Activity assay for His-tagged hPrx3

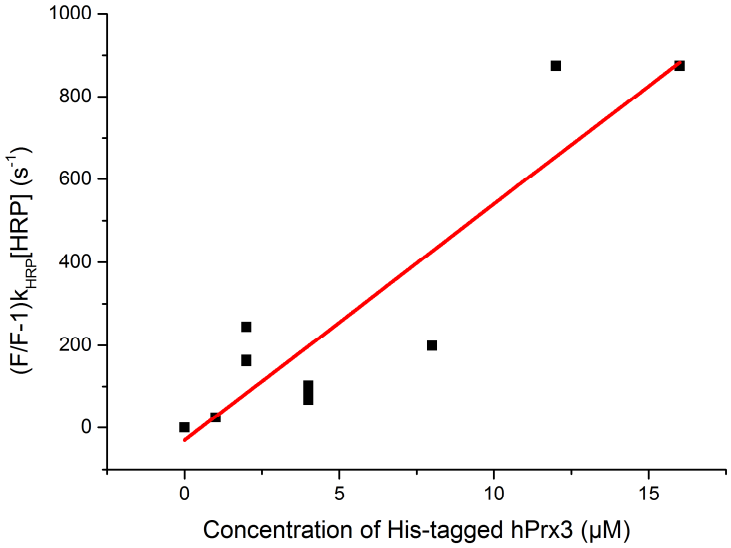

Figure 2.28: Results of the activity assay for tagged hPrx3.

The trend line of the graph for the activity assay of tagged hPrx3 gives a k_{cat}/k_M value of 5.7 $\times 10^7$ $M^{-1}s^{-1}$. This is again close to previously calculated peroxiredoxin k_{cat}/k_M values, and is also larger than the value for the wild type enzyme, indicating faster reaction with H_2O_2. However, the data does not fit to a line as well as that of the other protein variants, showing a distinct step between 2 and 4 μM, and an R^2 value of 0.82. This was seen over multiple replicates at this concentration. A possible cause for this is a shift in oligomeric state near this concentration. As the lowest concentration of tagged protein examined using SEC was 1 mg/ml, which is approximately 40 μM, further experiments would be necessary to investigate.

Activity measurements showed that all three enzyme variants had peroxide reducing activity and were able to compete with HRP. They also suggested that the variants that promoted the formation of higher order species had higher levels of activity than the wild type. However, more extensive experiments would be required to confirm this, as error in activity measurement is likely to be large.

2.6 Summary of Results

Three forms of hPrx3 were successfully purified: wild type hPrx3, hPrx3 S78A and His-tagged hPrx3. His-tagged hPrx3 S78A proved unstable in the buffers used during purification.

SEC analysis of these protein showed that each variant exhibited a different ratio of smaller and larger structures. Self-assembly in hPrx3 was shown to be complex, and influenced by protein concentration, pH and buffer as well as redox state. The size of the smaller species observed indicated it was a dimer, but the larger species did not correlate well in size to decameric or dodecameric species, likely due to their non-globular shape. TEM and SAXS indicated that these species were ring shaped, dodecameric species.

Both hPrx3 S78A and His-tagged hPrx3 showed increased proportions of higher order species compared to wild type hPrx3 across all conditions examined. In S78A, the large species showed a similar relationship between the calculated molecular weight of the dimer and that of the larger species as that seen in the wild type protein. This indicated that the larger species was likely to also be a ring shaped dodecamer.

His-tagged hPrx3 showed a very pronounced preference for self-assembly, with the protein being almost entirely present as larger species, even in the absence of reductant. The identity of the larger species was not clear, as TEM images indicated a dodecameric ring shaped species, but SAXS scattering indicated a larger species.

The increased proportions of larger species seen in His-tagged hPrx3 was found to be partially due to metal ion binding, as addition of EDTA decreased the proportion of large species seen, while the addition of nickel ions caused the protein to rapidly become insoluble. TEM analysis of the insoluble protein revealed it to be formed from dodecameric, ring shaped structures and even short stacks of rings.

Preliminary activity assays showed that all variants analysed had activity of similar levels to that seen in other peroxiredoxins, and suggested that the variants that favoured self-assembly had higher activity than wild type hPrx3. However, further investigation is necessary to confirm this.

CHAPTER THREE

Results and Discussion (TaqPrx)

Peroxiredoxins have the ability to self-assemble to form higher order species from smaller building blocks. This is controlled by the environment of the protein and its structure. A thermophilic peroxiredoxin demonstrating self assembly would be expected to have a very stable A-type interface in order to form higher order species at elevated temperatures. Higher heat tolerance would be a useful property for any nanodevice based on a peroxiredoxin system. However, no higher order structure forming thermophilic peroxiredoxins from the AhpC-Prx1 class (1.6.1) have been characterised. For this reason, it was an attempt was made to purify and characterise such a protein.

3.1 Sequence comparisons of hPrx3 and thermophilic peroxiredoxins

3.1.1 Clustal Omega alignment of peroxiredoxins

The peroxiredoxin genes of several thermophilic organisms were examined in order to determine their similarity to hPrx3 and their suitability for investigation of their quaternary structure. Peroxiredoxin genes for the archaean species *Pyrococcus furiosus*, *Pyrobaculum aerophilum*, *Sulfolobus acidocaldarius* and *Ignisphaera aggregans*, and the bacterial species *Thermotoga maritima* and *T. aquaticus* were compared using Clustal Omega (www.ebi.ac.uk/Tools/msa/clustalo/) (Sievers et al. 2011) (Figure 1). These organisms were selected as their genomic DNA was easily obtainable from other laboratories. Clustal Omega quickly aligns multiple sequences and has been demonstrated to have a high degree of accuracy (Sievers et al. 2011). No information other than the amino acid sequence was used to make the alignment.

```
H. sapiens            1 ----APAV-TQHAPYFKGTAVVNGEFKDLSLDDF--KGK-YLVLFFYPLDFTFVCPTEIVAFS 56
I. aggregans          1 MVGQIPLI-GEKFPE-MTV--VTTHGVKKLPDDY--KGK-WLVLFSHPADFTPVCTTEFYAFA 56
P. aerophilum         1 ----------MKIPEDLCF--NTDHGPKCFK-DY--KGK-WLLLFSHPADFTPVCTTEFVAFS 47
P. furiosus           1 ----MIVI-GEKFPE-VEV--KTTHGVIKLPDHFTKQGK-WFMLFSHPADFTPVCTTEFYGLQ 55
S. acidocaldarius     1 ----MALEKGNEAPD---FEGDSTIGKL-KLSSY--RGKSVVVLYFYPKAFTPGCTRETIKFG 53
T. maritima           1 MEGRIPLI-GEEFPR-VEV--KTTHGKKVLPDDF--RGK-WFVLFSHPADFTPVCTTEFVAFQ 57
T. aquaticus*         1 ----MSLV-GKKVQPFRAQAYHNGEFIEVTEQDF--MGK-WSIVCFYPADFTFVCPTELEDLQ 56
T. aquaticus          1 ----MPGMEGTLAPD---FALPDQEGRVHRLSDY--RGR-WVVLYFYPKDDTPGCTKEACGFR 54

H. sapiens           57 DKANEFHDVNCEVVAVSVDSHFSHLAWINTPRKNGGLGHMNIALLSDLTKQISRDYGVLLE-G 118
I. aggregans         57 KRYNDFKELNTELLGHSVDSVYSHIKWIEWIKEKLGI-EIPFPIIADPTGDVARKLGFLHAQS 118
P. aerophilum        48 RKYEEFKKRGVELLGLSVDTNYSHIEWKRQIEQAFGV-KVPFPIIADVDMKVASIFNAVPP-G 108
P. furiosus          56 IRLEKFRELGVEPIGLSVDQVFSHLKWMEWIKEKLGV-EIEFPVIADDRGDLAEKLGMIPS-G 116
S. acidocaldarius    54 QLYDQFKQLNAEVIGVSVDTVSTQKSFADKC-------GARFPIVSDSNKQIAKLYGVLNEKG 110
T. maritima          58 KRYDEFRKLNTELIGLSIDQVFSHIKWIEWIKEKLGV-EIEFPVIADDLGEVSRRLGLIHPNK 119
T. aquaticus*        57 DHYATFKELGVEVYSVSTDTHYTHKAWHDTSPA---ISKIEYVMIGDPSHQLSRMFDVLDE-E 115
T. aquaticus         55 DRMGDLQALGAVVLGVSADDVASHKRFAEKY-------GLNFPLLADPERQAILAYGAWGKKN 110

H. sapiens          119 S-----GLALRGLFIIDPNGVIKHLSVNDLPVGRSVEETLRLVKAFQYVET-HGEVCPANWTP 175
I. aggregans        119 A-----SHTVRAVFIVDPDGIIRAILYYPQEVGRNIDEILRLLKALQVNTQ-YKVALPANWPN 175
P. aerophilum       109 Q-----NLTVRTVALIDPDLKLAWFAAYPYTNGRNIDEILRVIDAIQFSYK-YGYATPADWKP 165
P. furiosus         117 S-----TITARAVFIVDDKGIIRAIVYYPAEVGRDWDEILRLVKALKISTE-KGVALPHKWPN 173
S. acidocaldarius   111 S------SAQRVTFIIDENGKIIEVLSGLGNAEEHANKSLEIIKRIRGKT------------- 154
T. maritima         120 G-----TNTVRAVFIVDPNGIIRAIVYYPQEVGRNIDEILRAVKALQTSDE-KGVAIPANWPS 176
T. aquaticus*       116 Q-----GLAQRGTFIIDPDGVIQAVEINADGIGRNASTLIDKIKAAQYVRNHPGEVCPAKWKE 173
T. aquaticus        111 LYGKEYEGVLRQTFLIDPEGRIAKVWRKVSP-EGHAEEVAEALRQARGE-------------- 157

H. sapiens          176 ----DSPTIKPSPAASKEYFQKVNQ----------------------------------- 196
I. aggregans        176 NELIGQNAIVPPASNVIDAAERL-----KQYKCYDWWFCYKEIPEQEAERARAFLKRVAGL 233
P. aerophilum       166 ----GDPVIVPPPPTTEGAA---------------------------------------- 181
P. furiosus         174 NELIGDKVIVPPASSVEQIKEREEAKAKGEIECYDWWFCYKKLE---------------- 220
S. acidocaldarius   155 ------------------------------------------------------------ 155
T. maritima         177 NELINDSVIVPPASSVEEARKRLES---KDFECYDWWFCYKKV----------------- 217
T. aquaticus*       174 ----GAETLKPSLDLVGKI---------------------------------------- 188
T. aquaticus        160 ------------------------------------------------------------ 160
```

Figure 3.1: Clustal Omega alignment of multiple thermophilic peroxiredoxins and hPrx3. The peroxiredoxin motif (PXXXTXXC) is highlighted in yellow, the overoxidation motifs (GLLG and YF) (1.8.4) are highlighted in yellow. The peroxidatic cysteines are shown in red text, while other cysteines, which may be resolving cysteines, are highlighted in blue. *T. aquaticus** refers to the protein sequence reported by Logan and Mayhew (Logan and Mayhew 2000)while the second sequence labelled *T. aquaticus* is that which was found in a search of the *Thermus aquaticus* genome. Proteins compared and Genbank accession numbers are: *Homo sapiens* (*H. sapiens*), AAH08435.1; *Ignisphaera aggregans* (*I. aggregans*), YP_003860235.1; *Pyrobaculum aerophilum* (*P. aerophilum*), NP_559755.1; *Pyrococcus furiosus* (*P. furiosus*), NP_578762.1; *Sulfolobus acidocaldarius* (*S. acidocaldarius*), YP_254780.1; *Thermotoga maritima* (*T. maritima*), NP_228616.1; *Thermus aquaticus* (*T. aquaticus*), AAF82118.1 and ZP_03495958.1.

When sequences were compared, the conserved peroxiredoxin motif (PXXXTXXC) (1.5.2) was aligned in all sequences. Sequence comparisons showed that the most similar enzyme to hPrx3 was that of *Thermus aquaticus* previously identified (Logan and Mayhew 2000), which while only 40% identical, conserved the amino acid sequence around both the peroxidatic and the resolving cysteine (C169 in *H. sapiens*), indicating that it is most likely a typical 2-cysteine peroxiredoxin of the AhpC-Prx1 class.

3.1.2 BLAST comparisons of reported peroxiredoxins in *T.aquaticus*

After PCR failed to amplify any products with primers for this gene (3.2), a BLAST alignment was used to compare the protein sequence to that reported in the Genbank database (www.ncbi.nlm.nih.gov/genbank/) in order to identify if any other similar proteins were known in related bacterial species. However, it was found that the amino acid sequence reported by Logan and Mayhew (2000) was almost identical to a protein found in the bacterium *Geobacillus stearothermophilus* (GenBank accession number YP_148428.1), showing only one amino acid difference. Many other peroxiredoxins of *Geobacillus* species are highly similar (80-90% identical) to the sequence proposed by Logan and Mayhew (2000). The genome of *T. aquaticus* published by Oak Ridge National Laboratory (http://genome.ornl.gov/microbial/taqu/) was then compared to the gene sequence of the enzyme identified by Logan and Mayhew (2000). The gene sequence was not identified in the *T. aquaticus* genome, nor were any sequences with significant similarity. Professor Mayhew was contacted, although he had subsequently retired. He suggested that the difference seen between the published *T. aquaticus* genome and the gene reported in his paper (Logan and Mayhew 2000) was due to differences in strain used. However, the high degree of similarity between the reported *T. aquaticus* gene and that of *Geobacillus* makes it seem likely that a *Geobacillus* species is the origin of the gene, whether due to contamination or horizontal gene transfer.

The genome search also identified a 157 residue protein called 'alkyl hydroperoxide reductase/ Thiol specific antioxidant/ Mal allergen' showing a degree of similarity. This protein contained the PXXXTXXC (1.5.2) motif conserved in almost all known peroxiredoxins. The protein sequence was obtained and compared to the NCBI protein database by BLAST, and was found to be most highly similar to peroxiredoxins from *Thermus scotoductus* and *Thermus thermophilus*, and very similar to peroxiredoxins of closely related thermophilic bacterial genera such as *Deinococcus*, *Marinithermus,* and *Meiothermus*. As genomic DNA for *T. aquaticus* had already been obtained, this protein was chosen for analysis.

Sequence analysis reveals that *T. aquaticus* Prx is 31% identical to hPrx3. Comparison of the sequence to the PREX database (http://csb.wfu.edu/prex/) (Soito et al. 2010) indicated it was a peroxiredoxin of the BCP-PrxQ group, a predominantly monomeric group. As the protein contains a second cysteine five residues after the peroxidatic cysteine, it could function as an atypical 2-Cys Prx, as other Prx in this family are known to have a resolving

cysteine in this position (Karplus and Hall 2007). This protein was termed TaqPrx, and the gene that encodes it *TaqPRDX1*.

3.2 PCR and transformation

Once identified, *TaqPRDX1* was amplified from genomic DNA and cloned into a plasmid vector. *E. coli* were transformed by the plasmid in order to express the protein. The Gateway cloning system was used to clone *TaqPRDX1* from genomic T. aquaticus DNA to the pDEST 17 plasmid (4.3). This technique uses a two-step PCR process to introduce the desired gene into a plasmid (Hartley 2000). The first step uses gene specific primers to amplify the gene from genomic DNA, and adds small adaptor sequences on either end. The second step uses generic primers that attach to the adaptor sequences added by the first primer pair. This creates a linear fragment of DNA containing the gene of interest flanked by adaptor regions called attB1 and attB2.

The next step is to transfer the fragment into a plasmid. To do this, an enzyme called BP clonase is used. This swaps the sequence from the fragment into a donor plasmid called pDONR221. This contains a gene for a toxic protein flanked by adaptor regions termed attP1 and attP2. This reaction, which results in the fragment being integrated into the donor plasmid, is called the BP reaction. Since donor plasmids that do not undergo the BP reaction contain the gene for the toxic protein, only plasmids where the reaction was successful can grow. Insertion of the fragment can be checked using a BsrG1 digest, which cleaves fragment from the plasmid (Walhout et al. 2000).

From the donor plasmid, the gene can be transferred into an expression plasmid. This uses a similar process, termed the LR reaction, using the enzyme LR clonase. The donor plasmid contains a pair of adaptor sequences called attL1 and attL2, while expression plasmids contain a pair called attR1 and attR2. LR clonase swaps the fragment from the donor plasmid to the expression plasmid, which again contains the gene for the toxic protein between its attR1 and attR2 (Walhout et al. 2000).

The advantage of this technique is that it does not require a pair of restriction enzymes to be found that do not have a recognition site with the gene of interest, and allows genes to be quickly swapped into different expression enzymes (Katzen 2007).

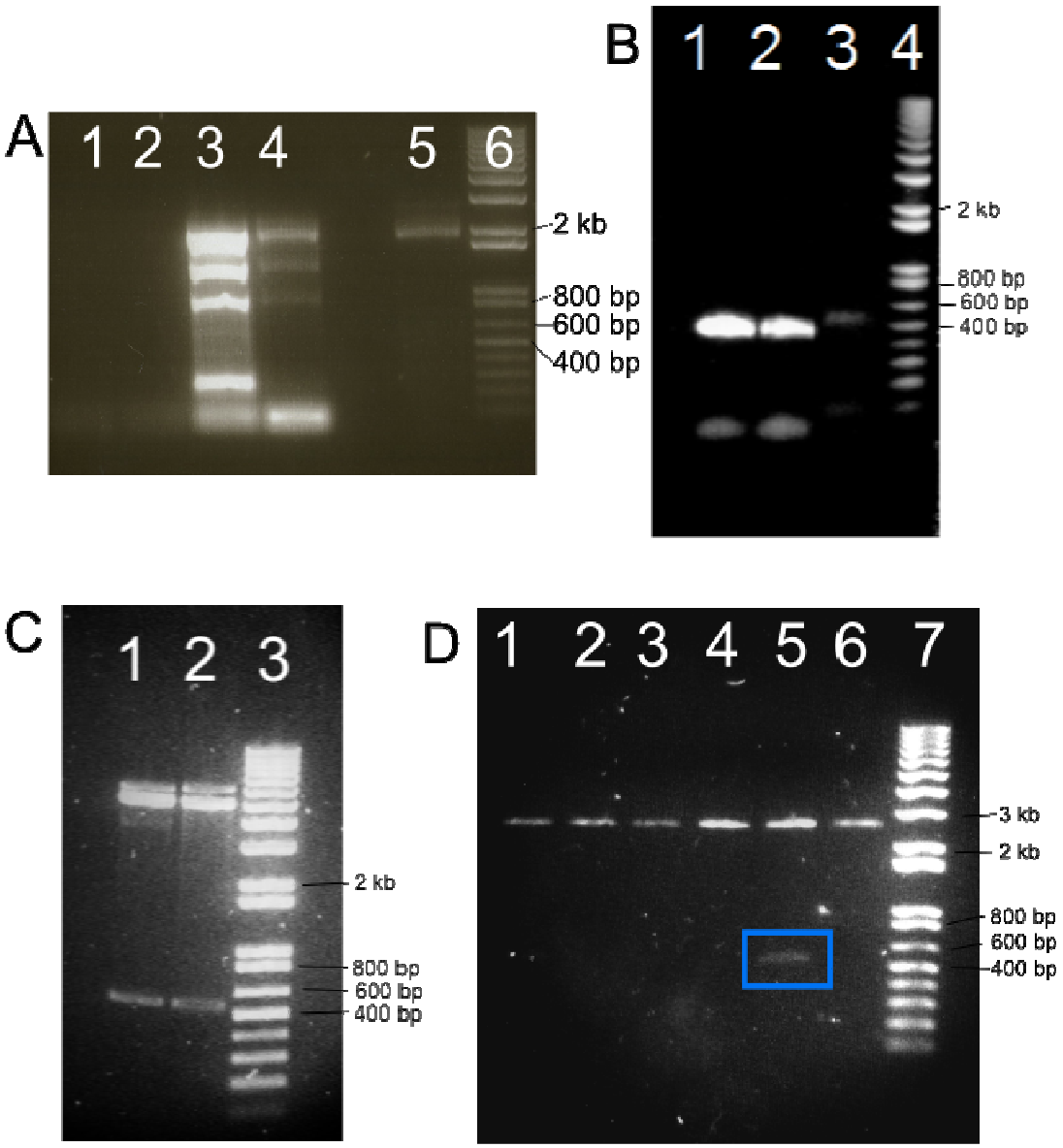

Figure 3.2: (A) Agarose gel showing results of the attempted amplification of the *T.aquaticus* peroxiredoxin previously reported (Logan and Mayhew 2000) from genomic *T. aquaticus* DNA. **Lane 1:** Attempted amplification of the gene, annealing temperature 65°C. **Lane 2:** The same reaction, annealing temperature 58°C. **Lane 3:** The same reaction, annealing temperature 51°C. **Lane 4:** The same reaction, annealing temperature 45°C. **Lane 5:** Control reaction. **Lane** 6**:** 1 kb plus DNA ladder. **(B)** Agarose gel showing results of PCR steps. **Lane 1:** Amplification of *TaqPRDX1* gene from *T. aquaticus* genomic DNA, annealing temperature 65°C. **Lane 2:** The same reaction, annealing temperature 60°C. **Lane 3:** Addition of clonase recognition sites to amplified gene. **Lane 4:** 1 kb plus DNA ladder. **(C)** Agarose gel showing BsrG1 digest of pDONR 221 plasmid after insertion of *TaqPRDX1* gene. **Lanes 1-6:** Plamid samples. **Lane 7:** 1 kb plus DNA ladder. Protein band is highlighted with a blue box. **(D)** Agarose gel showing BsrG1 digest of pDEST 17 plasmid after insertion of TaqPrx gene. **Lanes 1–2:** Plasmid samples. **Lane 3:** 1 kb plus DNA ladder.

Attempts to amplify a peroxiredoxin gene from genomic *T. aquaticus* using primers corresponding to the sequence identified by Logan and Mayhew (2000) showed no evidence of amplification apart from nonspecific amplification at low annealing temperatures (Figure 3.2A). None of the bands seen in the low annealing temperature reactions are consistent with the expected size of the gene, 564 bp. The control reaction shows that the lack of amplification was not due to errors in the method used to prepare reactions.

When primers for the *TaqPRDX1* were used, successful amplification was achieved (Figure 3.2B). The upper bands in lanes 1 and 2 show the amplified gene, with a length of approximately 500 bp, consistent with the expected 498 bp. The lower bands in these lanes show species of much lower molecular weight, most likely primer dimers. Lane 3 shows the addition of attB1 and attB2 sites by the second set of Gateway primers. The upper band corresponds to a size of approximately 550 bp, consistent with the expected 562 bp for the gene with the attB1 and attB2 sites attached. This lane also shows evidence of primer dimers. Although the band for product was faint, enough DNA was present to allow the next step.

After the gene had been transferred into the pDONR 221 plasmid (7.2.2), plasmid DNA was extracted from 6 colonies and checked for the presence of inserts by BrsG1 digest (7.2.4). Analysis of this reaction by gel electrophoresis (Figure 3.2C) revealed that an insert was present in lane 5, indicated by a band near 550 bp. Lanes 1-6 show a band near 2.8 kDa, indicating the presence of plasmid. A sample corresponding to lane 5 was used for the next reaction, transfer into the pDEST 17 plasmid (7.2.6). After cells had been transformed with the product of this reaction, plasmid was extracted and examined for the presence of insert by BsrG1 digest. Analysis of this reaction by gel electrophoresis (Figure 3.2C) showed that both samples examined contained an insert of the appropriate size, approximately 550 bp. Both samples also showed a pair of bands corresponding to a larger species. These bands are due to plasmid, with the paired bands likely caused by incomplete digestion of the plasmid by BsrG1. Sequencing of the plasmid with M13 primers confirmed that the plasmid contained the *TaqPRDX1* gene in the correct orientation and reading frame.

3.3 Overexpression and purification of TaqPrx

The method used for the overexpression and purification was based on that used in the purification of hPrx3 and is described in (7.3). After incubating cells overnight, *E. coli* Rosetta cells were harvested by centrifugation. Cells were lysed using a cell press, and debris was removed using centrifugation.

His-tagged TaqPrx was separated from the bacterial lysate using nickel affinity chromatography. After dialysis, His-tags were cleaved by incubation with 1 mg of TEV protease overnight. Cleaved TaqPrx was separated from any uncleaved protein, His-tags, and TEV protease using nickel affinity chromatography. After dialysis, a final purification step used anion exchange to produce TaqPrx. The concentration of purified TaqPrx was examined using a NanoDrop Spectrophotometer, measuring at 280 nm.Purification produced yields of TaqPrx of up to 20 mg per litre of culture. Protein purity was examined by SDS-PAGE (Figure 3.3).

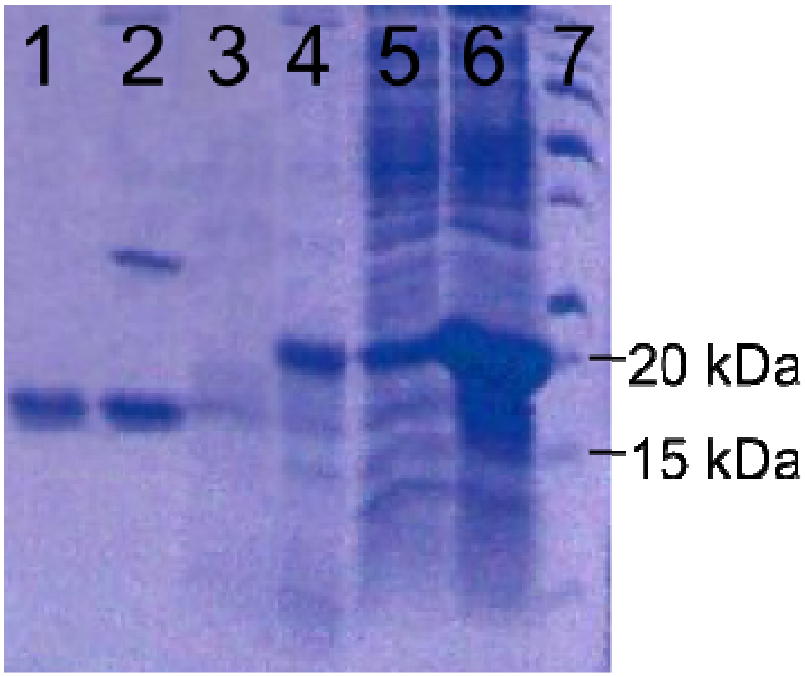

Figure 3.3: Purification of TaqPrx. **Lane 1:** Purified TaqPrx after anion exchange. **Lane 2:** TaqPrx after TEV cleavage. **Lane 3:** Nickel affinity column flowthrough. **Lane 4:** His-tagged TaqPrx. **Lane 5:** Bacterial lysate. **Lane 6:** Cell debris pellet. **Lane 7:** Novex Sharp pre-stained protein standard.

3.4 Melting temperature analysis or TaqPrx

The denaturation temperature of TaqPrx was investigated to test whether it displayed the high level of thermal stability expected in thermophilic bacterial protein. This was achieved by heating the protein in the presence of a dye that binds to hydrophobic regions of protein in a Bio-Rad iCycler iQ5 and measuring the absorbed fluorescence (7.4). When the protein denatures, hydrophobic regions are exposed, so a rapid increase in fluorescence is observed.

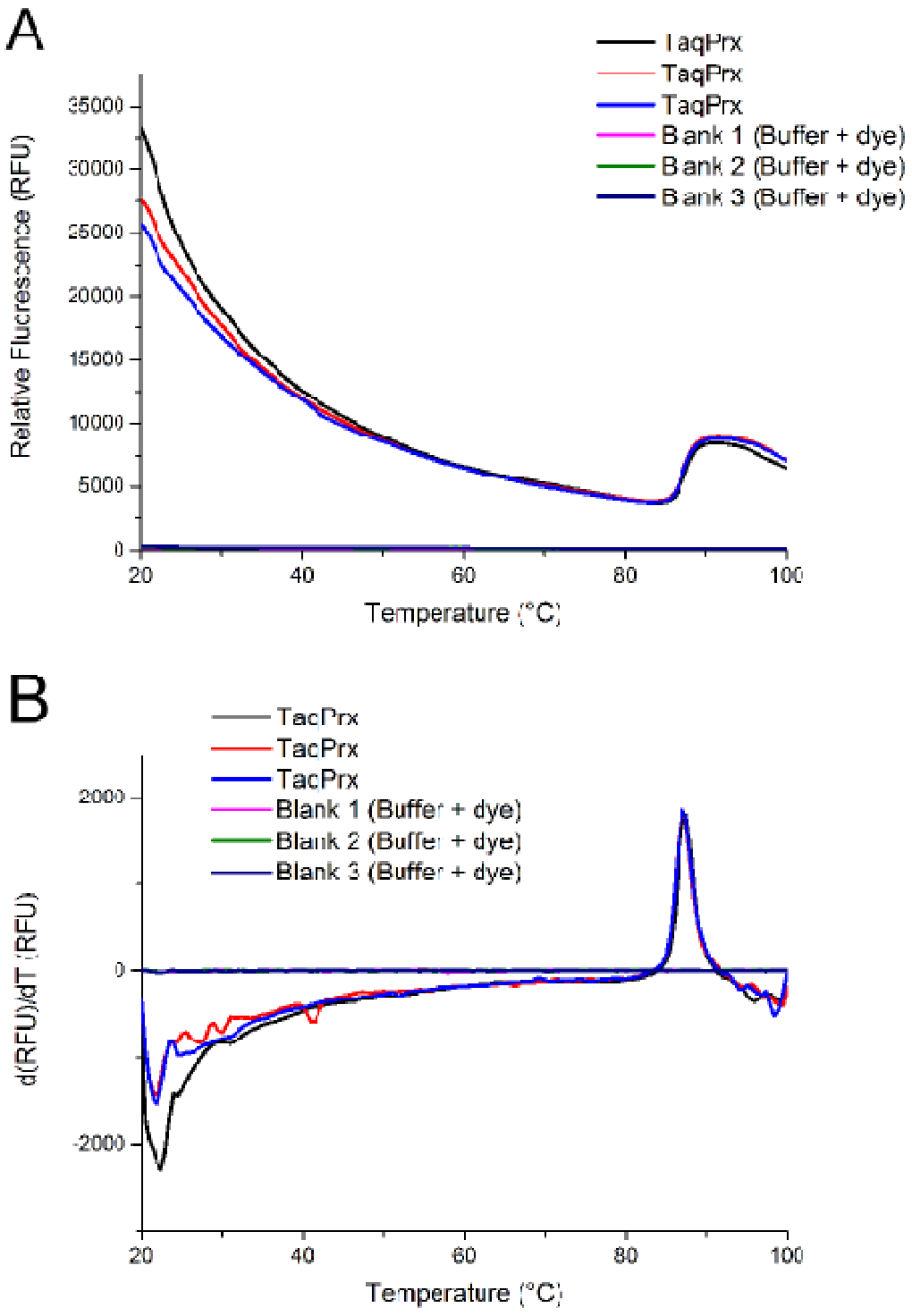

Figure 3.4: (A) Relative fluorescence measured with increasing temperature. **(B)** Change in relative fluorescence with increasing temperature. The large negative peak shows the point of most rapid increase in relative fluorescence, indicating exposing of hydrophobic protein regions due to denaturation.

In all samples, a high degree of initial fluorescence is present. A possible cause of this is that the protein is aggregating in the presence of the Sypro Orange dye. However, as temperature increases, this decreases, and a clear change in relative fluorescence can be seen (Figure 3.4A). Maximum increase in change occurs at 87.5°C (Figure 3.4B), revealing this as the denaturation point of TaqPrx. This shows that the enzyme is thermostable, consistent with its production by *T. aquaticus*, which grows optimally at approximately 75°C and can tolerate temperatures of up to 80°C (Brock and Freeze 1969).

3.5 Quaternary structure of TaqPrx by DLS

From its sequence, it was determined that TaqPrx is a member of the BCP-PrxQ group of enzymes (3.1), of which monomeric and dimeric forms are known. To determine the size of the species present, dynamic light scattering was used. This technique passes laser light through the sample, and detects the intensity of any scatter caused by particles in solution. As particles move through the laser, the change in intensity of scattering is recorded. This can be used to determine the hydrodynamic radius of the particles, as larger particles move more slowly than smaller ones. Larger particles scatter much more intensely than smaller ones, so samples must be free of large contaminants. Samples with particles of multiple sizes present are said to be polydisperse. The viscosity of the solution the particles are in must also be known, as this affects the rate of particle motion (Berne and Pecora 2000).

Samples are analysed using a statistical technique called the cumulant method. This gives a measure of the size of particles present, as well as the level of polydispersity, called the polydispersity index (PdI). A PdI of ~0.2 or lower indicates that a sample contains particles of uniform size, while a PdI of over ~0.5 indicates a sample is highly polydisperse (Koppel 1972; Frisken 2001).

Size distribution was analysed in three different ways: By intensity, which determines what proportion of the observed scattering was produced by each species present; by number, which evaluates the number of each species giving rise to scattering present; and by volume, which evaluates the total volume of each species giving rise to scatter. All are derived from the cumulant analysis of intensity.

Samples of 1 mg/ml TaqPrx were measured in phosphate buffered saline solution (137 mM NaCl, 2.7 mM KCl, 10 mM Na_2HPO_4. 1 mM KH_2PO_4, pH 7.4),examined using a Malvern Zetasizer Nano and analysed using the Zetasizer software. Three measurements were combined to estimate the size of the protein. The combined sample showed a high level of

polydispersity, with a PdI of 0.432 and a SD of 0.265. This indicates that multiple species are present in solution.

However, by number and volume, over 99% of material present was located in one peak. This indicates that the polydispersity observed is caused by a very small number of very large particles, most likely a small amount of TaqPrx aggregates.

By volume, this peak corresponded to an average radius of 1.740 nm with a SD of 0.057 nm and a peak width of 0.40 nm. By number, the peak corresponded to an average radius of 1.990 nm with a SD of 0.038 nm and a peak width of 0.527 nm. The low

These radius measurements indicate that the species present has a radius of approximately 17.4 to 19.9 Å. When the monomer crystal structure of another protein of the BCP-PrxQ class, from *Sulfolobus sulfataricus* (PDB number 3DRN (D'Ambrosio et al. 2009)) was examined, it was found to have a radius of approximately 20 Å. This shows that the DLS data is consistent with TaqPrx being a monomeric peroxiredoxin.

3.6 Structural homology modelling

In order to further investigate the structure of TaqPrx, a homology model was made using the online modelling software SWISS-MODEL (http://swissmodel.expasy.org/) (Kiefer et al. 2009). This program uses a BLAST search to identify a protein sequence with a crystal structure in the PDB and aligns them to the query sequence to find the best match. This is used as the basis of the model. The EVA-CM project (Koh et al. 2003) has been used to evaluate the accuracy of the SWISS-MODEL program, and shows that it compares favourably to other prediction programs. However, when the sequence identity of the query protein and the model is based on is over ~30%, all programs showed a similar level of accuracy.

3.6.1 Homology model of TaqPrx

The homology model produced by SWISS-MODEL used a peroxiredoxin from the archaen *S. sulfataricus* as the basis for its model (PDB number 3DRN). This protein has been shown to function with an atypical 2-Cys mechanism (D'Ambrosio et al. 2009). The two proteins belong to the same group, the PrxQ-BCP, and show 43% sequence identity, indicating that it likely has a very similar structure to TaqPrx.

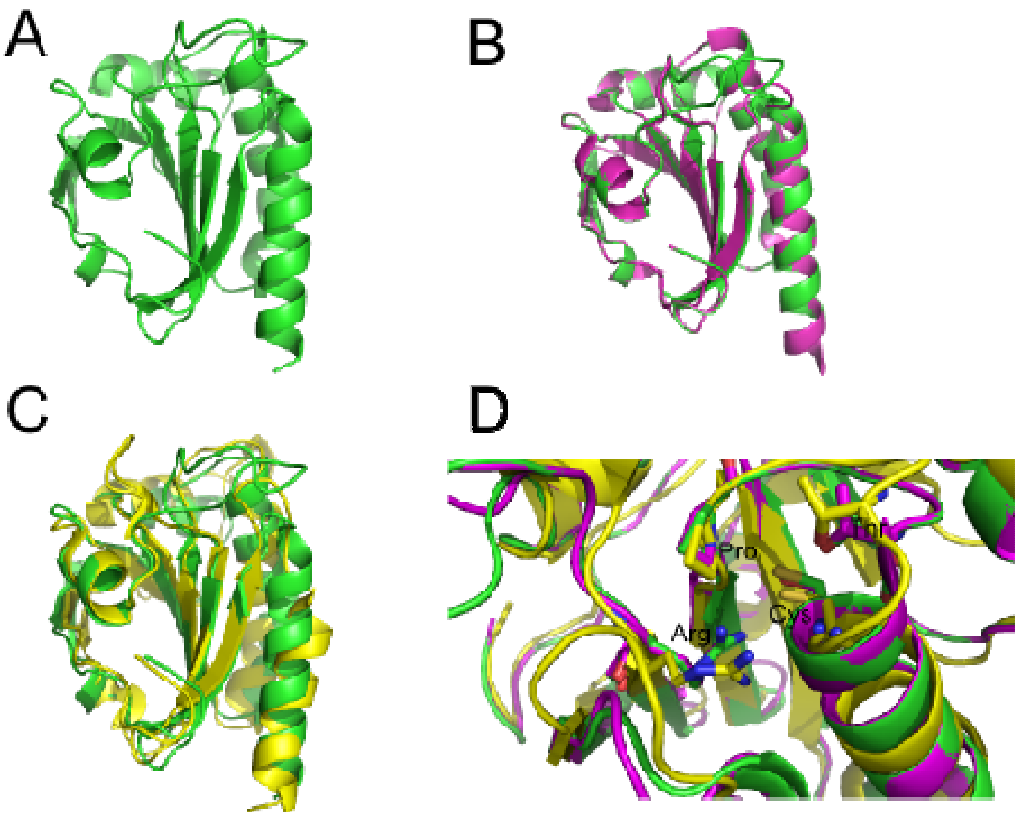

Figure 3.5: (A) Homology model of TaqPrx produced by SWISS-MODEL. **(B)** Alignment of TaqPrx (green) and *S. Sulfataricus* bcp 1(3DRN (D'Ambrosio et al. 2009)). **(C)** Alignment of TaqPrx (green) and hPrx3 (yellow) (1ZYE). **(D)** Alignment of key active site residues. Colours are as previously assigned. In *S.sulfataricus* bcp 1, the active cysteine has been mutated to a serine.

The core peroxiredoxin fold of 5 antiparallel β-sheets with flanking α-helices is conserved by the homology model (Figure 3.5A). It aligns very closely to *S. sulfataricus* bcp 1 with an RMSD of 0.08 Å over 129 atoms (Figure 3.5B), although this is expected as the model was based on this protein. However, it also aligns well to the much more distantly related bovine Prx3 (PDB number 1ZYE), which has a sequence identity of 31% with TaqPrx. The RMSD is 1.5 Å over 115 atoms (Figure 3.5C), with the main differences being in the positions of the loops between the secondary structural elements. Active sites also align well, with the key catalytic residues being positioned very similarly. The main difference is in the orientation of the arginine residue; however, both conformations have been previously identified in a survey of peroxiredoxin crystal structures (Hall et al. 2010).

3.6.2 Evaluation of homology model accuracy

In order to draw useful conclusions from the homology model, its accuracy was evaluated. The SWISS-MODEL program uses QMEAN4 to examine the model quality. This technique

combines 4 statistical terms – the torsion angles between sets of three amino acids, two measures of distant dependent interaction potentials (one between Cβ only and the other between all atoms in the structure) and a solvation potential (Benkert, Tosatto, and Schomburg 2008). These terms are weighted and combined to give a value between 0 and 1 for the homology model. This number is compared to QMEAN4 values of a library of high resolution crystal structures. QMEAN4 scores are then compared to a library of QMEAN4 derived from high resolution X-ray structures from the PDB, and their difference from the mean is calculated. This value is called the Z-score QMEAN (Benkert, Biasini, and Schwede 2011). Z-scores are also given for each of the terms used to make up the Z-score QMEAN. QMEAN scores can also be calculated per residue, termed QMEANlocal (Benkert, Schwede, and Tosatto 2009). This is calculated for a set of 9 amino acids at time, moving forward one amino acid per frame. This calculation uses the same terms as the QMEAN4 as well as terms for solvent accessibility and the proportion of residues not in a secondary structure. This can be used to estimate the accuracy of different sections within a model.

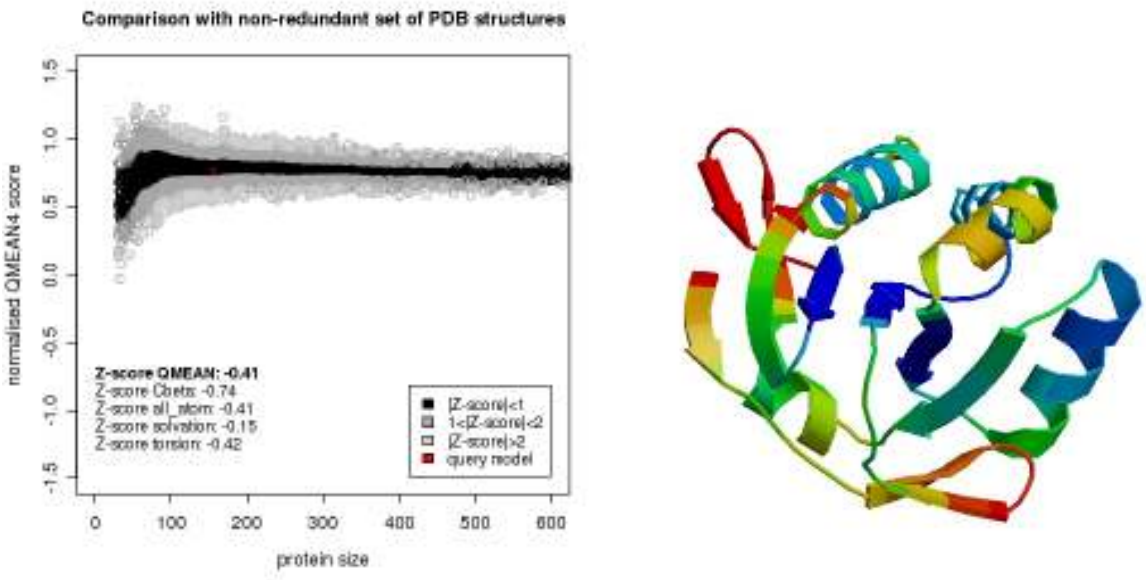

Figure 3.6: (A) Comparison of QMEAN4 score of the TaqPrx homology model to a library of scores from crystal structures in the PDB. The black area defines proteins that are within 1 standard score of the mean, while lighter shades indicate scores further from the mean. The red mark shows the position of the TaqPrx homology model. **(B)** Homology model showing estimated levels of reliability per residue using QMEANlocal. Blue regions have high QMEANlocal scores, indicating higher accuracy; while red have lower scores and lower accuracy.

The homology model of TaqPrx gives a QMEAN4 score of 0.76, and a Z-score QMEAN of -0.41 (Figure 3.6A). This indicates that the model's QMEAN4 score is within one SD of the

mean for proteins of similar length, indicating it is likely to be accurate. Examining the QMEANlocal scores (Figure 3.6B) shows that the central β-sheet and main α-helices including the active site show the most accuracy; while loops and peripheral α-helices have lower accuracy. This shows that TaqPrx is very likely to contain the conserved peroxiredoxins fold. The inaccuracy in the loop regions is not unexpected, as these regions are more variable across the peroxiredoxin family (Karplus and Hall 2007).

The homology model has a diameter of approximately 20 Å, correlating well with DLS (3.5).

3.7 Sparse matrix crystal screening

X-ray crystallography allows the very accurate determination of a proteins structure, as the position of every atom can be obtained. However, it requires protein to be in the crystalline state. For a protein to crystallise, it must be of sufficient concentration and in conditions that allow crystals to form and grow. Conditions allowing crystal formation and growth vary widely among proteins and are not easily predictable, so screens of a large number of conditions are carried out to look for evidence of crystallisation.

3.7.1 Initial screening

Screens were carried out to search for conditions that allowed crystals of TaqPrx to form. TaqPrx was screened at 10 mg/ml, using a custom screen based on Hampton Crystal Screen, Hampton Crystal Screen 2 and Hampton Index screen. These screens cover a broad range of conditions and have been widely used for protein crystallisation.

Two conditions in the first screen showed the formation of crystalline structures (Figure 3.7A). Both conditions produced small clusters of thin, needle shaped crystals. A fine screen of similar conditions resulted in slightly different crystal morphologies, but no usable crystals (7.7.1). Seeding growth by streaking crystal clusters into conditions from the fine screen where crystals did not form allowed the formation of another cluster like crystalline form, but did not yield any usable crystals (Figure 3.7B).

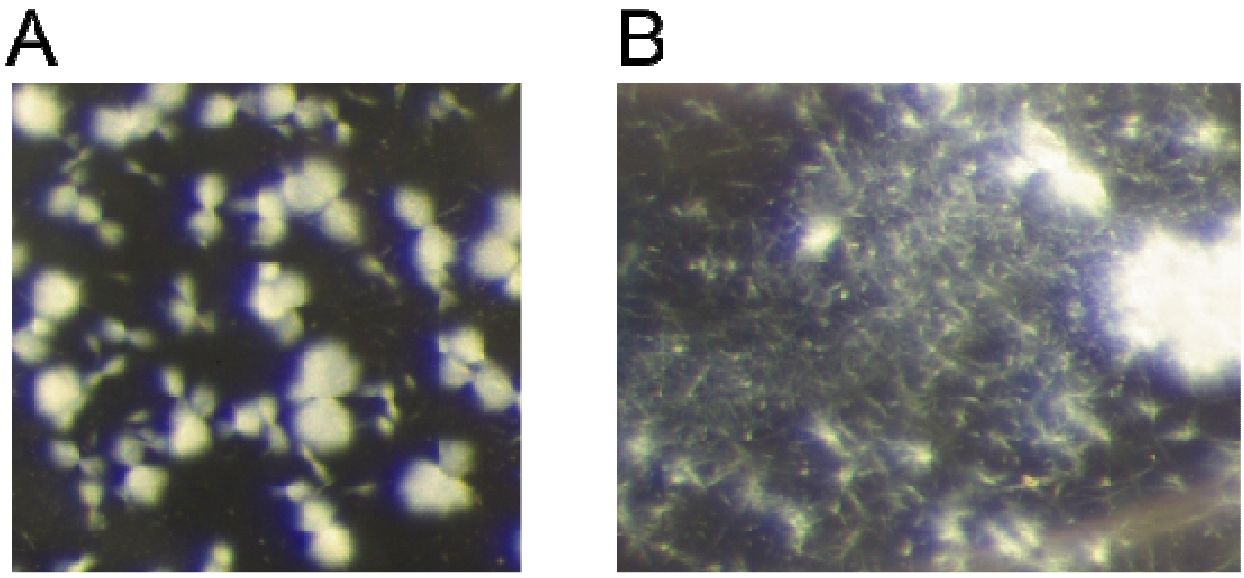

Figure 3.7: Representative photographs of cluster shaped crystal forms. **(A)** Cluster shaped crystals formed in 2 M $(NH_4)_2SO_4$, 0.1 M CH_3COONa, pH 4.6. **(B)** Cluster shaped crystals formed seeding crystal growth in 1.3 M $(NH_4)_2SO_4$, 0.1 M CH_3COONa, pH 4.5 by streaking crystals from 1.6 M $(NH_4)_2SO_4$, 0.1 M CH_3COONa, pH 4.5.

3.7.2 JCSG+ and PACT screens

As the previous screen (3.7.1) did not produce usable crystals, a second sparse matrix screen was carried out using two screens, the JCSG+ and PACT screens from Qiagen. These screens have proven successful in the past for protein crystallisation, and covers conditions not used in the previous screen.

In this screen, small triangular crystals were seen in conditions of 200 mM $LiSO_4$, 50% v/v PEG 400, 0.1 M CH_3COONa, pH 4.5 (Figure 3.8). However, these showed poor diffraction when examined at the MX1 Beamline at the Australian Synchrotron. A fine screen at similar conditions attempted to produce more useful crystals, but no crystals were observed under the conditions used (7.7.2).

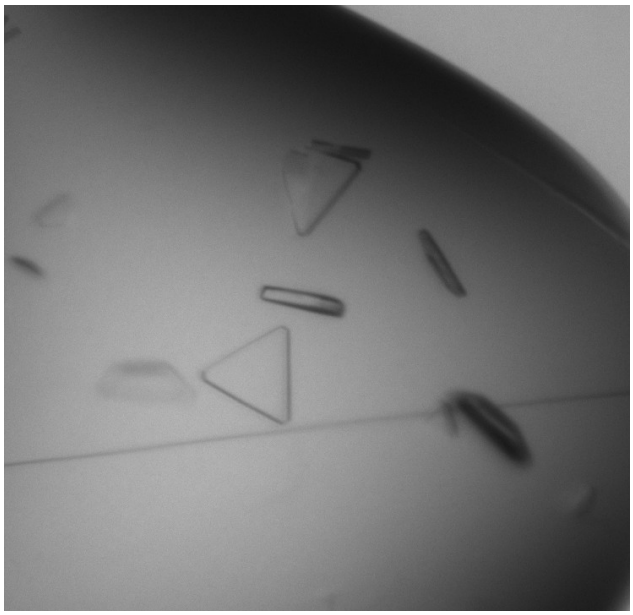

Figure 3.8: TaqPrx crystals formed in the JCSG+ screen in 200 mM $LiSO_4$, 50% v/v PEG 400, 0.1 M CH_3COONa, pH 4.5. The largest crystal is approximately 0.05 mm across.

3.8 Activity assay of TaqPrx

In order to confirm that TaqPrx is a peroxiredoxin, an assay to measure its peroxide activity was necessary. The assay used for hPrx3 (2.5) requires the activity of the peroxiredoxin to be close to that of horseradish peroxidase, and was therefore unsuitable. Instead, an assay based on mass spectrometry was developed with Dr Alexander Peskin from the University of Otago Centre for Free Radical Research. Samples of TaqPrx were examined in three conditions: Untreated, treated with H_2O_2 then *N*-ethyl maleimide (NEM) (termed the oxidised sample), and treated with NEM alone (called the blocked sample).

NEM reacts with cysteine thiol groups to form thioesters, while a thiol group that has reacted with peroxide would not. TaqPrx contains two cysteine residues (3.1) and thus two thiol groups. However only the peroxidatic cysteine would be expected to react with peroxide as the active site of peroxiredoxins favours the thiolate state.

Untreated conditions acted as a negative control, as there should be no oxidised derivatives in this sample. The oxidised sample shows if peroxide reduction is taking place. If TaqPrx has peroxide reducing activity, the peroxidatic cysteine would react with H_2O_2, creating an oxidised cysteine derivative. When NEM is added, it would react with the second cysteine, forming a species containing both an oxidised cysteine and an NEM blocked cysteine. However, if no peroxide reducing activity is present, a species containing two NEM blocked

cysteine residues would be observed. The blocked sample should contain this species as well, as both cysteines would react with NEM. All samples were examined by mass spectrometry by Dr Marie Squire from the University of Canterbury Department of Chemistry, using a Bruker maxis 3G mass spectrometer.

C_P	C_R	MW (Da)	C_P	C_R	MW
R—S—S—R		17813	R—SO_2H	HOS—R	17863
R—SH	HS—R	17815	R—SO_2H	HO_2S—R	17879
R—S^-	HS—R	17814	R—S-NEM	HS—R	17940
R—SOH	HS—R	17831	R—S-NEM	HOS—R	17956
R—SOH	HOS—R	17847	R—S-NEM	HO_2S—R	17972
R—SO_2H	HS—R	17847	R—S-NEM	NEM-S—R	18065

Table 3.1: Masses of possible species formed by adding H_2O_2 and/or NEM to TaqPrx. C_P is the putative peroxidatic cysteine, C_R is the putative resolving cysteine, NEM is N-ethyl maleimide, R is the rest of TaqPrx.

The possible species that could be formed and their masses are shown in Table 3.1. It is unlikely that any species containing a sulfenic acid (R-SOH in Table 3.1) would be seen, as this species would be expected to react quickly with either the other cysteine in the protein, or a second H_2O_2 to form a sulfinic acid (R-SO_2H) due to the large excess of H_2O_2 used.

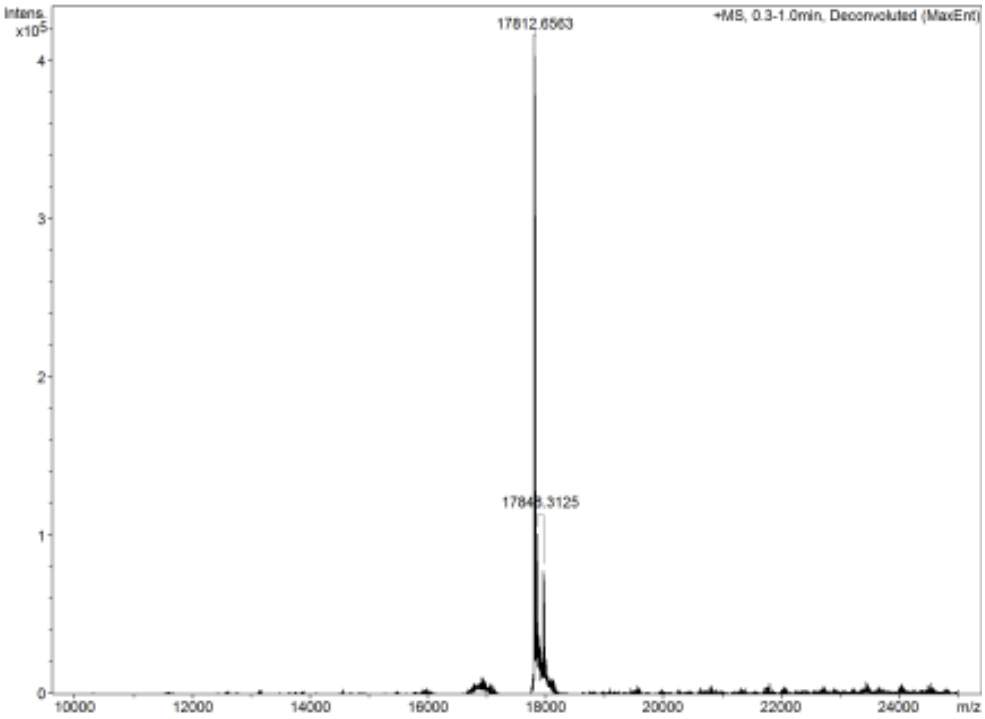

Figure 3.9: Deconvoluted mass spectrum of untreated TaqPrx. Peaks are at 17812 Da and 17848 Da.

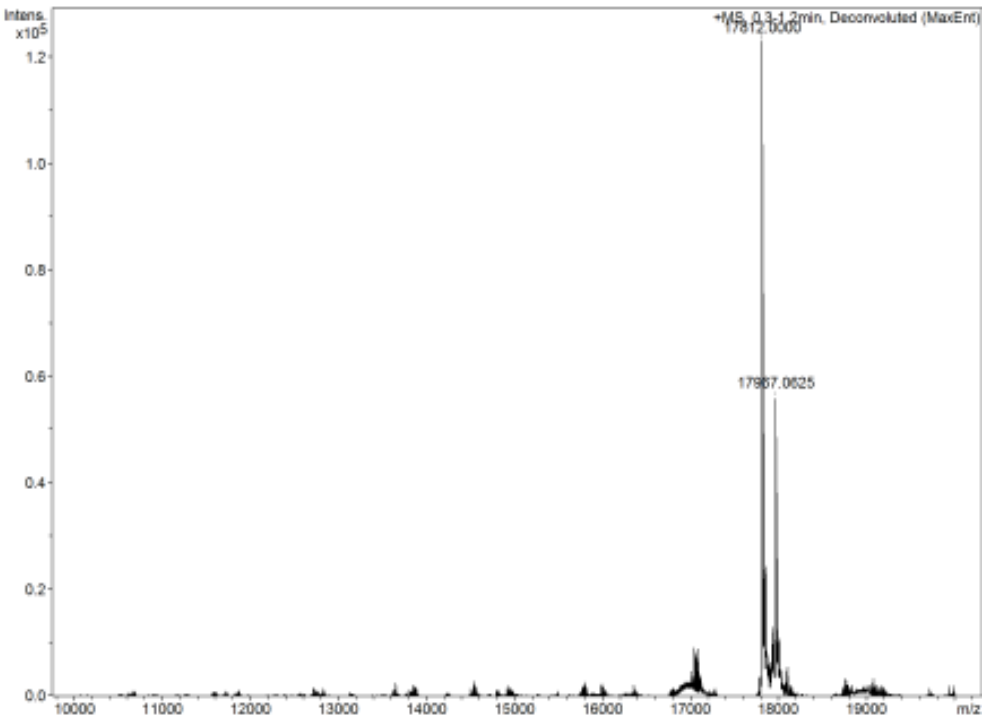

Figure 3.10: Deconvoluted mass spectrum of oxidised TaqPrx. Peaks are at 17812 Da and 17967 Da.

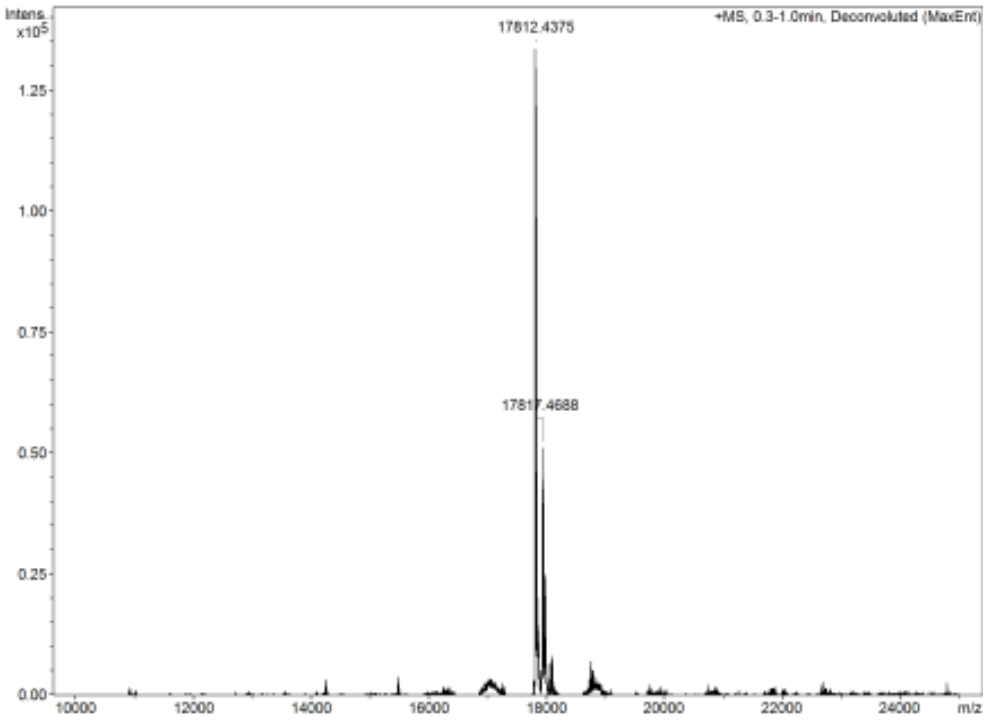

Figure 3.11: Deconvoluted mass spectrum of blocked TaqPrx. Peaks are at 17812 Da and 17967 Da.

In the untreated sample (Figure 3.9A) two peaks are seen. The first is at 17812 Da and shows a very strong signal. This corresponds most closely to the protein in the disulfide form. The second peak is at 17848 Da, and is much lower that the first peak. The most likely identity of this peak is the protein in the sulfinic acid form, which has a calculated mass of 17847 Da. The presence of the second peak was unexpected, as no H_2O_2 was added to the protein.

In the oxidised sample (Figure 3.9B), two peaks are again visible, the first corresponding to 17812 Da, the same mass as the main peak in Figure 3.9A, and thus, the same species. The second peak has a mass of 18967 Da. This corresponds most closely in mass to a species with cysteine as a sulfinic acid and the other NEM blocked. However, this species has a calculated mass of 18972 Da, 5 Da more than the species observed.

The blocked sample shows two peaks, one at 17812 Da and the other at 17817 Da (Figure 3.9C). Neither peak corresponds to a NEM containing species. The smaller species is of the same mass as the species seen in the other two conditions, while the larger corresponds most closely to the protein in the dithiol form.

In the oxidised sample (Figure 3.9B) the mass of the larger species present is close to what was expected to be seen if TaqPrx displayed peroxiredoxin activity. The sulfinic acid (RSO_2H) would be located on C_P, due to it quickly reacting with H_2O_2 to form a sulfenic acid (R-SOH), the reacting with another H_2O_2 due to the excess concentration present. The smaller peak shows a species that has not reacted with either of H_2O_2 or NEM. Also, there is a lack of protein that has reacted with only NEM. An explanation for this could be that TaqPrx was present in a mixture of an oxidised, disulfide form and a reduced form. Protein in the reduced form would quickly react with hydrogen peroxide though CP, leaving a thiol group free to react with NEM. The disulfide population would be unable to react with either H_2O_2 or NEM, explaining the peak seen a 17812 Da. A summary of this proposed mechanism is shown in Figure 3.10.

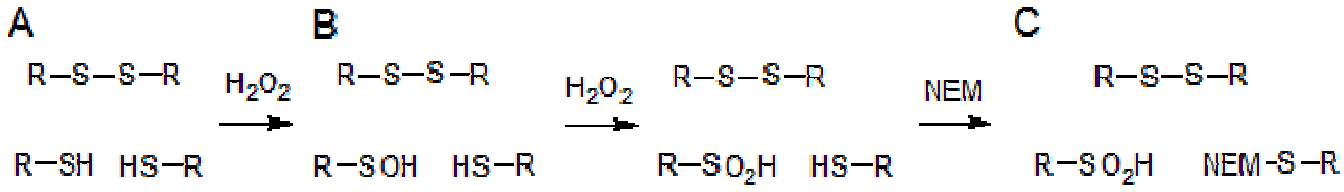

Figure 3.12: Proposed mechanism for the results seen in mass spectrometry of TaqPrx in the oxidised sample. **(A)** Initial solution contains both disulfide and dithiol TaqPrx. **(B)** The dithiol form of C_P rapidly reacts with two H_2O_2 molecules to form a sulfinic acid derivative. **(C)** NEM reacts with the dithiol of C_R.

The other two samples, however, have less easily explainable peaks present. In the untreated sample (Figure 3.9A), a peak with a mass indicating the presence of a sulfinic acid was seen although no H_2O_2 was used in the preparation of this sample. A possibility is that this species formed during the purification of the protein, and all TaqPrx used contains a proportion in the sulfinic acid form. However in the sample treated with NEM alone (Figure 3.9C), no such peak is present. This indicates that any sulfinic acid groups formed were not present before beginning the assay, as all protein used was from the same source. The sample also shows no evidence of NEM reacting with TaqPrx.

While the assay does provide evidence for TaqPrx being a peroxiredoxin enzyme, further study is necessary to confirm this. A positive control using a known peroxiredoxin enzyme should confirm that one cysteine reacts with H_2O_2, while the other reacts with NEM, and a higher number of replicates would find if the unexpected results seen were consistently observed.

3.9 Summary of results

Comparison of the sequences of thermophilic peroxiredoxins showed that the enzyme reported by Logan and Mayhew (2000) is unlikely to be present in *T. aquaticus*, but is likely to be from a bacterium of the *Geobacillus* genus. A gene was found in the *T. aquaticus* genome that showed evidence of being a peroxiredoxin of the BCP-PrxQ class, and was subsequently cloned, expressed and purified.

Denaturation temperature analysis showed that TaqPrx exhibited the thermal stability expected in a protein from a thermophilic organism. DLS showed no evidence of any species larger than a monomer, while homology modelling gave strong evidence that the protein contained the core peroxiredoxin fold and conserved active site. Production of crystalline protein for X-ray crystallography was attempted, but while promising conditions were identified, useable crystals were not produced.

The activity assay described gave some evidence that TaqPrx shows peroxiredoxin reducing activity. However, further experimentation is necessary to confirm these intial results.

CHAPTER FOUR

Summary and Conclusions

Many proteins demonstrate self-assembly, the formation of large structures from smaller basic units. This makes them attractive for use as nanoscale devices, as proteins are structurally and chemically diverse. Self-assembly in proteins is regulated by the structure of the monomeric units, using a variety of intermolecular forces. Peroxiredoxins are a diverse family of proteins with access to numerous oligomeric states, and exhibit redox controlled switching between larger and smaller forms. This makes them useful as a model system for investigating protein self-assembly.

This study mainly focussed on human peroxiredoxin 3, which is known to form large, ring shaped structures from a small subunit. This enzyme was examined under a variety of conditions to identify which conditions affected the quaternary structure of the protein. Two modified variants of the enzyme were created and purified: hPrx3 S78A and His-tagged hPrx3. These were then compared to the wild type enzyme.

In the purified wild type hPrx3, addition of reductant strongly favoured the formation of higher order structures, as reported in earlier literature for related peroxiredoxins. Increasing protein concentration also favoured oligomer formation, though not to as great an extent as the presence of reductant. Sodium phosphate buffer strongly favoured the formation of higher order structures compared to Tris buffer. Both increasing and decreasing pH favoured the dimer form when compared to pH 7.5; however, aggregation was apparent in many of these conditions. Analysis of SAXS measurements identified the two main species present as a having maximum diameters of 188 Å and 79 Å, and approximate masses of 293 kDa and 52 kDa. Comparison of the scattering curves observed for each species with those calculated from the crystal structure of bovine Prx3 indicated that these corresponded to a dodecamer and a dimer, respectively. Electron microscopy showed ring shaped structures with an average diameter of 140 Å, again consistent with the higher order species seen being a dodecamer.

The hPrx3 S78A mutant was examined in order to investigate whether it displayed increased proportions of larger species than the wild type, as a similar mutation had been

previously been shown to favour self-assembly in a bacterial peroxiredoxin (Parsonage et al. 2005).

When the hPrx3 S78A protein was examined, the same general trends were seen in the factors that affected oligomerisation as in the wild type. However, a greater proportion of higher order species were seen compared to wild type hPrx3. This was seen in all conditions observed. The likely cause of this is that the serine residue formed a hydrogen bond to the solution in the wild type, and removing this removed an interaction favouring the dimeric form. There would also be a gain in stability for the dodecameric form due to the methyl group of the alanine being buried in the interface.

In the His-tagged hPrx3 protein, the same trends seen in the wild type enzyme were observed. However, higher order species were very strongly favoured, with several conditions showing no observable presence of dimeric species. SAXS measurements showed that His-tagged hPrx3 has overall dimensions quite similar to that of the wild type, but has a significantly higher mass and volume. Its scattering curve did not match the dodecameric form, though it showed slightly more similarity to the calculated scattering of the catenane form of the protein. This may be caused by a change in the shape of the protein due to the His-tags. Examination of TEM images, however, revealed that dodecameric structures were present, with similar dimensions to those observed in wild type hPrx3.

It was found that the addition of nickel ions to the His-tagged protein caused the protein to rapidly become insoluble. TEM analysis revealed that this was formed from dodecameric structures, with external diameters of 140 Å and internal diameters of approximately 46 Å. This is somewhat different than what is observed for His-tagged hPrx3 in the absence, indicating that the presence of metal ions may cause the His-tag regions to become more structured. A small population of stacks of rings was also observed. These represent another possible oligomeric structure peroxiredoxins can form, and in some conditions may be present in both wild type and His-tagged hPrx3, as evidence for species larger than the dodecamer was present in some chromatography experiments.

Upon the addition of a chelating agent, a decrease in proportion of higher order species present was observed. This showed that metal binding played a role in favouring higher order species in His-tagged hPrx3. However, there was still a higher proportion of higher order species present than seen in the wild type enzyme, indicating that either metal binding does not completely explain the higher proportion of higher order species seen in His tagged

hPrx3, or that metal is bound too tightly for the chelating agent to fully remove. TEM images also revealed the presence of small stacks of rings. These represent another possible oligomeric structure peroxiredoxins can form, and in some conditions may be present in both wild type and His-tagged hPrx3, as evidence for species larger than the dodecamer was present in some chromatography experiments.

Purification of His-tagged hPrx3 S78A was attempted; however, this protein proved unstable and quickly aggregated during purification. Electron microscopy showed that aggregates formed were not higher order species. Different purification conditions may be able to allow purification of this enzyme variant, which was predicted to show very strong preference for self-assembly.

The activity of all three hPrx3 variants was analysed using a competitive assay with horseradish peroxidase. The wild type enzyme showed a k_{cat}/k_m of 1.95×10^7, which is consistent with previously reported values for other peroxiredoxin enzymes (Ogusucu et al. 2007; Nelson et al. 2011). In hPrx3 S78A, higher activity was seen, with a k_{cat}/k_m of 4.30×10^7. hPrx3 S78A also favoured the dodecameric form compared to the wild type enzyme; it is possible that this higher activity is linked to this altered quaternary structure. A link between redox state and activity has been suggested in another peroxiredoxin enzyme (Parsonage et al. 2005). For His-tagged hPrx3, a k_{cat}/k_m of 5.70×10^7 was seen. This is higher than what was observed for both the wild type hPrx3 and hPrx3 S78A, and as His-tagged hPrx3 shows a very strong preference the dodecameric form, it is possible that the increased activity is due to its preference for the dodecameric form. However, the data could not be linearly fitted as well as that of the other two variants.

A second enzyme was also examined, a thermophilic peroxiredoxin from the bacterium *Thermus aquaticus*. This was done to investigate if the protein also displayed self-assembly properties, and if these were significantly different from the mesophilic hPrx3. A combination of the redox controlled self-assembly and thermal stability would be useful for any nanodevices based on a peroxiredoxin enzyme.

Examination of the genome of *T. aquaticus* and reported gene sequences in the Genbank database showed that the peroxiredoxin enzyme previously reported (Logan and Mayhew 2000) is not present in *T. aquaticus* and is more likely from a bacteria of the genus *Geobacillus*. Instead, a potential peroxiredoxin gene was identified in the genome of *T. aquaticus* and cloned into a plasmid vector, allowing expression in *E. coli* and purification of the protein. Analysis of the sequence showed it belonged to the BCP-PrxQ group of

peroxiredoxins, and the presence of a second cysteine indicated it could use the atypical 2-Cys reaction mechanism.

After purification, the protein was investigated to determine its physical and biochemical properties. Dynamic light scattering measurement showed the protein was present as a single species, with an approximate diameter of 39 Å. This is close to the size of a monomer of related peroxiredoxin enzymes. Structural homology modelling of the protein using SWISS-MODEL agreed with this measurement, and suggested a protein structure containing the protein fold and active site conserved across all peroxiredoxins. Analysis of the melting curve of TaqPrx proved the thermal stability of the protein, giving a melting temperature of 87.5 °C, consistent with the known thermal tolerances of the *T. aquaticus* bacterium (Brock and Freeze 1969).

A novel mass spectrometry based activity assay was developed to test for peroxide reducing activity in TaqPrx, utilising the high reactivity of the active cysteine for hydrogen peroxide. This suggested that TaqPrx demonstrated peroxide reducing activity, as high reactivity to hydrogen peroxide was observed in one of its two cysteine residues. However further experimentation is necessary to confirm this result.

Crystals of TaqPrx were formed using the JCSG+ crystal screen. X-ray diffraction diffraction was poor, and fine screening was unable to produce for useful crystals. Further research would aim to produce a crystal structure for this enzyme, as it would confirm its structure as a member of the BCP-PrxQ peroxiredoxin group.

The experiments carried out on the peroxiredoxin of *T. aquaticus* confirmed that it has peroxiredoxin activity and a high level of thermal stability. They also showed that it lacks the self-assembly properties seen in the human peroxiredoxin investigated. However, it is likely that thermophilic enzymes exist that do display self-assembly, and identifying and investigating such enzymes would allow insight into how oligomerisation can be controlled at higher temperatures.

It was shown variant forms of peroxiredoxin enzymes can be produced by protein engineering that display altered quaternary structures, and that variants with altered quaternary structures show evidence of altered enzymatic activity. Further research could look at other mutations to residues involved in self-assembly either in the A-type interface, or in the regions closer to the active site involved in the structural shifts seen during catalysis. Another area to investigate is the interfaces involved in forming the stacks of rings seen in His-tagged hPrx3. A second result was the purification and identification of activity of a

previously unknown monomeric peroxiredoxin from *T. aquaticus*. While this protein does not show oligomeric activity, it does represent a member of a less well studied group of peroxiredoxins. Future work could aim to solve a crystal structure for this enzyme to confirm its structure.

In order to produce protein based self-assembling nanoscale devices, knowledge of the properties of proteins that allow this behaviour self-assembly is required. The work described in this thesis shows that peroxiredoxins are a useful model system for the investigation of these properties by protein engineering.

CHAPTER FIVE

General Methods

5.1 Chemicals, buffers and equipment

Chemical were generally purchased from Sigma-Aldritch, Invitrogen and Ajax Finechem. Protein standards for SDS-PAGE and SEC were purchased from Bio-Rad. Gateway cloning enzymes and DNA gel standards were purchased from Invitrogen. DNA and protein dyes were purchased from Roche. Filters were purchased from Sartorius Stedium Biotech. All columns used were from GE Healthcare.

All buffers were made in deionised water, except for buffers for TaqPrx activity assays (7.8) which used ultrapure water from Sigma. All buffers filtered using vacuum filtration. Buffer pH was adjusted by addition of HCl and NaOH and measured using a Denver Instrument UB-10 pH meter.

OD_{600} of cells was measured using a Bio-Rad Smartspec Plus spectrophotometer.

SDS-PAGE was carried out using a Bio-Rad Mini-PROTEAN Tetra Cell electrophoresis using precast gels.

All chromatography was carried out using a GE ÄKTA Explorer FPLC system. Samples were monitored by measuring UV absorbance at 280 nm.

For volumes of over 50 ml, centrifugation was carried out using a Sorvall RC6 plus centrifuge. For smaller volumes, either an Eppendorf 5819R centrifuge or an Eppendorf Minispin Plus centrifuge was used.

Protein was concentrated using Vivaspin 6 and 20 columns from GE Healthcare, using the appropriate molecular weight cutoff value for the protein used.

Protein concentration was measured using a NanoDrop ND 1000 spectrophotometer from Thermo Scientific after blanking with appropriate buffer, measuring absorbance at 280 nm.

All calculated molecular masses were found using the online tool Compute pI/MW tool from ExPASy (http://web.expasy.org/compute_pi/).

5.2 Bacterial cultures

All *E. coli* cultures were grown in sterile 20 gL^{-1} lysogeny broth (LB) in deionised water with the appropriate antiobiotics, shaking at 160 rpm. LB media were sterilised by autoclaving at 121°C. LB/Agar plates used for the growth of *E.coli* colonies were made using 20 gL^{-1} LB and 15 gL^{-1} agar dissolved in deionised water. This was sterilised by autoclaving at 121°C. Media were poured into sterile Petri dishes in a laminar flow hood and allowed to set before being sealed and stored at 4°C. Single colonies used to inoculate cultures were transferred using a sterile micropipette tip. Appropriate antibiotics were used in all cultures. Ampicillin (Amp) was used at 100 µg/ml, kanamycin (Kan) and chloramphenicol (Chl) were used at 30 µg/ml, and tetracycline was used at 15 µg/ml.

5.3 Plasmid extraction

Plasmids were purified from bacteria with an alkaline lysis based method using an Axygen Axyprep Plasmid Miniprep Kit. Bacteria were cultured overnight in 10 ml LB medium at 37°C. 4 ml of bacterial culture was pelleted by centrifugation at ~12,000 ×*g* for 1 minute. The supernatant was discarded and the pellet was resuspended in 250 µl of resuspension buffer. 250 µl of lysis buffer was then added, and the solution was mixed by inversion. 350 µl of neutralisation buffer was added and mixed by inversion. The solution was then centrifuged for 10 minutes at ~12,000 ×*g*, and the supernatant was transferred to a Miniprep column. This was centrifuged at ~12,000 ×*g* for 1 minute. 700 µl of wash buffer was applied to the column, which was again centrifuged for 1 minute at ~12,000 ×*g*. The filtrate was discarded, and 40 µl of eluant preheated to ~50 °C was added. This was allowed to stand for 1 minute at room temperature, before centrifugation for 1 minute at 12,000 ×*g*. Plasmid concentration was examined using a NanoDrop spectrophotometer measuring at 280 nm.

5.4 DNA gel electrophoresis

DNA gel electrophoresis was used to measure the size of plasmids and DNA fragments of interest. DNA gel electrophoresis was carried out using a 1% agarose/TAE gel, which were made by adding 0.3 g of agarose to 30 ml of TAE buffer (40 mM Tris, 20 mM acetic acid, 1 mM EDTA, pH 8.0). 3 µl of SybrSafe DNA dye was added to visualise DNA. Samples were prepared by adding 10 µl of sample to 2 µl of loading dye. 5 µl of 1 kb plus DNA ladder was used to estimate the size of sample DNA. Electrophoresis was carried out in TAE buffer, running at 110 V for 60 minutes. Gels were examined under UV light using a Syngene Chemi Genius^2 Bioimaging System.

5.5 Production of chemically competent cells

Cells were streaked out on LB/agar plates (containing Tet for XL1 Blue cells) and incubated overnight at 37 °C. Single colonies were used to inoculate 5 ml LB cultures, which were incubated overnight at 37 °C with shaking at 160 rpm. 4 ml was used to inoculate a 200 ml culture, which was incubated at 37 °C until it reached an OD_{600} of ~0.8. The culture was then cooled on ice for 15 minutes in sterile centrifuge bottles before centrifugation at 4,000 ×*g* for 10 minutes at 4 °C. Cells were resuspended in 40 ml of cooled, sterilised 100 mM $CaCl_2$, and then harvested by centrifugation at 4,000 ×*g* for 10 minutes at 4°C. Cells were finally resuspended in 8 ml 100 mM $CaCl_2$, and then frozen in liquid nitrogen in 100 µl aliquots. Competent cells were stored at -80°C.

5.6 Heat shock transformation

Transformation of chemically competent XL1 Blue and DH5α *Escherichia coli* (*E. coli*) cells was achieved using a heat shock method. Chemically competent cells were defrosted on ice in 100 µl aliquots. 1 µl of plasmid was added, and samples were incubated on ice for 30 minutes. Samples were heat shocked for 30 seconds at 42 °C. 1mL of LB media preheated to 37 °C was added, and samples were incubated at 37 °C with shaking at 160 rpm for 60 minutes. Cultured cells were pelleted by centrifugation at ~5,000 ×*g* for 1 minute. 900 µl of supernatant was removed and the pellet was resuspended in the remaining solution. This was used to inoculate an LB/Agar + Amp plate, which was incubated overnight at 37 °C.

Single colonies were selected and used to inoculate 10 ml LB media, which was incubated overnight at 37 °C with shaking at 160 rpm. Plasmid was extracted from cells (5.3). This was then used to transform chemically competent BL21 Star™ (DE3) cells using the above method.

5.7 Preparation of freezer stocks

Bacterial cells were cultured overnight at 37 °C in 10 ml of LB containing antibiotics appropriate for their growth. 1.5 ml of culture was harvested by centrifugation at ~12,000 ×*g* for 1 minute. This was resuspended in 750 µl of LB medium. 750 µl of 30% glycerol was added to the culture, and samples were frozen using liquid nitrogen and stored at -80 °C.

5.8 Protein SDS-PAGE

Protein gel electrophoresis was carried out using Bio-Rad Mini-PROTEAN TGX precast gels. Samples were prepared by adding 5 µl of protein sample to 4.75 µl Laemmli buffer and 0.25 µl β-mercaptoethanol, then heated at ~90°C for 5 minutes. 5 µl of Bio-Rad Precision Plus

Protein WesternC protein standard was used to determine band size. Gels were run for 30 minutes at 200 V. Gels were washed in deionised water for 2 minutes, then stained using SimplyBlue Coomassie-G250 stain.

5.9 Expression and purification of Tobacco etch virus protease

Tobacco etch virus (TEV) protease was expressed in *E. coli* and purified using a method based on that of Blommel and Fox (2007), which produces protease with a non-cleavable His-tag and a fused, TEV protease cleavable maltose binding protein domain (MBP). This increases solubility and yield. Single colonies of BL21 (DE3) *E. coli* containing a plasmid encoding the TEV gene were grown on a LB/Agar + Kan + Chl were used to inoculate 10 ml LB cultures. These were grown overnight at 37 °C overnight with shaking at 160 rmp, and were used to inoculate 0.5 l LB + Kan cultures. When the A_{600} reached ~0.8, expression was induced by adding IPTG to a concentration of 0.5 mM. Cultures were then incubated at 26 °C overnight with shaking at 160 rpm. Cells were harvested by centrifugation at 17,000 ×*g* and the supernatant was discarded. The cell pellet was resuspended in Buffer A (20 mM NaH_2PO_4, 500 mM NaCl, 0.3 mM TCEP, 50 mM imidazole, pH 7.5). Cells were lysed using a Microfluidics M-110P cell disrupter at 11500 Bar and cell debris was separated by centrifugation at 20,000 ×*g*. The supernatant was loaded onto a 5 ml GE HisTrap™ FF crude column, washed with the Buffer A and eluted using a gradient of Buffer B (20 NaH_2PO_4, 500 mM NaCl, 0.3 mM TCEP, 500 mM imidazole, pH 7.5). Fractions containing protein were then desalted using a GE HiPrep™ 26/10 desalting column into Buffer C (10 mM Tris, 0.3 mM TCEP, pH 7.5). Protein was incubated at 4 °C for 1 hour to allow cleaving of the MBP-tag, then loaded onto a GE HiTrap™ Q Sepharose FF anion exchange column. Protein was eluted with a gradient of Buffer D (10 mM Tris, 1000 mM NaCl, 0.3 mM Tris, pH 7.5). Protein containing fractions were pooled and diluted with Buffer C to bring the protein concentration to ~2 mg/ml. The protein was separated into 500 µl aliquots, 500 µl of glycerol was added to each and samples were frozen in liquid nitrogen and stored at -80 °C.

CHAPTER SIX

Experimental Methods (hPrx3)

Human peroxiredoxin 3 was examined in four forms: wild type hPrx3, His-tagged hPrx3, hPrx3 S78A, and His-tagged hPrx3 S78A to compare the oligomeric and self-assembly properties of each.

6.1 pEt 151 plasmids

Previous work in the Gerrard lab created (Zu and Littlejohn 2010, unpublished) a pEt 151 plasmid containing the gene for hPrx3 as well as mutant plasmid containing the gene for hPrx S78A. This plasmid attaches an N-terminal His_6-tag to the expressed protein. The tag is connected by a linker containing a TEV protease cleavage site and has the sequence:

HHHHHHGKPIPNPLLALDSTENLYFQ*EIDPFT

TEV cleavage occurs at the point marked with a '*' leaving 6 non-native amino acids attached to the protein. The calculated molecular masses of the hPrx3 variants are as follows: Wild type hPrx3 is 22.0 kDa, His-tagged hPrx3 is 25.2 kDa, hPrx3 S78A is 22.0 kDa, His-tagged hPrx3 S78A is 25.2 kDa.

6.2 Overexpression and purification

The method used for overexpression and purification was based on that of (Gourlay et al. 2003). Single colonies from LB/Agar + Amp plates were used to inoculate 10 ml LB + Amp cultures. These were grown overnight at 37°C with shaking at 160 rpm. These were used to inoculate 1 l LB + Amp cultures, which were grown at 37°C with shaking at 160 rpm until A_{600} reached ~0.6. Synthesis of protein was induced by adding IPTG to 0.3 mM and incubating cells overnight at 26°C with shaking at 160 rpm.

Cells were harvested by centrifugation at 8000 rpm and resuspended in a low imidazole buffer (30 mM imidazole, 500 mM NaCl, 20 mM NaH_2PO_4, pH 7.5). Cells were lysed by passing twice through a Microfluidics M-110P cell disrupter at 11500 Bar, and cell debris

was pelleted by centrifugation at 18000 rpm. Supernatant was loaded onto a 5 ml GE HisTrap™ FF crude column, washed with low imidazole buffer and eluted using a high imidazole buffer (300 mM imidazole, 500 mM NaCl, 20 mM NaH_2PO_4, pH 7.5), collecting in 1 ml fractions. Fractions were examined for protein content using a NanoDrop spectrophotometer measuring at 280 nm. Fractions containing protein were pooled.

1 mg of TEV protease was added to remove His-tags. This was then dialysed overnight into a cleavage buffer (20 mM Tris, 150 mM NaCl, 10 mM β-mercaptoethanol, pH 7.5), then incubated for 1 hour at 37°C.

TEV protease, cleaved His-tags and uncleaved proteins were separated from cleaved protein using a 5 ml GE HisTrap FF Crude column. Low imidazole buffer to elute before washing any bound proteins from the column using high imidazole buffer. 1 ml fractions were collected and the protein concentration was determined using a NanoDrop spectrophotometer. Protein containing fractions were pooled and desalted into a storage buffer (20 mM Tris, 150 mM NaCl, pH 7.5) using a GE 5 ml GE HiPrep 26/10 desalting column.

Cleaved protein was then desalted into a low salt buffer (20 mM Tris, pH 8.0) and loaded onto a GE HiTrap Q Sepharose FF anion exchange column. Protein was eluted using a gradient of high salt buffer (20 mM Tris, 1 M NaCl, pH 8.0). Samples containing protein were collected, then desalted into a storage buffer (20 mM Tris, 150 mM NaCl, pH 7.5).

To produce protein with the His-tag attached, tagged protein was desalted into low salt buffer and loaded onto the anion exchange column. His-tagged protein was eluted with a gradient of high salt buffer and protein containing fraction were pooled and desalted into a storage buffer.

Purification was analysed using SDS-PAGE (5.8).

6.3 Transition electron microscopy

Samples were prepared for examination by TEM using a Morgagni 268D TEM, measuring at 100 kV and capturing images using a SIS/Olympus Megapixel III digital camera. Samples were prepared on copper grids coated with formvar, size 200 mesh from ProSciTech. 10 µl of protein was added, then rinsed 3 times with distilled water. Samples were then negatively stained using 3% uranyl acetate.

Wild-type and tagged wild-type protein was examined at concentrations of 1 and 10 mg/ml in 20 mM Tris, 150 mM NaCl, pH 7.5 buffer. Tagged protein was also examined at concentrations between 3 and 5 mg/ml and $NiCl_2$ concentrations of between 1, 2, 5 and 10 mg/ml.

6.4 Analytical size exclusion chromatography

6.4.1 Concentration, pH and buffer variations

Protein oligomeric structure was estimated using analytical size exclusion chromatography (SEC). A GE Sephadex 200 10/300 GL column was used. The column was first calibrated with Bio-Rad Gel Filtration Standards (bovine thyroglobulin, 670 kDa; γ-globulin, 158 kDa; chicken ovalbumin, 44 kDa; horse myoglobin, 17 kDa and vitamin B_{12}, 0.135 kDa). Wild type hPrx3, hPrx3 S78A and His-tagged hPrx3 were examined in the following conditions:

20 mM Tris, 150 mM NaCl, pH 7.5

20 mM Tris, 150 mM NaCl, 10 mM DTT pH 7.5

20 mM NaPi, 150 mM NaCl, pH 7.5

20 mM NaPi, 150 mM NaCl, 10 mM DTT pH 7.5

20 mM Tris, 150 mM NaCl, pH 9.0

20 mM Tris, 150 mM NaCl, 10 mM DTT pH 9.0

20 mM NaPi, 150 mM NaCl, pH 6.0

20 mM NaPi 150 mM NaCl, 10 mM DTT pH 6.0

At each condition, protein was analysed at concentrations of 1, 5 and 10 mg/ml. Elution was monitored for protein by recording the UV absorbance at 280 nm.

6.4.2 EDTA and His-tagged hPrx3

The oligomeric structure of His-tagged hPrx3 was investigated by SEC using a GE Sephadex 200 10/300 GL column. The column was calibrated with Bio-Rad Gel Filtration Standards (bovine thyroglobulin, 670 kDa; γ-globulin, 158 kDa; chicken ovalbumin, 44 kDa; horse myoglobin, 17 kDa and vitamin B_{12}, 0.135 kDa). The protein was examined in 20 mM

Tris, 150 mM NaCl, 10 mM EDTA, pH 7.5, at concentrations of 1, 5 and 10 mg/ml. Elution was monitored for the protein by recording the UV absorbance at 280 nm.

6.5 SAXS measurement

SAXS measurements of wild type and wild type tagged hPrx3 were made at the SAXS-WAXS beamline of the Australian Synchrotron in Melbourne, Australia. Proteins were examined at ~4 mg/ml in storage buffer (20 mM Tris, 150 mM NaCl, pH 7.5). Samples were run through a 3 ml gel filtration column at a flow rate of 0.2 ml/min before passing through a 1 mm quartz capillary. Measurements were collected every 2 seconds, at 25 °C. Scattering intensity was compared to elution time, and measurements that showed protein were averaged. Scattering was normalised by comparison to water scatter and the resulting forward scatter was used to estimate the molecular weights of the scattering species. A 1.6 m camera was used, which provided a q range from 0.01 to 0.5 $Å^{-1}$, where q is the magnitude of the scattering vector, and is related to the scattering angle (2θ) and the wavelength (λ) by the equation: $q = (4\pi/\lambda)$. Data were collected on a Pilatus 1M detector (170 mm×170mm, effective pixel size 172×12 μm)

Averaging of images, subtraction of blanks and radial integration was performed using the beamline control software ScatterBrain (Australian Synchrotron). Further analysis was carried out using the ATSAS software package (Konarev et al. 2006; Petoukhov et al. 2012) from EMBL Hamburg (http://www.embl-hamburg.de/biosaxs/software.html).

6.6 Competitive activity assay

The activity of wild type, tagged wild type and S78A hPrx3 was estimated using a competitive assay with horseradish peroxidase (HRP). HRP contains a heme group that absorbs at 403 nm, but loses this absorbance when it reacts with H_2O_2. The assay compares the decrease of absorbance seen when hPrx3 is in competition with HRP for a limited amount of H_2O_2 and is based on that of Oguscu et al. (2007).

Protein samples were reduced with 70 mM β-mercaptoethanol and incubated on ice for 60 minutes. Samples were then desalted into 100μ 50 mM NaH_2PO_4, 100 μM DTPA, pH 7.5 using a Bio-Rad Bio-spin 6 desalting column. This buffer was prepared with ultrapure water to ensure no oxidising agents were present. Exact protein concentration after buffer exchange was determined using the Lowry assay (Lowry et al. 1951). HRP concentration used in each assay was determined by measurement of absorbance at 403 nm, and that of

H_2O_2 used was determined by measurement of absorbance at 240 nm. Absorbance measurements were carried out using an Agilent 8453 UV-visible spectroscopy system in a quartz cuvette with a 10 mm path length.

Absorbance was first measured of HRP alone, which was done by adding 5 µl of HRP was to 95 µl of buffer. Next, the absorbance of HRP in the presence of H_2O_2 was measured, by adding 5 µl of HRP and 5 µl of H_2O_2 to 90 µl of buffer. Absorbance of HRP was then measured in the presence of H_2O_2 and increasing concentrations of enzyme samples. Measurements were made immediately after addition of H_2O_2, to limit reduction of oxidised hPrx3 by reduced HRP.

CHAPTER SEVEN

Experimental Methods (TaqPrx)

7.1.1 Comparisons of thermophilic peroxiredoxin genes to hPrx3

The amino acid sequences of six thermophilic peroxiredoxin enzymes from both bacteria and archaea were identified in the Genbank database (www.ncbi.nlm.nih.gov) (Benson et al. 2000). From achaea, the amino acid sequences for peroxiredoxins from *Pyrococcus furiosus*, *Pyrobaculum aerophilum*, *Sulfolobus acidocaldarius* and *Ignisphaera aggregans* were identified, while from bacteria, sequences from *Thermotoga maritima* and *T. aquaticus* were identified. These were aligned together with the hPrx3 using Clustal Omega www.ebi.ac.uk/Tools/msa/clustalo/) (Sievers et al. 2011) to search for sequences similar to hPrx3.

7.1.2 The *TaqPRDX1* gene

Genomic DNA from the bacterium *T. aquaticus* was obtained from Professor Hugh Morgan of the University of Waikato. Examination of the Genbank database found a gene that was a likely peroxiredoxin candidate, containing the key active site motif found in all Prx proteins. This was annotated as 'Alkyl hydroperoxidase reductase/Thiol specific antioxidant/Mal allergen [*Thermus aquaticus* Y51MC23]' with accession number ZP_03495958.1. Four other *T. aquaticus* proteins were identically annotated (Table X), however none contained the key peroxiredoxin catalytic motif, PXXXTXXC (1.5.2) (Poole 2007). Examination of the sequence using the Peroxiredoxin Classification Index (PREX) (www.csb.wfu.edu/prex/) (Soito et al. 2010) showed that the protein was likely a 1-Cys peroxiredoxin in the BCP-PrxQ class. The sequence was also examined for rare codons using an online rare codon calculator tool, (www.nihserver.mbi.ucla.edu/RACC).

7.2 Gateway cloning of *TaqPRDX1*

7.2.1 PCR

The *TaqPRDX1* gene was cloned into a plasmid using the Gateway system from Invitrogen (Walhout et al. 2000). Primers were designed using the NetPrimer tool at

(www.premierbiosoft.com/netprimer/) and ordered from IDT DNA. The sequence for the gene-specific primers was:

Forward: 5' – GGC AGC GGC GCG **ATG CCC GGC ATG GAA** – 3'
Reverse: 5' – GAA AGC TGG GTG **CTA CTC CCC CCT TGC CT** – 3'
The bold section complements the genomic DNA sequence, while non-bold sections introduce binding sites for the second set of primers.
Reactions contained:

T. aquaticus genomic DNA	0.25 µl
dNTP mix	2 µl
5× PrimeSTAR® Buffer	5 µl
Gene specific primer (forward)	0.75 µl
Gene specific primer (reverse)	0.75 µl
PrimeSTAR® HS Polymerase	0.25 µl
dH_2O	16 µl

PCR was carried out in a Eppendof Mastercycle Gradient Thermocycler. Parameters were:

Step	Temperature	Time
Initial Denaturation	98°C	10 min
25 Cycles of:		
Denaturation	98°C	5 sec
Annealing	60 / 65°C	5 sec
Extension	72°C	60 sec
1 Repeat of:		
Final Extension	72°C	120 sec
Hold	4°C	-

Reactions were run at both 60°C and 65°C. Products were analysed by gel electrophoresis on a 1% agarose gel at 100 V for 40 minutes. SybrSafe dye was used for visualisation at 280 nm. Products were used for the second PCR reaction. The generic primers used were:

Forward: 5' – GGGG **ACA AGT TTG TAC AAA AAA GCA GGC T**TC GAA AAC CTG TAT TTT CAG GGC AGC CGC GCG – 3'

Reverse: 5' – GGGG **AC CAC TTT GTA CAA GAA AGC TGG GT**G – 3'

The bold section introduces the attB sites to the linear fragment produced by reaction 1.

This reaction contained:

PCR 1 product	1 µl

dNTP mix	4 µl
5X PrimeSTAR® Buffer	10 µl
Generic primer (forward)	1.5 µl
Generic primer (reverse)	1.5 µl
PrimeSTAR® HS Polymerase	0.5 µl
dH_2O	to 50 µl

The reaction was run in the same thermocycler as the previous reaction, with the parameters:

Step	Temperature	Time
Initial Denaturation	94°C	10 min
10 Cycles of:		
Denaturation	94°C	20 sec
Annealing	45°C	5 sec
Extension	72°C	1 min
20 Cycles of:		
Denaturation	94°C	15 sec
Annealing	45°C	5 sec
Extension	72°C	1 min
Final Extension	72°C	2 min
Hold	4°C	-

Products were analysed by gel electrophoresis on a 1% agarose gel at 100 V for 40 minutes. SybrSafe dye was used for visualisation at 280 nm.

7.2.2 Cloning of *TaqPRDX1* into pDONR221 donor plasmid

Product from PCR reaction 2 was inserted into the donor plasmid pDONR 221 using the BP reaction (3.2). The reaction mixture contained:

PCR 2 product	2.5 µl
pDONR 221 plasmid	0.5 µl
BP clonase II	1 µl
dH_2O	1 µl

This was incubated at room temperature for 5 hours. Proteinase K was then added to digest the clonase enzyme, and the reaction was incubated at 37°C for 10 minutes.

7.2.3 Transformation of pDONR221 plasmid into *E.coli* DH5α

Plasmids were then transformed into electro DH5α *E. coli* cells using a Bio-Rad Micropulser^{TM} in a 0.2 cm electroporation cuvette. 1 ml of LB medium (10 gl^{-1}) was added and cells were incubated at 37°C for 1 hour, then plated on an LB/Agar + Kan and incubated at 37°C overnight. Single colonies were selected to inoculate 10 ml LB + Kan cultures, which were incubated at 37°C overnight with shaking at 160 rpm.

7.2.4 BsrG1 digest of pDONR221 plasmid

Plasmids were extracted (5.3) and digested using the restriction enzyme BsrG1 to determine if the gene insertion was successful. The reaction mixture was:

pDONR211 plasmid	5 µl
BSA	1 µl
10x 'Buffer 2'	1 µl
BsrG1 enzyme	0.5 µl
dH_2O	2.5 µl

Reactions were incubated at 37°C for 2 hours, and products were analysed by gel electrophoresis using a 1% agarose gel ran at 100 V for 40 minutes. SybrSafe dye was used for visualisation at 280 nm. Samples containing inserts of an appropriate size were sequenced using an Applied Biosystems 9700 Gold Block thermal cycler.

7.2.5 Cloning of *TaqPRDX1* into pDEST 17 expression plasmid

The gene was then cloned into the expression vector pDEST17, which adds an N-terminal His-Tag connected to the protein by a linker including a TEV protease cleavage site. The reaction mixture was:

pDONR211 Plasmid	1 µl
pDEST 17 vector	0.5 µl
LR Clonase II	1 µl
dH_2O	2.5 µl

The mixture was incubated at room temperature for 5 hours. Proteinase K was then added to digest the clonase enzyme, and the reaction was incubated at 37°C for 10 minutes.

7.2.6 Transformation of pDEST17 into *E.coli* Rosetta

Plasmids were transformed into electrocompetent Rosetta *E. coli* cells by electroporation using a Bio-Rad Micropulser^{TM} in a 0.2 cm electroporation cuvette. 1 ml of LB medium was added and cells were incubated at 37°C for 1 hour, and then plated on a LB/agar + Amp +

Kan plates and incubated overnight at 37°C. Plasmids were extracted (5.3) and insertion was confirmed using a BsrG1 and DNA sequencing (7.2.4). Freezer stocks were also produced (5.7).

7.3 Overexpression and purification of TaqPrx

Freezer stocks of *E. coli* Rosetta cells containing pDEST17 with the TaqPrx gene were cultured on an LB/agar + Amp + Kan plate overnight at 37°C. Single colonies were used to inoculate 10 ml LB + Amp + Kan cultures. These were grown overnight at 37°C, shaking at 160 rpm. These cultures were used to inoculate 1 l LB + Amp + Kan cultures, which were grown at 37°C, shaking at 160 rpm until the OD_{600} reached ~0.6. Synthesis of TaqPrx was induced by adding IPTG to 0.3 mM and incubating cells at 26°C with 160 rpm shaking overnight.

Cells were then harvested by centrifugation at 8000 rpm and resuspended in a low imidazole buffer (30 mM imidazole, 500 mM NaCl, 20 mM NaH_2PO_4, pH 7.5). Cells were lysed in a Microfluidics M-110P cell disrupter at 11500 bar, and cell debris was pelleted by centrifugation at 18000 rpm. Supernatant was loaded onto a 5 ml GE HisTrap™ FF Crude column, washed with low imidazole buffer and eluted using a high imidazole buffer (300 mM imidazole, 500 mM NaCl, 20 mM NaH_2PO_4, pH 7.5), collecting 1 ml fractions. Fractions were examined for protein content using a NanoDrop spectrophotometer measuring at 280 nm. Fractions containing protein were pooled and 1 mg of TEV protease (5.9) was added. This was then dialysed overnight into a cleavage buffer (20 mM Tris, 150 mM NaCl, 10 mM β-mercaptoethanol, pH 7.5), then incubated for 1 hour at 37°C.

Cleaved protein was separated from protease, cleaved His-tags and uncleaved protein using a 5 ml GE HisTrap FF Crude column, using low imidazole buffer to elute before washing any bound proteins from the column using high imidazole buffer. 1 ml fractions were collected and examined for protein using a NanoDrop spectrophotometer. Protein containing fractions were pooled and desalted into a low salt buffer (20 mM Tris, pH 8.0) using a 5 ml GE HiTrap 26/10 desalting column. Cleaved protein was loaded onto a GE HiTrap Q Sepharose FF anion exchange column. Protein was eluted using a gradient of high salt buffer (20 mM Tris, 1 M NaCl, pH 8.0). Samples containing TaqPrx were collected, then desalted into a storage buffer (20 mM Tris, 150 mM NaCl, pH 7.5)

Samples from each step of the purification were examined by SDS-PAGE (5.8).

7.4 Protein melting temperature analysis

The temperature of denaturation of TaqPrx was examined using a Bio-Rad iCycler iQ5. 25 µl samples were prepared in a 96 well plate, each containing 2.5 µl of 50× Sypro Orange protein dye and 22.5 µl of 1 mg/ml TaqPrx in 20 mM Tris, 150 mM NaCl, pH 7.5. Blanks were prepared containing 2.5 µl of 50× Sypro Orange protein dye and 22.5 µl 20 mM Tris, 150 mM NaCl, pH 7.5 buffer. Both samples and blanks were run in triplicate, and heated from 20°C to 100°C, measuring fluorescence every 0.5°C.

7.5 Dynamic light scattering measurement of TaqPrx

Oligomeric state of TaqPrx was examined using a Malvern Zetasizer Nano. Samples of 1 mg/ml TaqPrx were desalted into phosphate buffered saline solution (137 mM NaCl, 2.7 mM KCl, 10 mM Na_2HPO_4. 1 mM KH_2PO_4, pH 7.4). Six 1 ml samples were analysed, allowing the software to identify the correct attenuation level for the laser. Samples showing the highest level of agreement were combined and used for analysis.

7.6 Structural homology modelling

The online program SWISS-MODEL from ExPASy (www.swissmodel.expasy.org/) was used to model the structure of TaqPrx from its amino acid sequence (Arnold et al. 2006; Kiefer et al. 2009; Peitsch 1995). The amino acid sequence of TaqPrx was entered, and the modelling program run in automated mode, which allows the program to search the PDB for a sequence that aligns with the query on which to base its model.

The accuracy of the model was examined using the QMEAN4 tool provided by SWISS-MODEL (Benkert, Tosatto, and Schomburg 2008; Benkert, Biasini, and Schwede 2011) as well as structural alignment with other peroxiredoxin enzymes using the program PyMOL from DeLano Scientific.

7.7 Sparse matrix crystal screening

7.7.1 Initial screening

A Hampton Research pre-crystallisation test was carried out in order to find the appropriate protein concentration for further screening. Two samples were prepared containing TaqPrx at a concentration of 10 mg/ml using a hanging drop method, with reservoir solutions of 0.1 M Tris, 2.0 M $(NH_4)_2SO_4$, pH 8.5 and 0.1 M Tris, 0.2 M MgCl $(H_2O)_6$, 30% (w/v) PEG 4000,

pH 8.5. Incubation overnight gave a light precipitate in both conditions, showing that concentration was appropriate for crystal screening.

Robotic crystal screening was carried out using a Hamilton Robotics Cartesian Honeybee Nanodispensor at the University of Auckland. Screens were of in-house design, based on the Hampton Crystal Screen, Hampton Crystal Screen 2 and Hampton Index screen. Drops were examined after 24 hours using a Leica Microsystems optical microscope, then every two days over several weeks.

Conditions that showed evidence of crystal structure were recorded. Fresh samples were prepared with similar conditions in order to find conditions that would promote larger crystal growth. The hanging drop vapour diffusion method was used in 24 well Hampton crystallisation plates. The conditions used are summarised in Table 7.1 and 7.2.

1.1 M $AmSO_4$ pH 4.0	1.2 M $AmSO_4$ pH 4.0	1.3 M $AmSO_4$ pH 4.0	1.4 M $AmSO_4$ pH 4.0	1.5 M $AmSO_4$ pH 4.0	1.6 M $AmSO_4$ pH 4.0
1.1 M $AmSO_4$ pH 4.5	1.2 M $AmSO_4$ pH 4.5	1.3 M $AmSO_4$ pH 4.5	1.4 M $AmSO_4$ pH 4.5	1.5 M $AmSO_4$ pH 4.5	1.6 M $AmSO_4$ pH 4.5
1.1 M $AmSO_4$ pH 5.0	1.2 M $AmSO_4$ pH 5.0	1.3 M $AmSO_4$ pH 5.0	1.4 M $AmSO_4$ pH 5.0	1.5 M $AmSO_4$ pH 5.0	1.6 M $AmSO_4$ pH 5.0
1.1 M $AmSO_4$ pH 5.5	1.2 M $AmSO_4$ pH 5.0	1.3 M $AmSO_4$ pH 5.0	1.4 M $AmSO_4$ pH 5.0	1.5 M $AmSO_4$ pH 5.0	1.6 M $AmSO_4$ pH 5.0

Table 7.1 Fine screen of potential crystallisation conditions. All conditions contain 0.1 M CH_3COONa. $AmSO_4$ is $(NH_4)_2SO_4$.

1.7 M $AmSO_4$ pH 4.0	1.8 M $AmSO_4$ pH 4.0	1.9 M $AmSO_4$ pH 4.0	2.0 M $AmSO_4$ pH 4.0	2.1 M $AmSO_4$ pH 4.0	2.2 M $AmSO_4$ pH 4.0
1.7 M $AmSO_4$ pH 4.5	1.8 M $AmSO_4$ pH 4.5	1.9 M $AmSO_4$ pH 4.5	2.0 M $AmSO_4$ pH 4.5	2.1 M $AmSO_4$ pH 4.5	2.2 M $AmSO_4$ pH 4.5
1.7 M $AmSO_4$ pH 5.0	1.8 M $AmSO_4$ pH 5.0	1.9 M $AmSO_4$ pH 5.0	2.0 M $AmSO_4$ pH 5.0	2.1 M $AmSO_4$ pH 5.0	2.2 M $AmSO_4$ pH 5.0
0.2 M $AmSO_4$ 24% mPEG2K	0.2 M $AmSO_4$ 26% mPEG2K	0.2 M $AmSO_4$ 28% mPEG2K	0.2 M $AmSO_4$ 30% mPEG2K	0.2 M $AmSO_4$ 32% mPEG2K	0.2 M $AmSO_4$ 34% mPEG2K

Table 7.2 Fine screen of potential crystallisation conditions. All conditions contain 0.1 M CH_3COONa, all conditions containing mPEG 2,000 are at pH 4.0. $AmSO_4$ is $(NH_4)_2SO_4$, mPEG2K is mPEG 2,000.

Crystal streaking was also used to try and seed growth of TaqPrx crystals (Stura and Wilson 1991). A hair was run through droplets containing microcrystals, then consecutively through 6 droplets of buffers that did not form microcrystals in the earlier screen. Microcrystals were streaked from two conditions, termed I and II. I was: 1.7 M $(NH_4)_2SO_4$, 0.1 M CH_3COONa at pH 4.5. II was 1.5 M $(NH_4)_2SO_4$, 0.1 M CH_3COONa at pH 4.0. Microcrystals from I and II were each streaked through four conditions. These are summarised in Table 7.3.

1.1 M $AmSO_4$ pH 4.5	1.3 M $AmSO_4$ pH 4.5
1.1 M $AmSO_4$ pH 5.0	1.3 M $AmSO_4$ pH 5.0

Table 7.3 Fine screen of potential crystallisation conditions. All conditions contain 0.1 M CH_3COONa. $AmSO_4$ is $(NH_4)_2SO_4$.

7.7.2 JCSG+ and PACT screening

A second sample of TaqPrx was prepared at screened at the Collaborative Crystallisation Centre in Melbourne, Australia. TaqPrx was used at 15 mg/ml in two screens, JCSG+ and (OTHER). A crystal produced by the screen was examined at the MX1 Beamline at the Australian Synchrotron in Melbourne, Australia.

TaqPrx samples were prepared in condition similar to those that produced the observed crystals in an effort to produce larger and more useful crystals. Conditions used are summarised in Table 7.4.

50 mM $LiSO_4$ 40% PEG 400	100 mM $LiSO_4$ 40% PEG 400	150 mM $LiSO_4$ 40% PEG 400	200 mM $LiSO_4$ 40% PEG 400	250 mM $LiSO_4$ 40% PEG 400	300 mM $LiSO_4$ 40% PEG 400
50 mM $LiSO_4$ 45% PEG 400	100 mM $LiSO_4$ 45% PEG 400	150 mM $LiSO_4$ 45% PEG 400	200 mM $LiSO_4$ 45% PEG 400	250 mM $LiSO_4$ 45% PEG 400	300 mM $LiSO_4$ 45% PEG 400
50 mM $LiSO_4$ 50% PEG 400	150 mM $LiSO_4$ 50% PEG 400	150 mM $LiSO_4$ 50% PEG 400	200 mM $LiSO_4$ 50% PEG 400	250 mM $LiSO_4$ 50% PEG 400	300 mM $LiSO_4$ 50% PEG 400
50 mM $LiSO_4$ 55% PEG 400	150 mM $LiSO_4$ 50% PEG 400	200 mM $LiSO_4$ 50% PEG 400	200 mM $LiSO_4$ 50% PEG 400	250 mM $LiSO_4$ 50% PEG 400	300 mM $LiSO_4$ 50% PEG 400

Table 7.1 Fine screen of potential crystallisation conditions. All conditions contain 0.1 M CH_3COONa and are at pH 4.5.

7.8 Activity assay

Purified TaqPrx was examined for evidence of peroxide reducing activity. This was done using mass spectrometry to determine if the purported reactive cysteine of the protein reacted with H_2O_2.

Protein at 3 mg/ml was desalted using a Bio-Rad BioSpin desalting column into a reduction buffer (20 mM Tris, 1 mM β-ME at pH 7.5). This, and all other buffers used in the assay were made with ultrapure water to ensure the absence of any oxidants. Samples were incubated at room temperature for 30 minutes, then desalted into a storage buffer (20 mM Tris, pH 7.5), leaving reduced protein in the absence of any oxidants.

The first sample was made by adding NEM (*N*-ethylmaleimide) to 1 mM into a sample of reduced protein. The sample was incubated at room temperature for 10 minutes, before being desalted back into storage buffer.

The second sample was made by adding H_2O_2 to 1 mM into a sample of reduced protein. This was incubated at room temperature for 10 minutes, and then desalted into storage buffer. Following this, NEM was added to 1 mM and the sample was incubated at room temperature for a further 10 minutes. Finally protein was desalted back into storage buffer.

The third sample was reduced protein in the storage buffer.

The concentration of all samples was examined using a NanoDrop spectrophotometer measuring at 280 nm. All samples were diluted in storage buffer to a concentration of ~1 mg/ml and analysed by mass spectrometry using a Bruker maXis 3G mass spectrometer to look for differences in molecular weights of the species present.

References

Ali, M.H. and Imperiali, B. (2005) Protein oligomerization: How and why. *Bioorganic & Medicinal Chemistry* **13**: 5013–5020.

Allen, R.G, and Tresini, M. 2000. Oxidative stress and gene regulation. *Free Radical Biology and Medicine* 28: 463–499.

Alphey, M.S., Bond, C. S., Tetaud, E., Fairlamb, A.H. and Hunter, W.N. (2000) The structure of reduced tryparedoxin peroxidase reveals a decamer and insight into reactivity of 2Cys-peroxiredoxins. *Journal of Molecular Biology* **300**: 903–916.

Angelescu, D.G. and Linse, P. (2008). Viruses as supramolecular self-assemblies: Modelling of capsid formation and genome packaging. *Soft Matter* **4**: 1981.

Ansari, S. and Helms, V. (2005) Statistical analysis of predominantly transient protein–protein interfaces. *Proteins: Structure, Function, and Bioinformatics* **61**: 344–355.

Arnold, K., Bordoli, L., Kopp, J. and Schwede, T. (2006) The SWISS-MODEL workspace: A web-based environment for protein structure homology modelling. *Bioinformatics* **22**:195–201.

Astier, Y., Bayley, H., and Howorka, S. (2005). Protein components for nanodevices. *Current Opinion in Chemical Biology* **9**: 576–584

Barranco-Medina, S., Kakorin, S., Lázaro, J.J. and Dietz, K.-J. (2008) Thermodynamics of the dimer−decamer transition of reduced human and plant 2-Cys peroxiredoxin. *Biochemistry* **47**: 7196–7204.

Barranco-Medina, S., Lázaro, J.J. and Dietz, K.-J. (2009) The oligomeric conformation of peroxiredoxins links redox state to function. *FEBS Letters* **583**:1809–1816.

Bath, J. and Turberfield, A.J. (2007) DNA nanomachines. *Nature Nanotechnology* **2**: 275–284.

Benesch, J. L. P., Ayoub, M., Robinson, C.V. and Aquilina J.A. (2008) Small heat shock protein activity is regulated by variable oligomeric substructure. *Journal of Biological Chemistry* **283**: 28513–28517.

Benkert, P., Biasini, M. and Schwede, T. (2011) Toward the estimation of the absolute quality of individual protein structure models. *Bioinformatics* **27**: 343–350.

Benkert, P., Schwede, T., and Tosatto, S. (2009) QMEANclust: Estimation of protein model quality by combining a composite scoring function with structural density information. *BMC Structural Biology* **9**: 35.

Benkert, P, Tosatto, S.C.E. and Schomburg, D. (2008) QMEAN: A comprehensive scoring function for model quality assessment. *Proteins: Structure, Function, and Bioinformatics* **71**: 261–277.

Benson, D.A., Karsch-Mizrachi, I., Lipman, D.J., Ostell, J., Rapp, B.A. and Wheeler, D.L. (2000) GenBank. *Nucleic Acids Research* **28**: 15.

Berne, B.J., and Pecora, R. (2000) *Dynamic light scattering: With applications to chemistry, biology, and physics*. Courier Dover Publications.

Bernier-Villamor, L., Navarro, E., Sevilla, F., and Lázaro J.-J. (2004) Cloning and characterization of a 2-Cys peroxiredoxin from *Pisum sativum*. *Journal of Experimental Botany* **55**: 2191 –2199.

Biteau, B., Labarre, J., and Toledano, M.B. (2003) ATP-dependent reduction of cysteine–sulphinic acid by *S. Cerevisiae* Sulphiredoxin. *Nature* **425**: 980–984.

Blommel, P.G., and Fox, B.G. (2007) A combined approach to improving large-scale production of tobacco etch virus protease. *Protein Expression and Purification* **55**: 53–68.

Bogan, A.A, and Thorn, K.S. (1998) Anatomy of hot spots in protein interfaces. *Journal of Molecular Biology* **280**: 1–9.

Boveris, A., and Chance, B. (1973) The mitochondrial generation of hydrogen peroxide. General properties and effect of hyperbaric oxygen. *Biochemical Journal* **134**: 707.

Brock, T.D., and Freeze, H. (1969) *Thermus aquaticus* Gen. N. and Sp. N., a nonsporulating extreme thermophile. *Journal of Bacteriology* **98**: 289.

Bromley, E.H. C., Channon, K., Moutevelis, E. and Woolfson, D.N. (2008) Peptide and protein building blocks for synthetic biology: From programming biomolecules to self-organized biomolecular systems. *ACS Chem. Biol.* **3**: 38–50.

Bryk, R., Griffin, P. and Nathan, C. (2000) Peroxynitrite reductase activity of bacterial peroxiredoxins. *Nature* **407**: 211–215.

Cao, Z., Bhella, D. and Lindsay, J.G. (2007) Reconstitution of the mitochondrial PrxIII antioxidant defence pathway: General properties and factors affecting PrxIII activity and oligomeric state. *Journal of Molecular Biology* **372**: 1022–1033.

Cao, Z., Lindsay, J.G. and Isaacs, N.W. (2007) Mitochondrial peroxiredoxins. *Subcellular Biochemistry*, **44**:295–315.

Cao, Z., Roszak, A.W., Gourlay, L.J., Lindsay, J.G. and Isaacs, N.W. (2005) Bovine mitochondrial peroxiredoxin III forms a two-ring catenane. *Structure* **13**: 1661–1664.

Chae, H.Z., Robison, K., Poole, L.B. Church, G., Storz, G, and Rhee, S.G. (1994) Cloning and sequencing of thiol-specific antioxidant from mammalian brain: Alkyl hdroperoxide reductase and thiol-specific antioxidant define a large family of antioxidant enzymes. *Proceedings of the National Academy of Sciences* **91**: 7017 –7021.

Choi, H.-J., Kang, S.W. Yang, C.-H. Rhee, S.G. and Ryu, S.-E.. (1998) Crystal structure of a novel human peroxidase enzyme at 2.0 Å resolution. *Nature Structural & Molecular Biology* **5**: 400–406.

Cox, A.G., Peskin, A.V., Paton, L.N., Winterbourn, C.C and Hampton, M.B. (2009) Redox potential and peroxide reactivity of human peroxiredoxin 3. *Biochemistry* **48**: 6495–6501.

Cox, A.G., Winterbourn, C.C and Hampton, M.B. (2010) Mitochondrial peroxiredoxin involvement in antioxidant defence and redox signalling. *Biochemical Journal* **425**: 313–325.

D'Ambrosio, K., Limauro, D., Pedone, E., Galdi, I., Pedone, C., Bartolucci, S. and De Simone, G. (2009) Insights into the catalytic mechanism of the Bcp family: Functional and structural analysis of Bcp1 from *Sulfolobus solfataricus*. *Proteins: Structure, Function, and Bioinformatics* **76**: 995–1006.

Dekker, C., Willison, K.R. and Taylor, W.R. (2011) On the evolutionary origin of the caperonins. *Proteins: Structure, Function, and Bioinformatics* **79**: 1172–1192.

Deponte, M. and Becker, K. (2005) Biochemical characterization of *Toxoplasma gondii* 1-Cys peroxiredoxin 2 with mechanistic similarities to typical 2-Cys Prx. *Molecular and Biochemical Parasitology* **140**: 87–96.

Dill, Ken A. (1990) Dominant forces in protein folding. *Biochemistry* **29**: 7133–7155.

Dolman, D., Newell, G.A., Thurlow, M.D. and Dunford, H.B. (1975) A kinetic study of the reaction of horseradish peroxidase with hydrogen peroxide. *Biochemistry and Cell Biology* **53**: 495–501.

Edgar, R.S., Green, E.W., Zhao, Y., van Ooijen, G., Olmedo, M., Qin, X. and Xu, Y. (2012) Peroxiredoxins are conserved markers of circadian rhythms. *Nature* **485**: 459–464.

Ferrer-Sueta, G. and Radi R. (2009) Chemical biology of peroxynitrite: Kinetics, diffusion, and radicals. *ACS Chem. Biol.* **4**: 161–177.

Frisken, Barbara J. (2001) Revisiting the method of cumulants for the analysis of dynamic light-scattering data. *Applied Optics* **40**: 4087–4091.

Gourlay, L.J, Bhella, D., Kelly, S.M., Price, N.C. and Lindsay, J.G. (2003) Structure-function analysis of recombinant substrate protein 22 kDa (SP-22): A mitochondrial 2-Cys peroxiredoxin organised as a decameric toroid. *Journal of Biological Chemistry* **278**: 32631–32637.

Griffin, M.D.W. and Gerrard, J.A. (2012) The relationship between oligomeric state and protein function. *Advances in Experiment Medicine and Biology*, **747**:74–90. New York, NY: Springer New York.

Griffin, M.D.W., Dobson, R.C.J., Pearce, F.G., Antonio, L., Whitten, A.E., Liew, C.K. and Mackay, J.P. (2008) Evolution of quaternary structure in a homotetrameric enzyme. *Journal of Molecular Biology* **380**: 691–703.

Guimarães, B.G., Souchon, H., Honoré, N., Saint-Joanis, B., Brosch, R., Shepard, W., Cole, S.T. and Alzari, P.M. (2005) Structure and mechanism of the alkyl hydroperoxidase AhpC, a key element of the *Mycobacterium tuberculosis* defense system against oxidative stress. *Journal of Biological Chemistry* **280**: 25735–25742.

Hall, A.P., Karplus, A. and Poole, L.B. (2009) Typical 2-Cys peroxiredoxins – Structures, mechanisms and functions. *FEBS Journal* **276**: 2469–2477.

Hall, A., Nelson, K., Poole, L.B. and Karplus, P.A. (2011) Structure-based insights into the catalytic power and conformational dexterity of peroxiredoxins. *Antioxidants & Redox Signaling* **15**: 795–815.

Hall, A., Parsonage, D., Poole, L.B. and Karplus, P.A. (2010) Structural Evidence That Peroxiredoxin Catalytic Power Is Based on Transition-State Stabilization. *Journal of Molecular Biology* **402**: 194–209.

Hartley, J. L. (2000) DNA cloning using in vitro site-specific recombination. *Genome Research* **10**: 1788–1795..

Hendsch, Z.S., and Tidor, B. (1994). Do salt bridges stabilize proteins? A continuum electrostatic analysis. *Protein Science* **3**: 211–226.

Hirotsu, S., Abe, Y., Okada, K., Nagahara, N., Hori, H., Nishino, T. and Hakoshima T. (1999). Crystal structure of a multifunctional 2-Cys peroxiredoxin heme-bindingpProtein 23 kDa/proliferation-associated gene product. *Proceedings of the National Academy of Sciences* **96**: 12333–12338.

Hofmann, B., Hecht, H.-J. and Flohé, L. (2005) Peroxiredoxins. *Biological Chemistry* **383**: 347–364.

Hol, W.G.J., van Duijnen, P.T. and Berendsen, H.J.C. (1978) The A-helix dipole and the properties of proteins. *Nature* **273**: 443–446.

Horton, N. and Lewis, M. (1992). Calculation of the free energy of association for protein complexes. *Protein Science* **1**: 169–181.

Hugo, M., Turell, L., Manta, B., Botti, H., Monteiro, G., Netto, L.E.S., Alvarez, B., Radi, R. and Trujillo, M. (2009) Thiol and sulfenic acid oxidation of AhpE, the one-cysteine peroxiredoxin from *Mycobacterium tuberculosis*: Kinetics, acidity constants, and conformational dynamics. *Biochemistry* **48**: 9416–9426.

Jang, H.H., Lee, K.O., Chi, Y.H., Jung, B.G., Park, S.K., Park, J.H. and Lee, J.R. (2004) Two enzymes in one: Two yeast peroxiredoxins display oxidative stress-dependent switching from a peroxidase to a molecular chaperone function. *Cell* **117**: 625–635.

Job, D., Valiron, O. and Oakley, B. (2003) Microtubule nucleation. *Current Opinion in Cell Biology* **15**: 111–117.

Jones, S. (2012) Computational and structural characterisation of protein associations. *Advances in Experimental Medicine and Biology*, **747**:42–54.

Karplus, P.A. and Hall, A. (2007) Structural survey of the peroxiredoxins.*Subcellular Biochemistry*, **44**:41–60.

Katzen, F. (2007) Gateway ® recombinational cloning: A biological operating system. *Expert Opinion on Drug Discovery* **2**: 571–589.

Kiefer, F., Arnold, K., Kunzli, M., Bordoli, L. and Schwede, T. (2009) The SWISS-MODEL repository and associated resources. *Nucleic Acids Research* **37**: D387–D392.

Kim, K., Kim, I.H., Lee, K.Y., Rhee, S.G. and Stadtman, E.R. (1988) The isolation and purification of a specific “protector” protein which inhibits enzyme inactivation by a thiol/Fe(III)/O_2 mixed-function oxidation system. *Journal of Biological Chemistry* **263**: 4704–4711.

Kitano, K., Niimura, Y., Nishiyama, Y. and Miki, K. (1999) Stimulation of peroxidase activity by decamerization related to ionic strength: AhpC protein from *Amphibacillus xylanus*. *Journal of Biochemistry* **126**: 313–319.

Klotz, I.M, Langebman, N.R. and Dahnall, D.W. (1970) Quaternary structure of proteins. *Annual Review of Biochemistry* **39**: 25–62.

Koh, I.Y.Y., Eyrich, V.A., Marti-Renom, M.A., Przybylski, D., Madhusudhan, M.S., Eswar, N. and Graña, O. (2003) EVA: Evaluation of protein structure prediction servers. *Nucleic Acids Research* **31**: 3311.

Konarev, P.V., Volkov, V.V., Petoukhov, M.V. and Svergun, D.I. (2006) ATSAS 2.1, a program package for small-angle scattering data analysis. *Journal of Applied Crystallography* **39**: 277–286.

Koo, K.H., Lee, S., Jeong, S.Y., Kim, E.T., Kim, H.J., Kim, K., Song, K. and Chae, H.Z. (2002) Regulation of thioredoxin peroxidase activity by C-terminal truncation. *Archives of Biochemistry and Biophysics* **397**: 312–318.

Koppel, D.E. (1972) Analysis of macromolecular polydispersity in intensity correlation spectroscopy: The method of cumulants. *The Journal of Chemical Physics* **57**: 4814–4820.

Lee, W.S., Choi, K.-S. Riddell, J., Ip, C., Ghosh, D., Park, J.-H. and Park, Y.-M. (2007) Human peroxiredoxin 1 and 2 are not duplicate proteins. *Journal of Biological Chemistry* **282**: 22011 –22022.

Li, L., Shoji, W., Takano, H., Nishimura, N., Aoki, Y., Takahashi, R., Goto, S., Kaifu, T., Takai, T. and Obinata, M. (2007) Increased susceptibility of MER5 (peroxiredoxin III) knockout mice to LPS-induced oxidative stress. *Biochemical and Biophysical Research Communications* **355**: 715–721.

Li, S., Peterson, N.A., Kim, M.-Y., Kim, C.-Y., Hung, L.-W., Yu, M., Lekin, T., Segelke, B.W., Lott, J.S. and Baker, E.N. (2005) Crystal structure of AhpE from *Mycobacterium tuberculosis*, a 1-Cys peroxiredoxin. *Journal of Molecular Biology* **346**: 1035–1046.

Liao, S.-J., Yang, C.-Y., Chin, K.-H., Wang, A.H.-J. and Chou S.-H. (2009) Insights into the alkyl peroxide reduction pathway of *Xanthomonas campestris* bacterioferritin comigratory protein from the trapped intermediate–ligand complex structures. *Journal of Molecular Biology* **390**: 951–966.

Link, A.J., Robison, K. and Church, G.M. (1997) Comparing the predicted and observed properties of proteins encoded in the genome of *Escherichia coli* K-12. *Electrophoresis* **18**: 1259–1313.

Logan, C. and Mayhew, S.G. (2000) Cloning, overexpression, and characterization of peroxiredoxin and NADH peroxiredoxin reductase from *Thermus aquaticus*. *Journal of Biological Chemistry* **275**: 30019 –30028.

Lowe, C.R. (2000) Nanobiotechnology: The fabrication and applications of chemical and biological nanostructures. *Current Opinion in Structural Biology* **10**: 428–434.

Lowry, O.H., Rosebrough, N.J., Farr, A.L. and Randall, R.J. (1951) Protein measurement with the folin phenol reagent. *Journal of Biological Chemistry* **193**: 265–275.

Manta, B., Hugo, M., Ortiz, C., Ferrer-Sueta, G., Trujillo, M. and Denicola, A. (2009) The peroxidase and peroxynitrite reductase activity of human erythrocyte peroxiredoxin 2. *Archives of Biochemistry and Biophysics* **484**: 146–154.

Marianayagam, N.J., Sunde, M. and Matthews, J.M. (2004) The power of two: protein dimerization in biology. *Trends in Biochemical Sciences* **29**: 618–625.

Matsumura, T., Okamoto, K., Iwahara, S., Hori, H., Takahashi, Y., Nishino, T. and Abe, Y.. (2008) Dimer-oligomer interconversion of wild-type and mutant rat 2-Cys peroxiredoxin. *Journal of Biological Chemistry* **283**: 284 –293.

Matthews, J.M. and Sunde, M. (2012). Dimers, oligomers, everywhere. *Advances in Experimental Medicine and Biology* **747**:1–18.

Meissner, U., Schröder, E., Scheffler, D., Martin, A.G. and Harris, J.R. (2007) Formation, TEM study and 3D reconstruction of the human erythrocyte peroxiredoxin-2 dodecahedral higher-order assembly. *Micron* **38**: 29–39.

Mertens, H.D.T., and Svergun, D.I. (2010) Structural characterization of proteins and complexes using small-angle X-ray solution scattering. *Journal of Structural Biology* **172**: 128–141.

Miles, E.W., Rhee, S. and Davies, D.R. (1999) The molecular basis of substrate channeling. *Journal of Biological Chemistry* **274**: 12193–12196.

Nakamoto, R.K., Baylis Scanlon, J.A. and Al-Shawi, M.K. (2008) The rotary mechanism of the ATP synthase. *Archives of Biochemistry and Biophysics* **476**: 43–50.

Nelson, K.J., Knutson, S., Soito, L., Klomsiri, C., Poole, L.B. and Fetrow, J.S. (2011) Analysis of the peroxiredoxin family: Using active-site structure and sequence information for global classification and residue analysis. *Proteins: Structure, Function, and Bioinformatics* **79**: 947–964.

Nelson, K.J., Parsonage, D., Hall, A., Karplus, P.A. and Poole, L.B. (2008) Cysteine pK_a values for the bacterial peroxiredoxin AhpC. *Biochemistry* **47**: 12860–12868.

Nogoceke, E., Gommel, D.U., Kieß, M., Kalisz, H.M. and Flohé, L. (1997) A unique cascade of oxidoreductases catalyses trypanothione-mediated peroxide metabolism in *Crithidia fasciculata*. *Biological Chemistry* **378**: 827–836.

Ogusucu, R., Rettori, D., Munhoz, D.C., Netto, L.E.S. and Augusto, O. (2007) Reactions of Yeast Thioredoxin Peroxidases I and II with hydrogen peroxide and peroxynitrite: Rate constants by competitive kinetics. *Free Radical Biology and Medicine* **42**: 326–334.

Ovádi, J. (1991) Physiological significance of metabolic channelling. *Journal of Theoretical Biology* **152**: 1–22.

Pacher, P., Beckman, J.S. and Liaudet, L. (2007) Nitric oxide and peroxynitrite in health and disease. *Physiological Reviews* **87**: 315–424.

Papapostolou, D., and Howorka, S. (2009) Engineering and exploiting protein assemblies in synthetic biology. *Molecular BioSystems* **5**: 723.

Park, S.-H., Chung, Y.M., Lee, Y.-S., Kim, H.J., Kim, J.S., Chae, H.Z. and Yoo, Y.D. (2000) Antisense of human peroxiredoxin II enhances radiation-induced cell death. *Clinical Cancer Research* **6**: 4915–4920.

Parsonage, D., Youngblood, D.S., Sarma, G.S., Wood, Z.A., Karplus, P.A. and Poole, L.B. (2005) Analysis of the link between enzymatic activity and oligomeric state in AhpC, a bacterial peroxiredoxin. *Biochemistry* **44**: 10583–10592.

Pascual, M.B., Mata-Cabana, A., Florencio, F.J., Lindahl, M. and Cejudo F.J. (2010) Overoxidation of 2-Cys peroxiredoxin in prokaryotes. *Journal of Biological Chemistry* **285**: 34485 –34492.

Pedrajas, J.R., Padilla, C.P., McDonagh, B. and Bárcena, J.A. (2010) Glutaredoxin participates in the reduction of peroxides by the mitochondrial 1-Cys peroxiredoxin in *Saccharomyces cerevisiae*. *Antioxidants & Redox Signaling* **13**: 249–258.

Peitsch, M.C. (1995) Protein modeling by e-mail. *Nature Biotechnology* **13**: 658–660.

Petoukhov, M.V., Franke, D., Shkumatov, A.V., Tria, G., Kikhney, A.G., Gajda, M., Gorba, C., Mertens, H.D.T., Konarev, P.V. and Svergun, D.I. (2012) New developments in the ATSAS program package for small-angle scattering data analysis. *Journal of Applied Crystallography* **45**: 342–350.

Poole, L.B. (2005) Bacterial defenses against oxidants: Mechanistic features of cysteine-based peroxidases and their flavoprotein reductases. *Archives of Biochemistry and Biophysics* **433**: 240–254.

Poole, L.B. (2007) The catalytic mechanism of peroxiredoxins. *Subcellular Biochemistry*, **44**:61–81.

Poole, L.B., Reynolds, C.M., Wood, Z.A., Karplus, P.A., Ellis, H.R. and Calzi, M.L. (2000). AhpF and other NADH:peroxiredoxin oxidoreductases, homologues of low M_r thioredoxin reductase. *European Journal of Biochemistry* **267**: 6126–6133.

Porath, J. and Flodin, P. (1959) Gel filtration: A method for desalting and group separation. *Nature* **183**: 1657–1659.

Rhee, S.G., Chae, H.Z. and Kim, K. (2005) Peroxiredoxins: A historical overview and speculative preview of novel mechanisms and emerging concepts in cell signaling. *Free Radical Biology and Medicine* **38**: 1543–1552.

Rothemund, P.W.K. (2006) Folding DNA to create nanoscale shapes and patterns. *Nature* **440**: 297–302.

Saccoccia, F., Micco, P.D., Boumis, G., Brunori, G., Koutris, I., Miele, A.E. and Morea, V. (2012) Moonlighting by different stressors: Crystal structure of the chaperone species of a 2-Cys peroxiredoxin. *Structure* **20**: 429–439.

Salvi, M., Battaglia, V., Brunati, A.M., La Rocca, N., Tibaldi, N., Pietrangeli, P., Marcocci, L., Mondovì, B., Rossi, C.A. and Toninello, A. (2007) Catalase takes part in rat liver mitochondria oxidative stress defense. *Journal of Biological Chemistry* **282**: 24407–24415.

Sarma, G.N., Nickel, C., Rahlfs, S., Fischer, M., Becker, K. and Karplus, P.A. (2005) Crystal structure of a novel *Plasmodium falciparum* 1-Cys peroxiredoxin. *Journal of Molecular Biology* **346**: 1021–1034.

Sayed, A.A., and Williams, D.L. (2004) Biochemical characterization of 2-Cys peroxiredoxins from *Schistosoma mansoni*. *Journal of Biological Chemistry* **279**: 26159–26166.

Schonbaum, G.R., and Chance, B.. (1976) Catalase. *Enzymes* **13**:363–408.

Schröder, E., Littlechild, J.A., Lebedev, A.A., Errington, N., Vagin, A.A. and Isupovm M.N. (2000) Crystal structure of decameric 2-Cys peroxiredoxin from human erythrocytes at 1.7Å resolution. *Structure* **8**: 605–615.

Schröder, E., and Ponting, C.P. (1998) Evidence that peroxiredoxins are novel members of the thioredoxin fold superfamily. *Protein Science* **7**: 2465–2468.

Sheinerman, F.B., Norel, R. and Honig, B. (2000) Electrostatic aspects of protein–protein interactions. *Current Opinion in Structural Biology* **10**: 153–159.

Sievers, F., Wilm, A., Dineen, D., Gibson, T.J., Karplus, K., Li, W. and Lopez, R. (2011) Fast, scalable generation of high-quality protein multiple sequence alignments Using Clustal Omega. *Molecular Systems Biology* **7**:539

Soito, L., Williamson, C., Knutson, S.T., Fetrow, J.S., Poole, L.B. and Nelson, K.J. (2010) PREX: PeroxiRedoxin classification indEX, a database of subfamily assignments across the diverse peroxiredoxin family. *Nucleic Acids Research* **39**: D332–D337.

Sonavane, S., and Chakrabarti, P. (2008) Cavities and atomic packing in protein structures and interfaces. *PLoS Comput Biol* **4**: e1000188.

Stura, E.A. and Wilson, I.A. (1991) Applications of the streak seeding technique in protein crystallization. *Journal of Crystal Growth* **110**: 270–282.

Svergun, D., Barberato, C. and Koch, M.H.J. (1995) CRYSOL – a program to evaluate X-ray solution scattering of biological macromolecules from atomic coordinates. *Journal of Applied Crystallography* **28**: 768–773.

Tavender, T.J., Sheppard, A.M. and Bulleid, N.J. (2008) Peroxiredoxin IV is an endoplasmic reticulum-localized enzyme forming oligomeric complexes in human cells. *Biochemical Journal* **411**: 191-199.

Tohru, Y., Yasuhisa, M., Shunji, N. and Masuo, O. (1989) Cloning of a housekeeping-type gene (MERS) preferentially expressed in murine erythroleukemia cells. *Gene* **80**: 337–343.

Trujillo, M., Clippe, A., Manta, B., Ferrer-Sueta, G., Smeets, A., Declercq, J.-P., Knoops, B. and Radi, R. (2007) Pre-steady state kinetic characterization of human peroxiredoxin 5: Taking advantage of Trp84 fluorescence increase upon oxidation. *Archives of Biochemistry and Biophysics* **467**: 95–106.

Trujillo, M., Ferrer-Sueta, G., Thomson, L., Flohé, L. and Radi, R. (2007) Kinetics of peroxiredoxins and their role in the decomposition of peroxynitrite. *Subcellular Biochemistry* **44**:83–113.

Tsai, C.-J., Lin, S.L., Wolfson, H.J. and Nussinov, R. (1997) Studies of protein-protein interfaces: A statistical analysis of the hydrophobic effect. *Protein Science* **6**: 53–64.

Ursini, F., Maiorino, M. and Gregolin, C. (1985) The selenoenzyme phospholipid hydroperoxide glutathione peroxidase. *Biochimica Et Biophysica Acta (BBA) - General Subjects* **839**: 62–70.

Wakita, M., Masuda, S., Motohashi, K., Hisabori, T., Ohta, H. and Takamiya, K. (2007) The significance of Type II and PrxQ peroxiredoxins for antioxidative stress response in the purple bacterium *Rhodobacter sphaeroides*. *Journal of Biological Chemistry* **282**: 27792–27801.

Walhout, A.J.M., Temple, G.F., Brasch, M.A., Hartley, J.L., Lorson, M.L., van den Heuvel, S. and Vidal, M.. (2000) GATEWAY recombinational cloning: Application to the cloning of large numbers of open reading frames or ORFeomes. *Methods in Enzymology*, **328**:575–592.

Watabe, S., Kohno, H., Kouyama, H., Hiroi, T., Yago, N. and Nakazawa, T. (1994) Purification and characterization of a substrate protein for mitochondrial ATP-dependent protease in bovine adrenal cortex. *Journal of Biochemistry* **115**: 648–654.

Whitesides, G.M. (2003) The “right” size in nanobiotechnology. *Nature Biotechnology* **21**: 1161-1165.

Whitesides, G.M. and Boncheva, M. (2002) Beyond molecules: Self-assembly of mesoscopic and macroscopic components. *Proceedings of the National Academy of Sciences* **99**: 4769–4774.

Whitesides, G.M., and Grzybowski, B. (2002) Self-assembly at all scales. *Science* **295**: 2418–2421.

Winterbourn, C.C. (2008) Reconciling the chemistry and biology of reactive oxygen species. *Nature Chemical Biology* **4**: 278–286.

Winzor, D.J. (2003) Analytical exclusion chromatography. *Journal of Biochemical and Biophysical Methods* **56**: 15–52.

Woo, H.A, Chae, H.Z., Hwang, S.C., Yang, K.-S., Kang, S.W., Kim, K. and Rhee, S.G. (2003) Reversing the inactivation of peroxiredoxins caused by cysteine sulfinic acid formation. *Science* **300**: 653–656.

Wood, Z.A., Schröder, E., Harris, J.R. and Poole, L.B. (2003) Structure, mechanism and regulation of peroxiredoxins. *Trends in Biochemical Sciences* **28**: 32–40.

Wood, Z.A., Poole, L.B., Hantgan, R.R. and Karplus, P.A. (2002) Dimers to doughnuts: Redox-sensitive oligomerization of 2-cysteine peroxiredoxins. *Biochemistry* **41**: 5493–5504.

Wood, Z.A., Poole, L.B. and Karplus, P.A. (2003) Peroxiredoxin evolution and the regulation of hydrogen peroxide signaling. *Science* **300**: 650 –653.

Yang, K.S., Kang, S.W., Woo, H.A., Hwang, S.C., Chae, H.Z., Kim, K. and Rhee, S.G. (2002) Inactivation of human peroxiredoxin I during catalysis as the result of the oxidation of the catalytic site cysteine to cysteine-sulfinic acid. *Journal of Biological Chemistry* **277**: 38029–38036.

Zhang, S. (2003) Fabrication of novel biomaterials through molecular self-assembly. *Nature Biotechnology* **21**: 1171–1178.